AD-A035 607 SYSTEMS SCIENCE AND SOFTWARE LA JOLLA CALIF F/G 18/6
E-BEAM BENCHMARK CALCULATIONS. PROBLEM NO. 1.(U)
APR 76 J HARVEY, I KATZ, A WILSON DNA001-76-C-0121
UNCLASSIFIED SSS-R-76-2898 DNA-3974T NL

1 OF 1
ADA035607

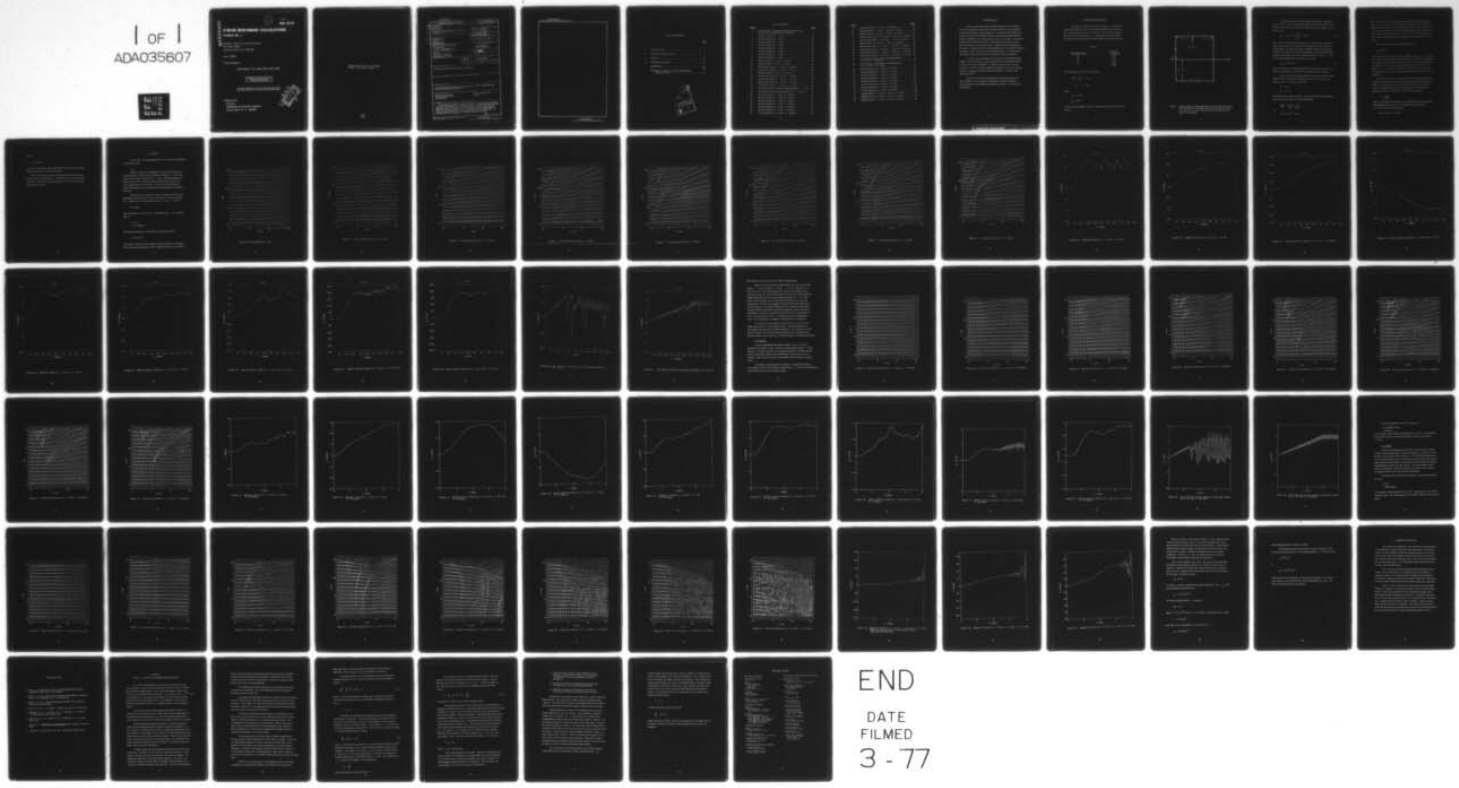

END

DATE
FILMED
3 - 77

DNA 3974T

# E-BEAM BENCHMARK CALCULATIONS

## Problem No. I

Systems, Science and Software
P.O. Box 1620
La Jolla, California 92038

April 1976

Topical Report

CONTRACT No. DNA 001-76-C-0121



THIS WORK SPONSORED BY THE DEFENSE NUCLEAR AGENCY
UNDER RDT&E RMSS CODE B323076464 R99QAXEB06960 H2590D.



Prepared for
Director
DEFENSE NUCLEAR AGENCY
Washington, D. C. 20305

Destroy this report when it is no longer needed. Do not return to sender.

UNCLASSIFIED

SECURITY CLASSIFICATION OF THIS PAGE (When Data Entered)

**REPORT DOCUMENTATION PAGE**

READ INSTRUCTIONS BEFORE COMPLETING FORM

| | |
|---|---|
| 1. REPORT NUMBER: DNA 3974T | 2. GOVT ACCESSION NO. |
| 3. RECIPIENT'S CATALOG NUMBER | |
| 4. TITLE (and Subtitle): E-BEAM BENCHMARK CALCULATIONS, Problem No. 1 | 5. TYPE OF REPORT & PERIOD COVERED: Topical Report |
| 6. PERFORMING ORG. REPORT NUMBER: SSS-R-76-2898 | |
| 7. AUTHOR(s): James Harvey, Ira Katz, Andrew Wilson | 8. CONTRACT OR GRANT NUMBER(s): DNA 001-76-C-0121 |
| 9. PERFORMING ORGANIZATION NAME AND ADDRESS: Systems, Science and Software, P.O. Box 1620, La Jolla, California 92038 | 10. PROGRAM ELEMENT, PROJECT, TASK AREA & WORK UNIT NUMBERS: NWED Subtask R99QAXEB069-60 |
| 11. CONTROLLING OFFICE NAME AND ADDRESS: Director, Defense Nuclear Agency, Washington, D.C. 20305 | 12. REPORT DATE: Apr 76 |
| | 13. NUMBER OF PAGES: 76 |
| 14. MONITORING AGENCY NAME & ADDRESS (if different from Controlling Office): 74p. | 15. SECURITY CLASS (of this report): UNCLASSIFIED |
| | 15a. DECLASSIFICATION/DOWNGRADING SCHEDULE |

16. DISTRIBUTION STATEMENT (of this Report)

Approved for public release; distribution unlimited.

17. DISTRIBUTION STATEMENT (of the abstract entered in Block 20, if different from Report)

18. SUPPLEMENTARY NOTES

This work sponsored by the Defense Nuclear Agency under RDT&E RMSS Code B323076464 R99QAXEB06960 H2590D.

19. KEY WORDS (Continue on reverse side if necessary and identify by block number)

Benchmark Experiment
Electron Beam Transport
Finite Pressure
Electromagnetic Codes
SGEMP

20. ABSTRACT (Continue on reverse side if necessary and identify by block number)

The transport of a large area electron beam in a cylindrical tank is analyzed using the 2-D FRED/EM and GFRED particle codes. Calculations were performed under both vacuum and non-zero density conditions using prescribed injected electron energies and current pulses. The results illustrate, dynamically, the effects of space-charge limiting and neutralization by the gas background. At the highest pressures examined, a collective instability develops.

DD FORM 1 JAN 73 1473 EDITION OF 1 NOV 65 IS OBSOLETE

UNCLASSIFIED

SECURITY CLASSIFICATION OF THIS PAGE (When Data Entered)

388 507

TABLE OF CONTENTS



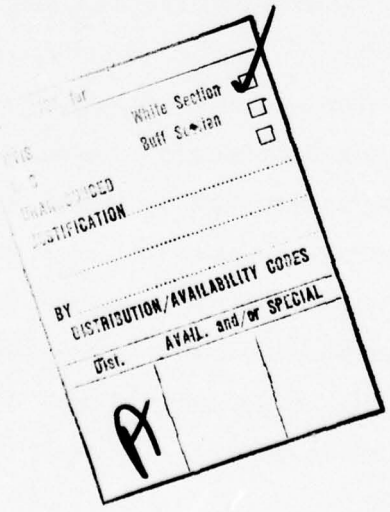

LIST OF FIGURES

# 1. INTRODUCTION

The first of the DNA series of IEMP benchmark code calculations involves the transport of electrons in a simple cylindrical cavity under both vacuum and finite gas pressure conditions. The purpose of this problem was to check the various DNA SGEMP codes in performing calculations when the manner in which they were performed was as close as possible. The electron emission data was specified by HDL. It was particularly simple to model and was not based on experimental data. In addition, the grid spacings and time-steps were specified so that a close comparison of the calculations should be possible. This is discussed in the following section. The results of the calculations are presented in Section 3 and these are then summarized.

To carry out the calculations, we used the $S^3$ codes FRED/EM and GFRED. The first of these is a 2-D axisymmatric electromagnetic particle code and is described elsewhere[1]. It was used for the vacuum case calculations. In order to handle the relativistic dynamics of the more energetic electrons a relativistic particle pusher was included. It is based on the method of Boris[2].

The non-zero pressure calculations were performed using a new code, GFRED. It is an adaption of FRED/EM, in which the secondary electron dynamics and ionization processes are included. It is described in the Appendix.

## 2. PROBLEM SPECIFICATION

The problem configuration is shown in Figure 1. It consists of a cylindrical tank whose sides are conducting and grounded to each other. The radius R and the length L are both 15 cm. The electron emission is uniform over the omitting surface z = 0 and contains no angular spread. The spectrum of the electrons is shown in Table 1 and is uniform in time.

TABLE 1

| Mean Energy (keV) | Fraction of Total Charge |
|---|---|
| 15 | 0.23 |
| 25 | 0.34 |
| 35 | 0.16 |
| 45 | 0.13 |
| 60 | 0.14 |
| | 1.00 |

The emitted current pulse has an amplitude

$$J(t) = J_o \frac{t}{t_R}, \quad t \le t_R$$

$$= J_o, \quad t > t_R$$

where

$$J_o = 5 \text{ A/cm}^2$$

$$t_R = 6 \text{ nsec}.$$

The electric and magnetic fields are calculated at the positions indicated in Figure 1.

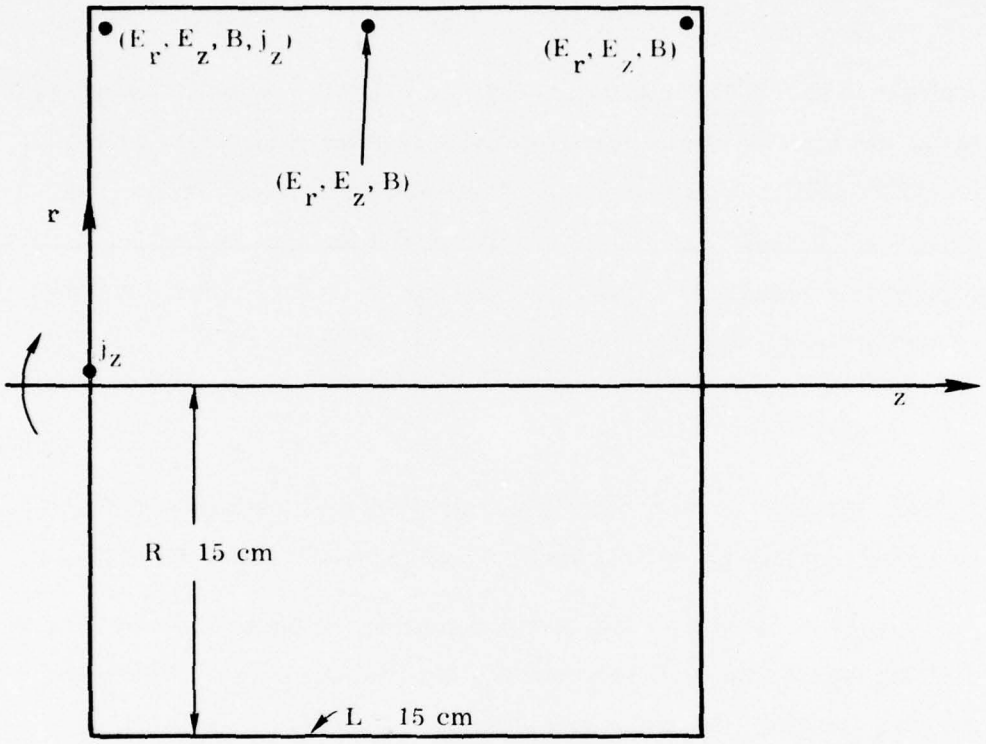


Figure 1. Cavity geometry, showing approximate positions where the desired output quantities are calculated (accurate to dimensions of a cell $\Delta r = 1$ cm, $\Delta z = 0.5$ cm). Exact positions are indicated on the respective output plots.

Before proceeding, it is worth considering the basic phenomena involved. In the zero pressure case the emitted current will be limited by its own space charge if it exceeds the (non-relativistic) Child-Langmuir current limit, namely

$$J_{CL} = 2.33 \times 10^{-6} \frac{\varepsilon^{3/2}}{(L/2)^2} \quad A/cm^2 \tag{1}$$

where $\varepsilon$ is the emitted electron energy (in eV). This is only a rough estimate, and ignores electromagnetic cavity resonances as well as electron inertia effects, 2-D radial spreading and polychromaticity in the electron emission. We shall make one further assumption, namely that the limiting current is determined by the most energetic electrons. Taking $\varepsilon = 6 \times 10^4$ eV and ignoring relativistic corrections, we see that

$$J_{CL} \sim 0.6 \ A/cm^2 \ . \tag{2}$$

This corresponds to less than one-eighth of the peak emitted current. Consequently, we should expect limiting to occur fairly early in the pulse.

There is no very low energy component of emitted electrons in this problem and, as we shall see, limiting does not occur very close to the emitting surface. The cell size used was

$$\Delta r = 1 \text{ cm}$$

$$\Delta z = 0.5 \text{ cm}$$

and this proved to be quite adequate. The codes used were electromagnetic and the time-step stability criterion demands that

$$\left(\frac{1}{c\Delta t}\right)^2 \gtrsim \frac{1}{(\Delta r)^2} + \frac{1}{(\Delta z)^2}$$

or

$$\Delta t \lesssim 1.5 \times 10^{-11} \text{ secs} \ .$$

Since some of the electrons have velocities comparable with the velocity of light ($\beta \sim 0.45$), it is important they be pushed using a time-step which is comparable with the above. In FRED/EM, the two time-steps were identical. In the original specifications of this problem, particles were permitted to be pushed with a much longer time-step ($\sim 5 \times 10^{-10}$ secs). With such a time-step, particles cross many cells in a single cycle and this will lead to noisy results.

The vacuum case is essentially quasi-static since

$$ct_R = 150 \text{ cm}$$

and this is much larger than the radius or length of the cavity. Cavity resonances will be of small amplitude and high frequency. However, the advantages to be gained by using a quasi-static code are not very great for this problem since there are many fast moving electrons and the time savings are only about $\beta^{-1} \sim 2$. In any case, FRED/E was not used as the point of these calculations was to compare codes performing under closely similar running conditions.

In the non-zero pressures cases (50 and 200 mtorr), the production of secondary electrons leads to a reduction of the space-charge potential. Secondaries are accelerated away from such regions and the beam electron charge is largely neutralized by the remaining ions. The time taken to neutralize the beam space-charge is, very crudely, given by[3]

$$t_N = \frac{1}{n_o \sigma \beta_c}$$

where $n_o$ is the gas number density, $\sigma$ is the ionization cross section and $\beta c$ is the average electron velocity. At a pressure of 50 microns ($n_o \sim 1.8 \times 10^{15}$ cm$^{-3}$) for 40 keV electrons

$$\sigma \beta c \sim 2.9 \times 10^{-8} \text{ cm}^3/\text{sec}$$

so that

$$t_N \sim 19 \text{ nsec.}$$

Thus, gas neutralization, while important for the 50 mtorr case, should dominate the behavior in the 200 mtorr case.

When neutralization occurs, the beam electron number density is similar to that of the secondaries. With beam electrons moving rapidly through the cold secondary electron plasma, it is possible for collective instabilities to develop.

## 3. RESULTS

In this section, the results obtained for each of the three calculations are described in turn.

P = 0

Figures 2 through 9 are snapshots at nanosecond intervals of the electron dynamics. Deceleration of the beam is evident at $t = 2$ nsec and trajectory turnaround is important by $t = 3$ nsec. Radial spreading of the beam is greatest far from the axis of the tank where the peel-off of the lower energy groups is most obvious. It is also clear that the spatial zoning is appropriate to this problem and that no limiting occurs within the first cells.

Time histories of a number of electric, magnetic and current field quantities at points specified in Figure 1 are shown in Figures 10 through 20. In Figure 10, the peak magnetic field at ($r = 15$ cm, $z = 15$ cm) is

$$B \simeq 5 \text{ gauss}$$

This corresponds to a total current I transmitted to the $z = 15$ cm surface given by

$$I = 5\, r\, B$$
$$= 375 \text{ Amperes} \quad .$$

The average transmitted current density on this surface is then

$$j \simeq 0.5 \text{ A/cm}^2 \quad .$$

This result is close to the Child-Langmuir result (Equation 1), especially in view of the various assumptions made. Probably the largest error made in

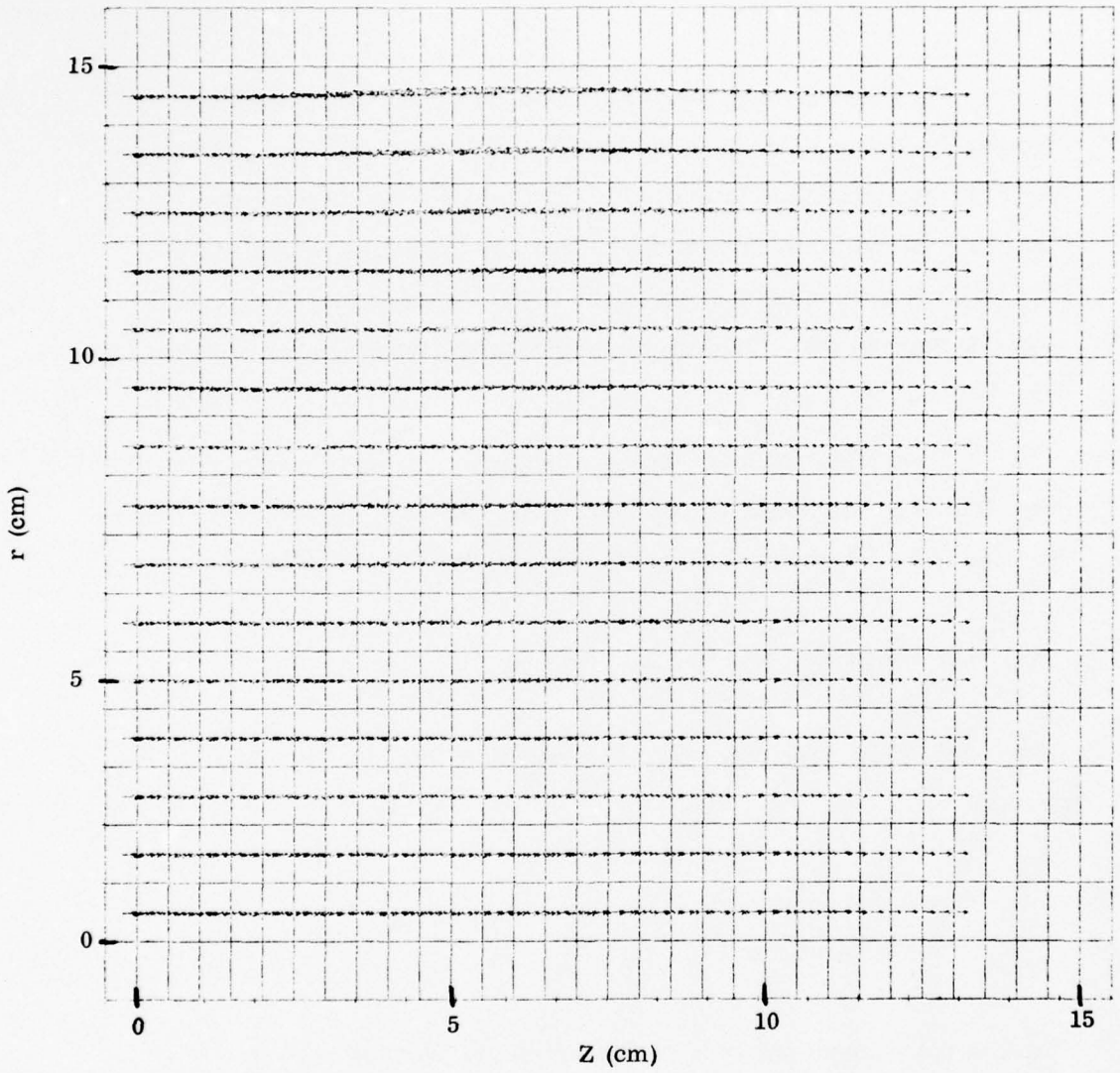


Figure 2. Particle positions at t = 1 nsec.

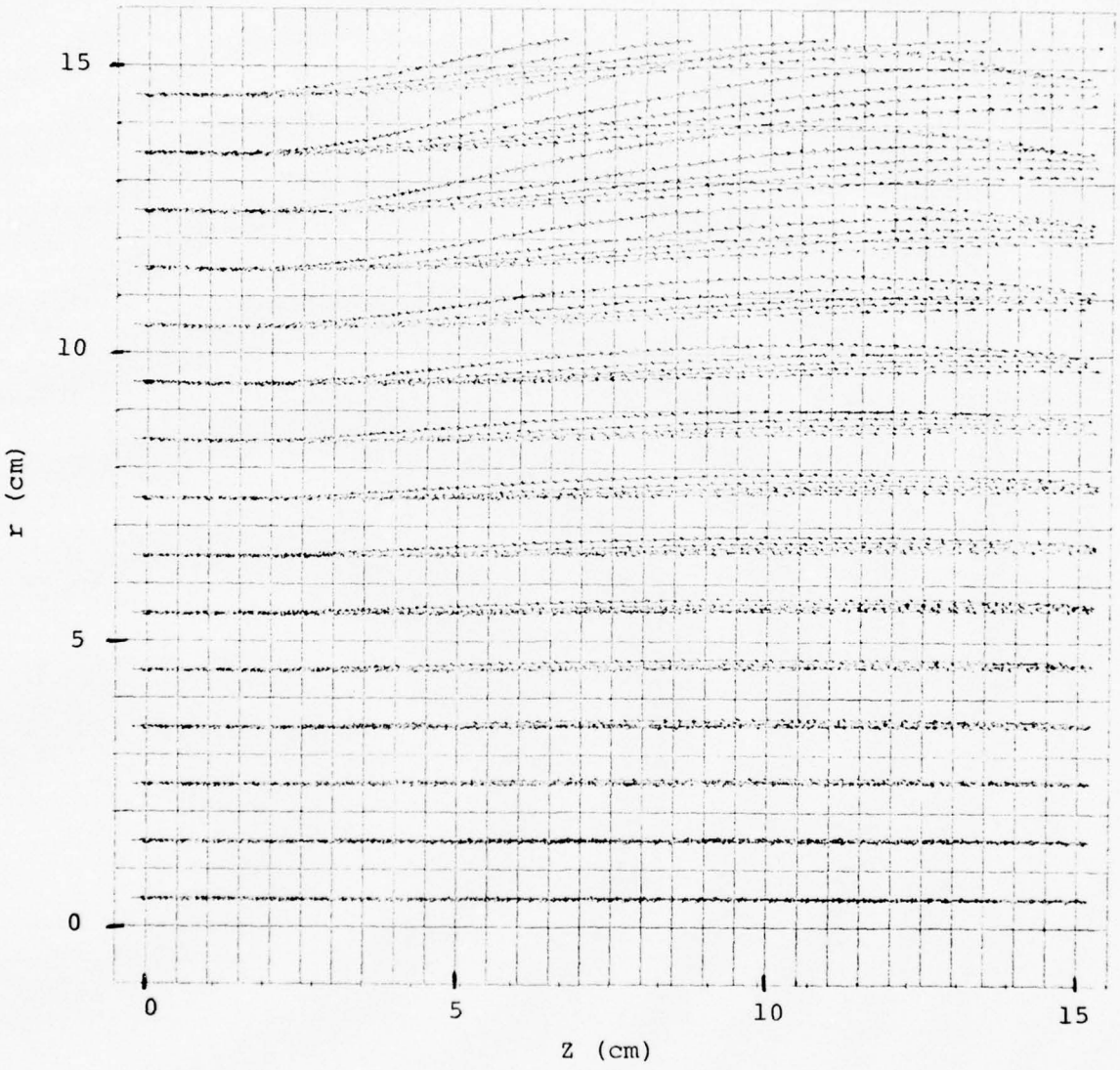


Figure 3. Particle positions at t = 2 nsec.

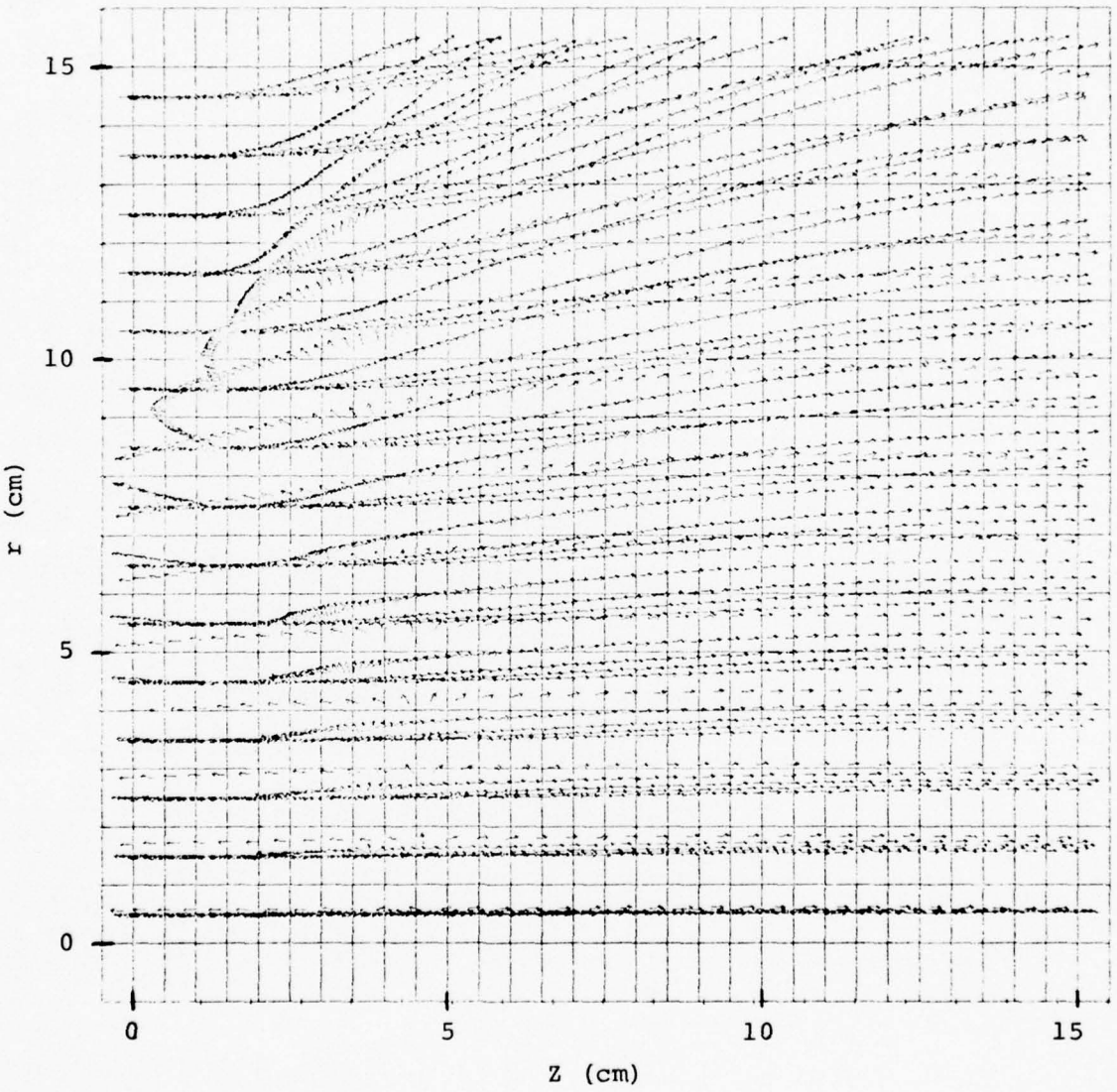


Figure 4. Particle positions at t = 3 nsec.

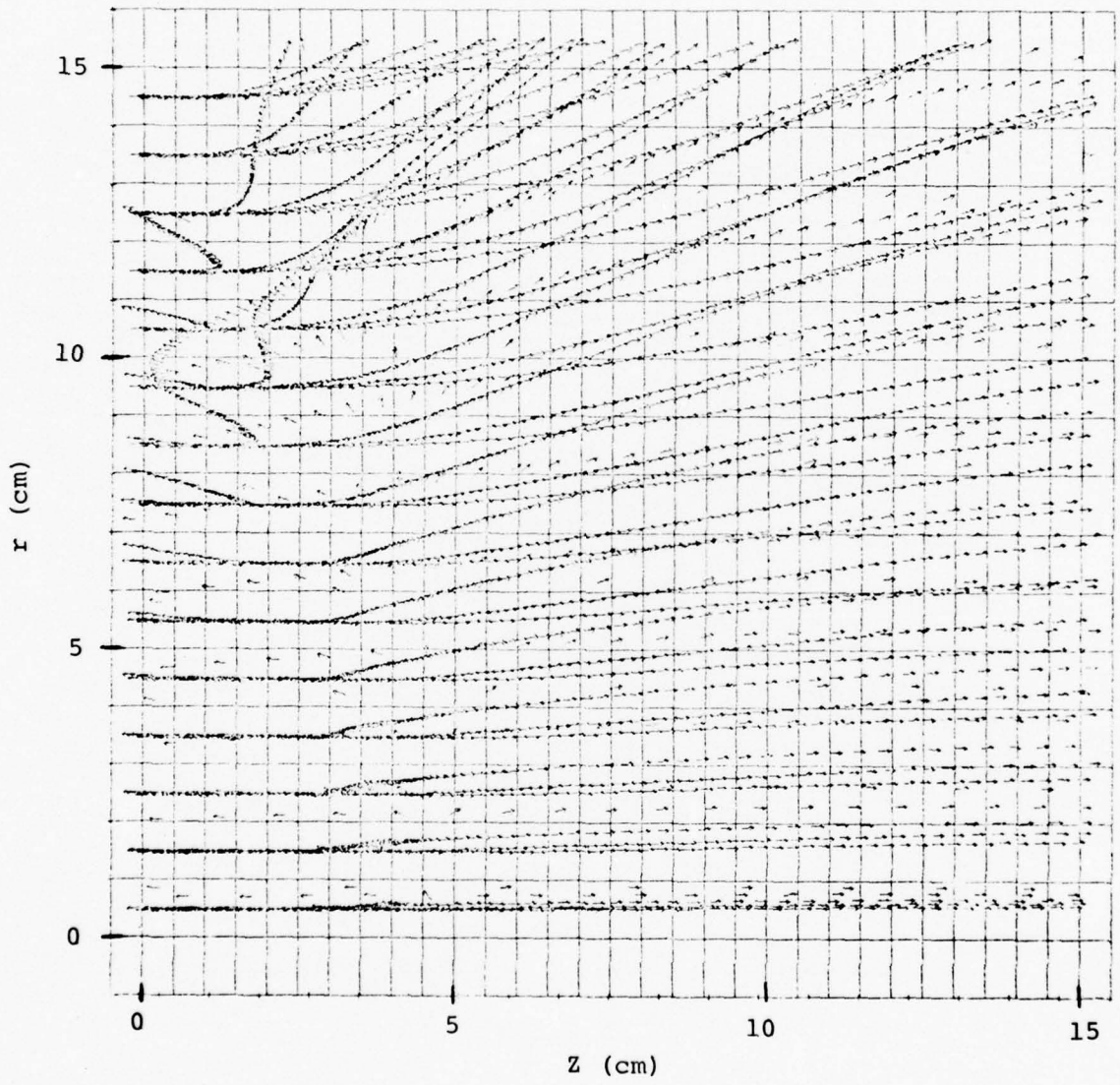


Figure 5. Particle positions at t = 4 nsec.

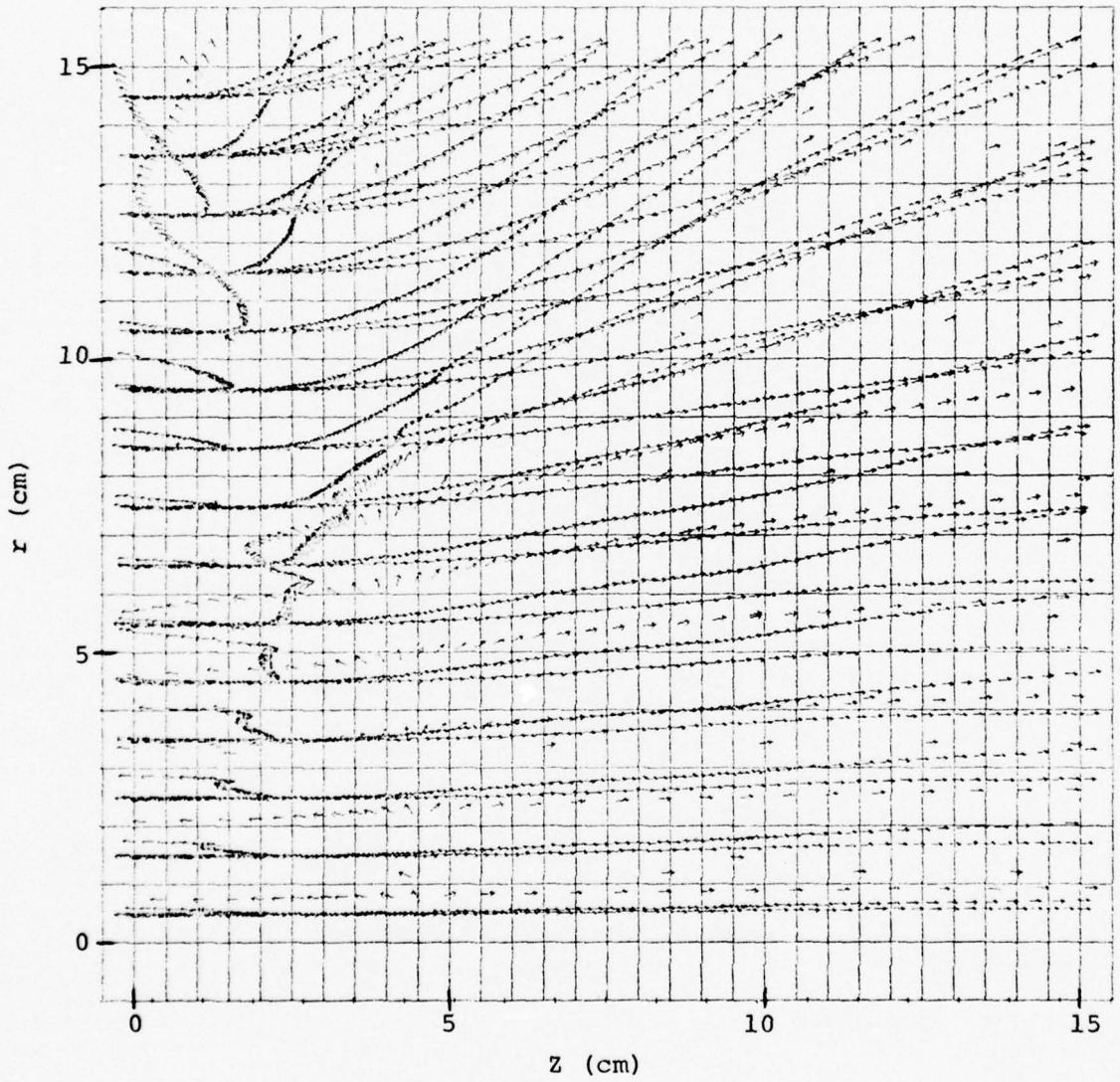


Figure 6. Particle positions at t = 5 nsec.

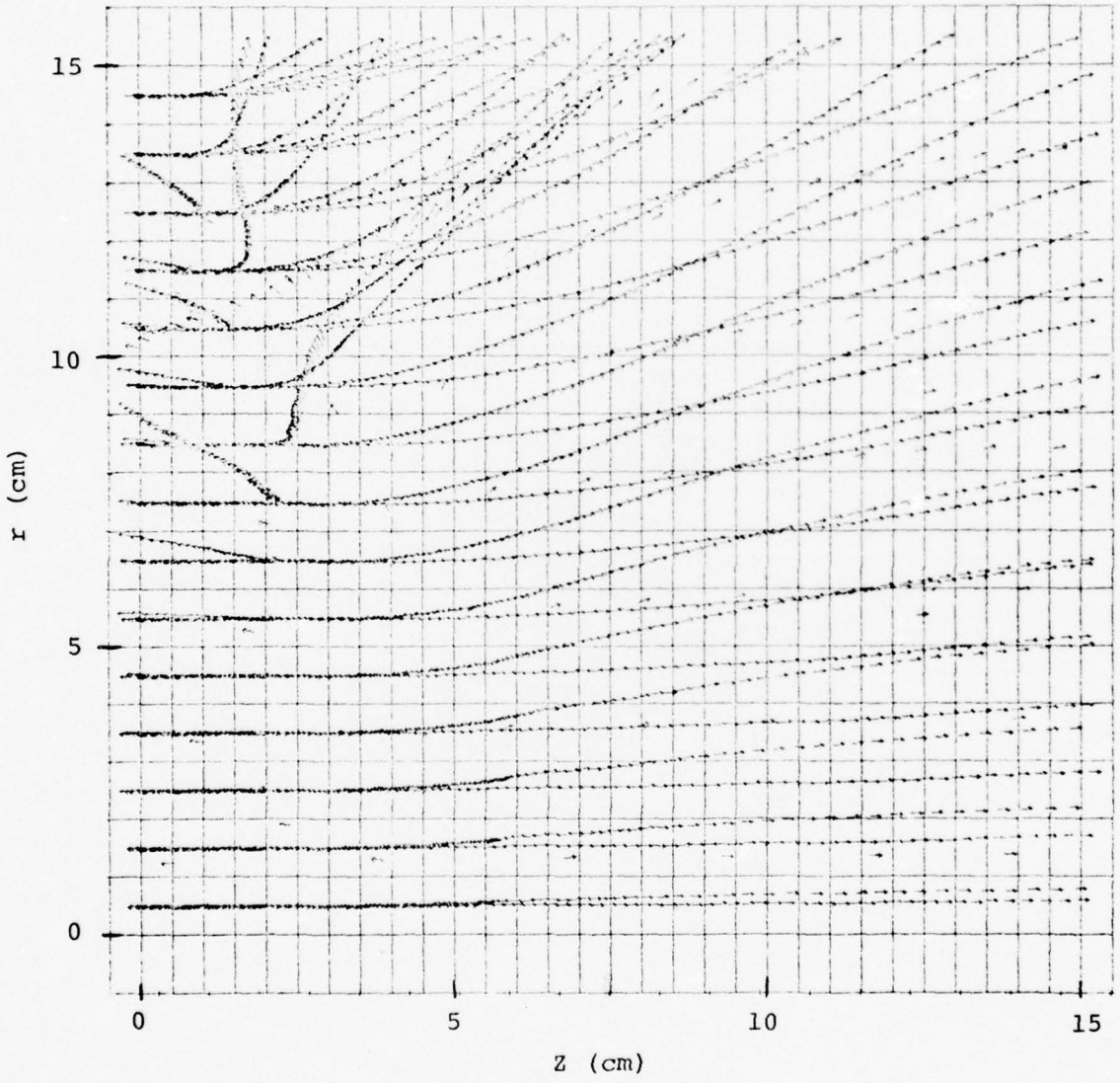


Figure 7. Particle positions at t = 6 nsec.

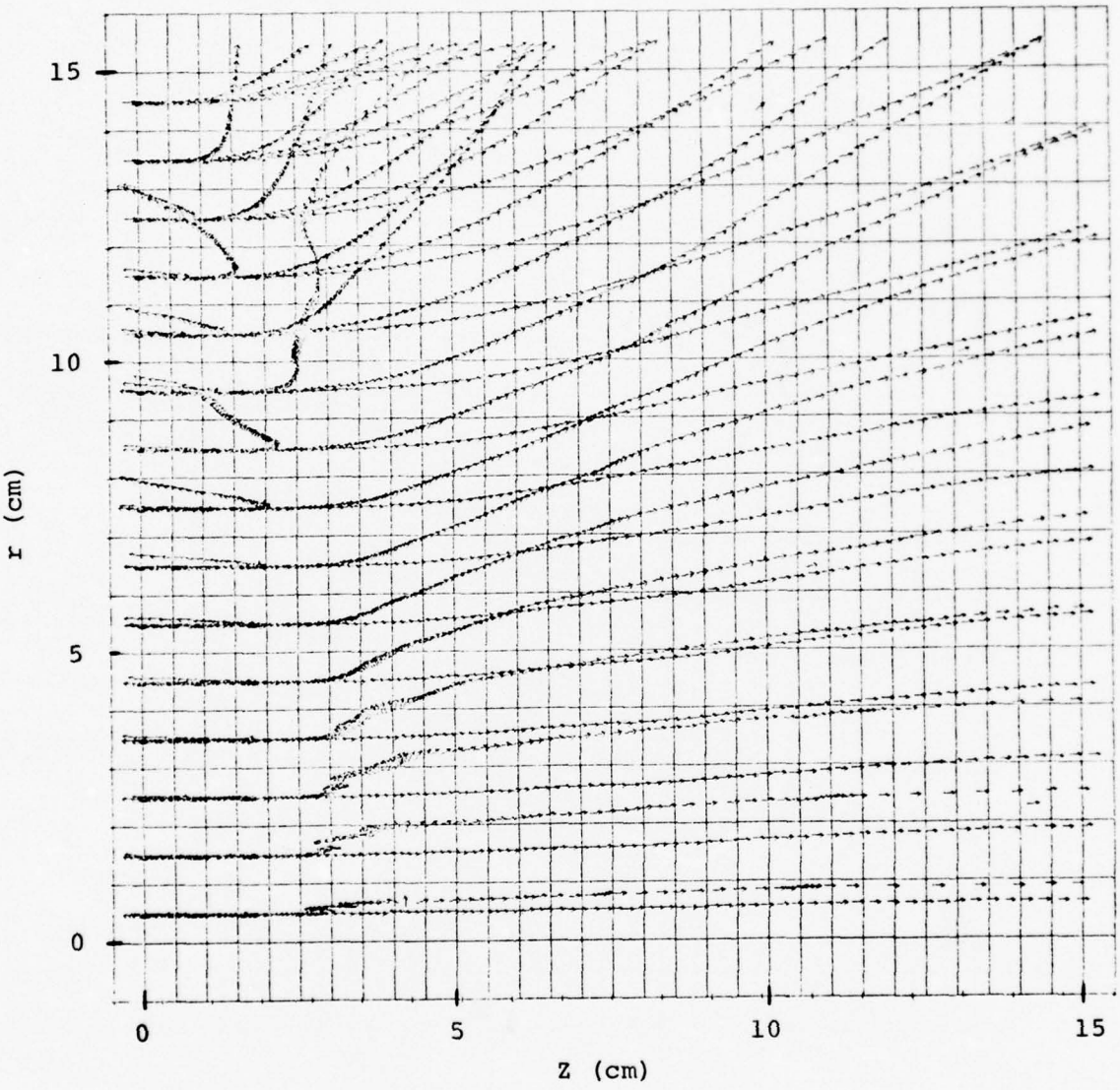


Figure 8. Particle positions at t = 7 nsec.

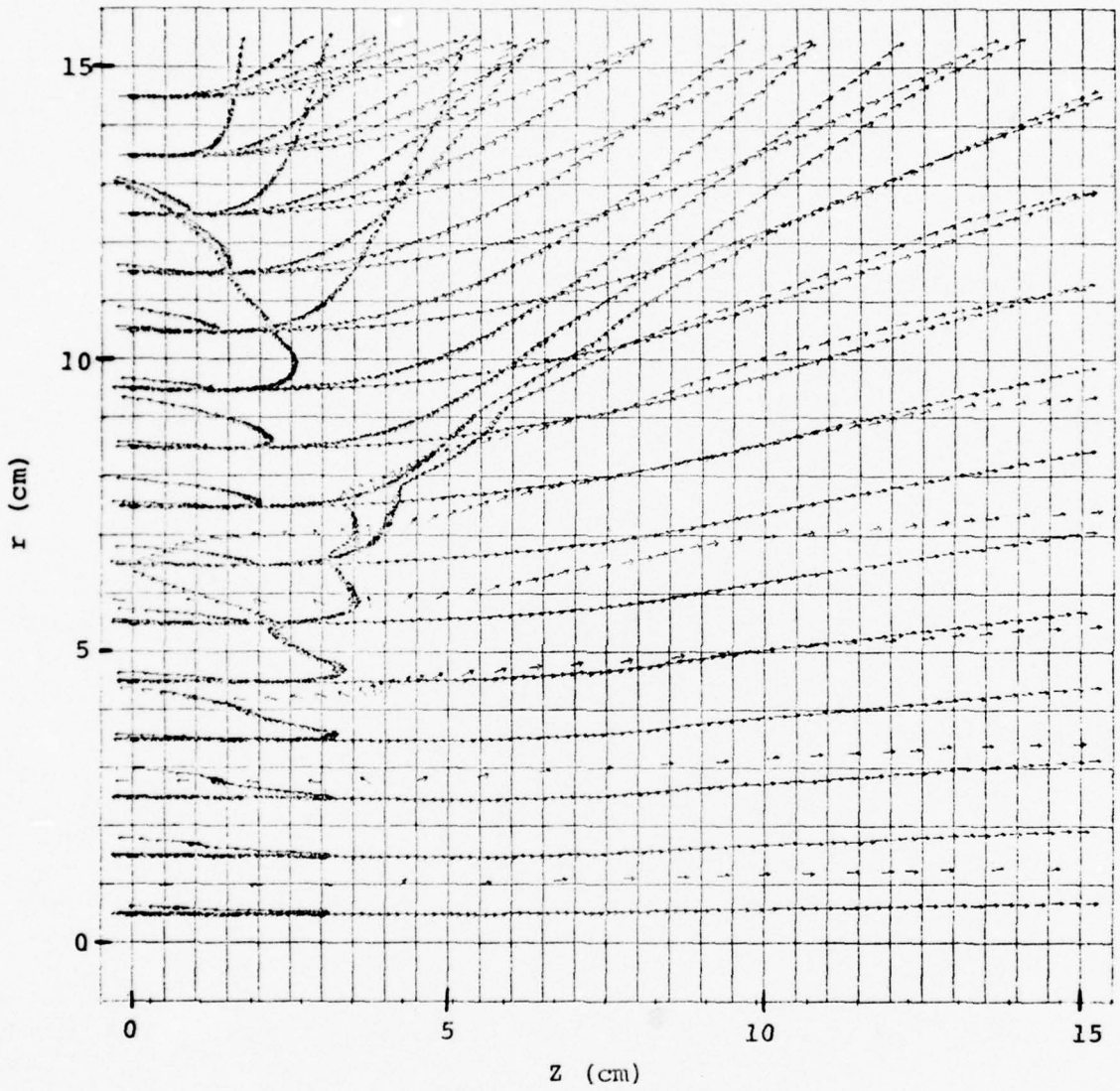


Figure 9. Particle positions at t = 8 nsec.

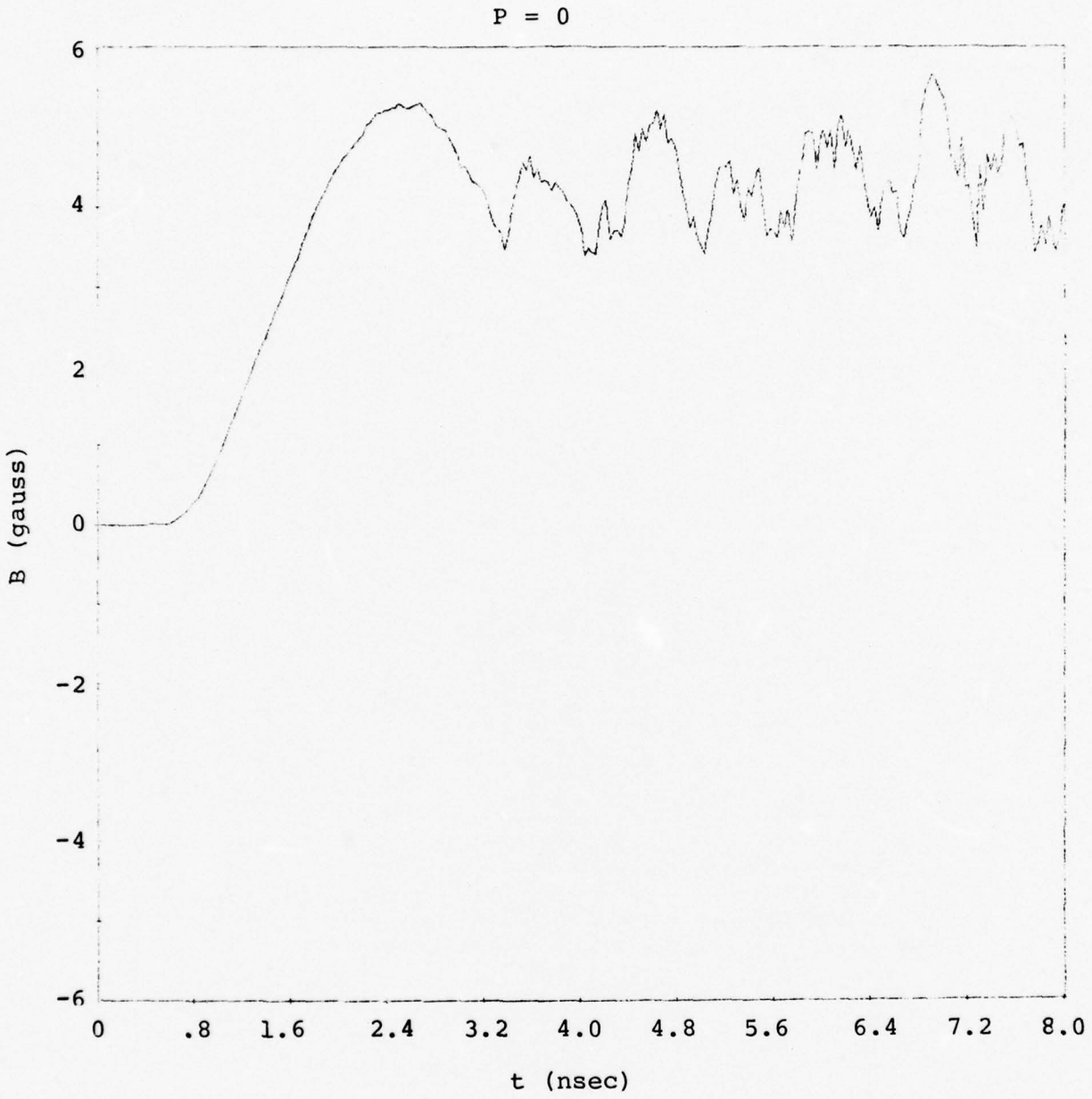


Figure 10. Magnetic field at r = 15 cm, z = 15 cm.

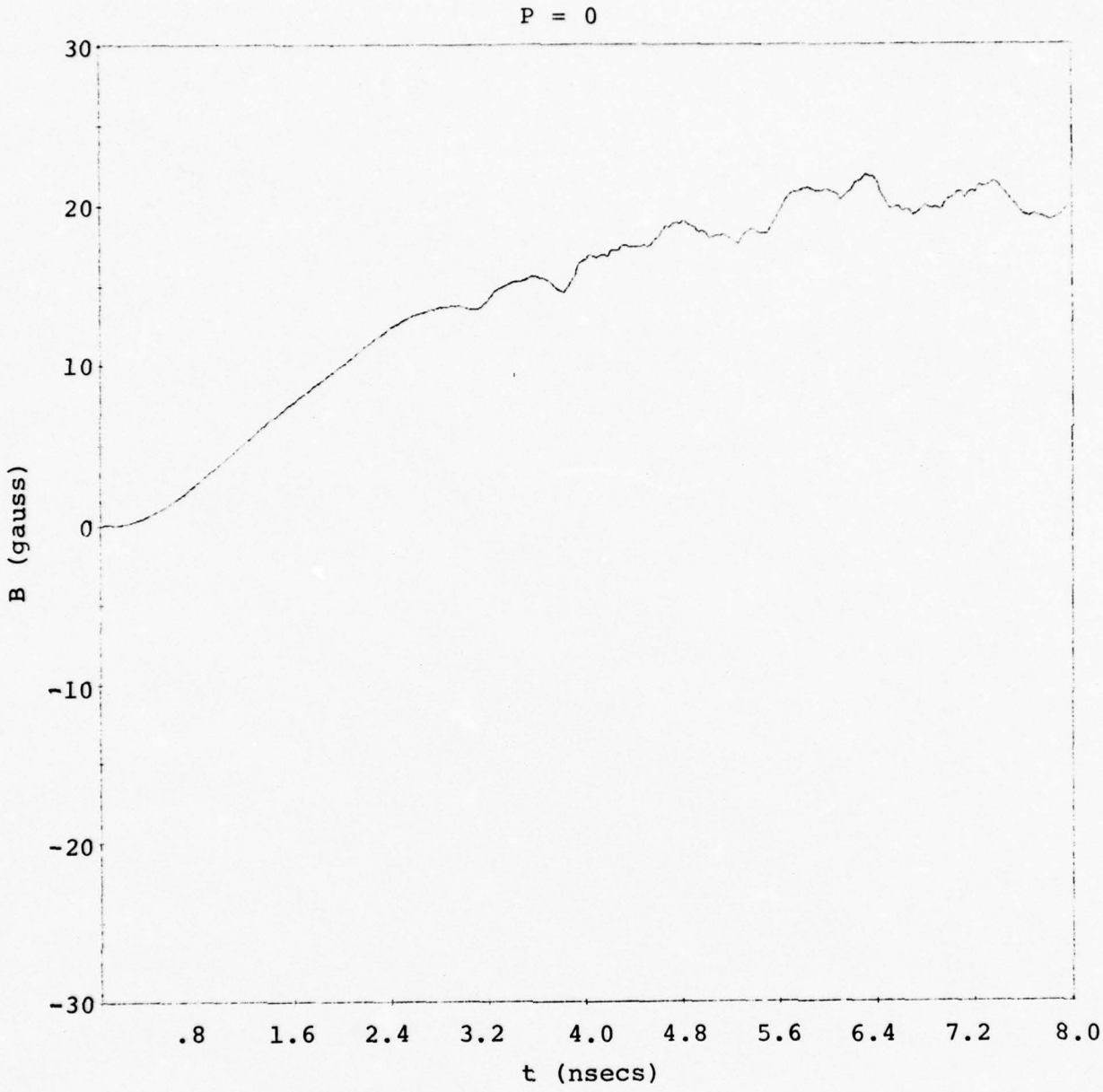


Figure 11. Magnetic field at r = 14 cm, z = 0 cm.

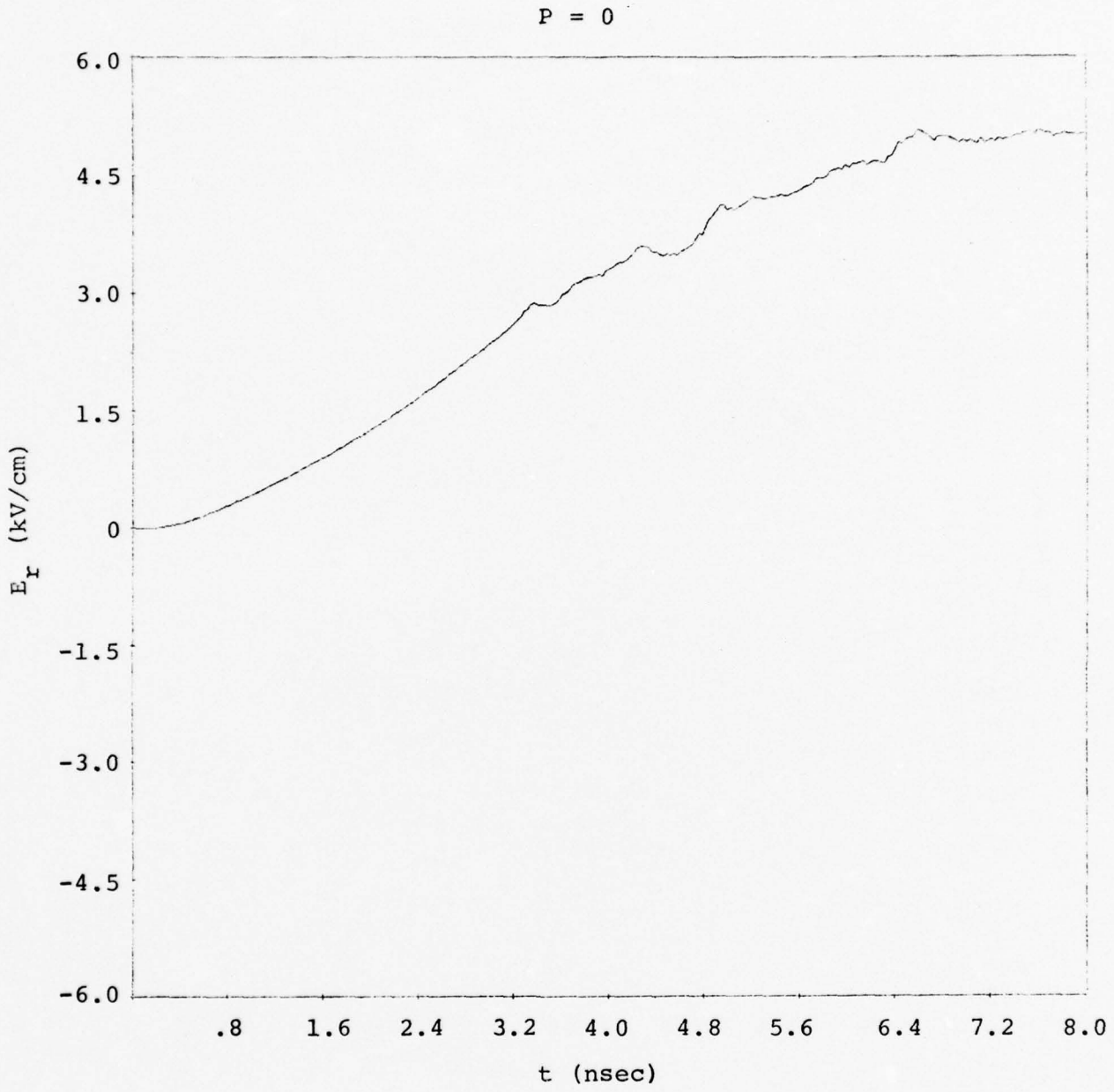


Figure 12. Radial electric field at r = 14 cm, z = 0.25 cm.

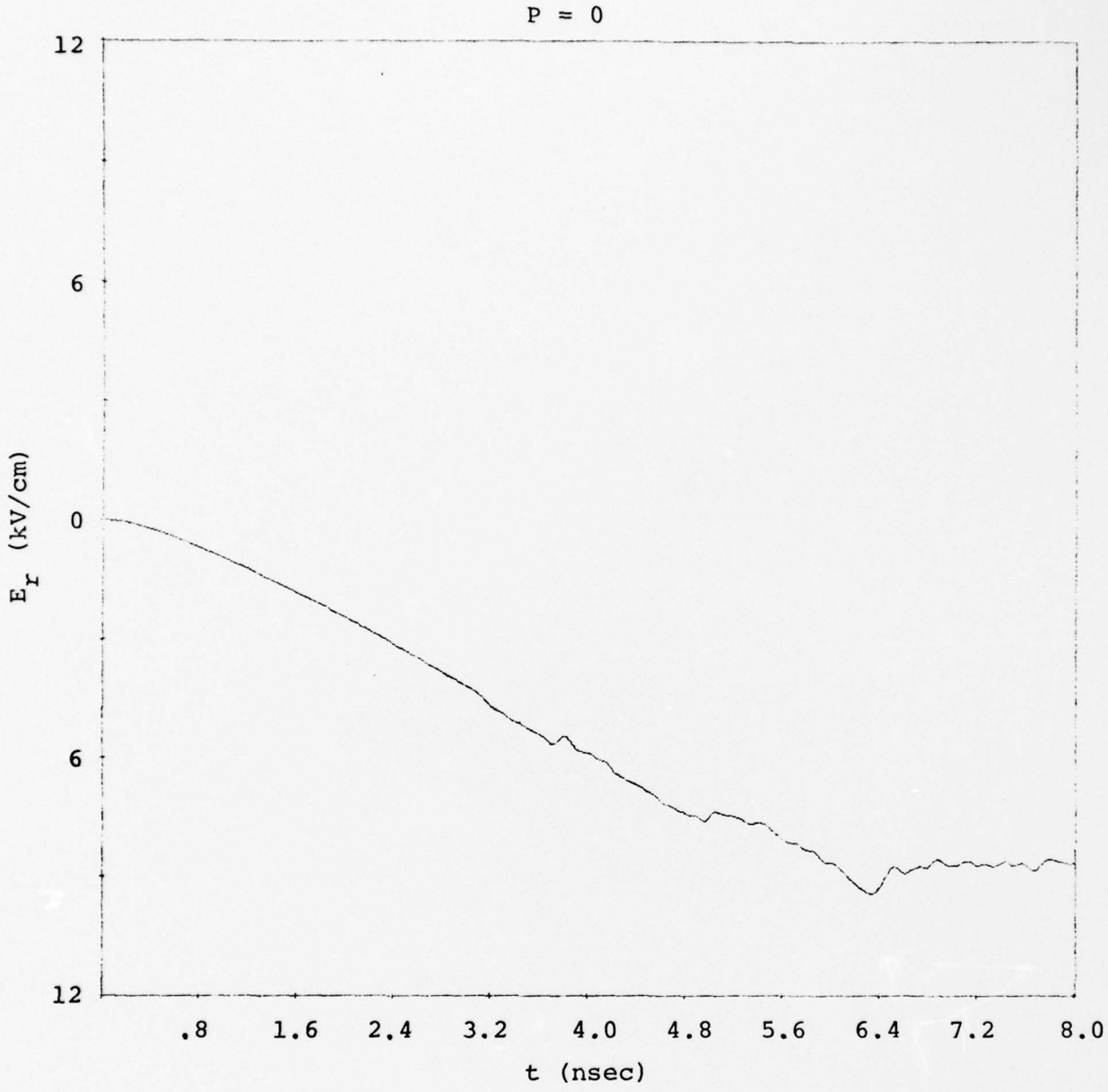


Figure 13. Axial electric field at r = 14.5 cm, z = 0 cm.

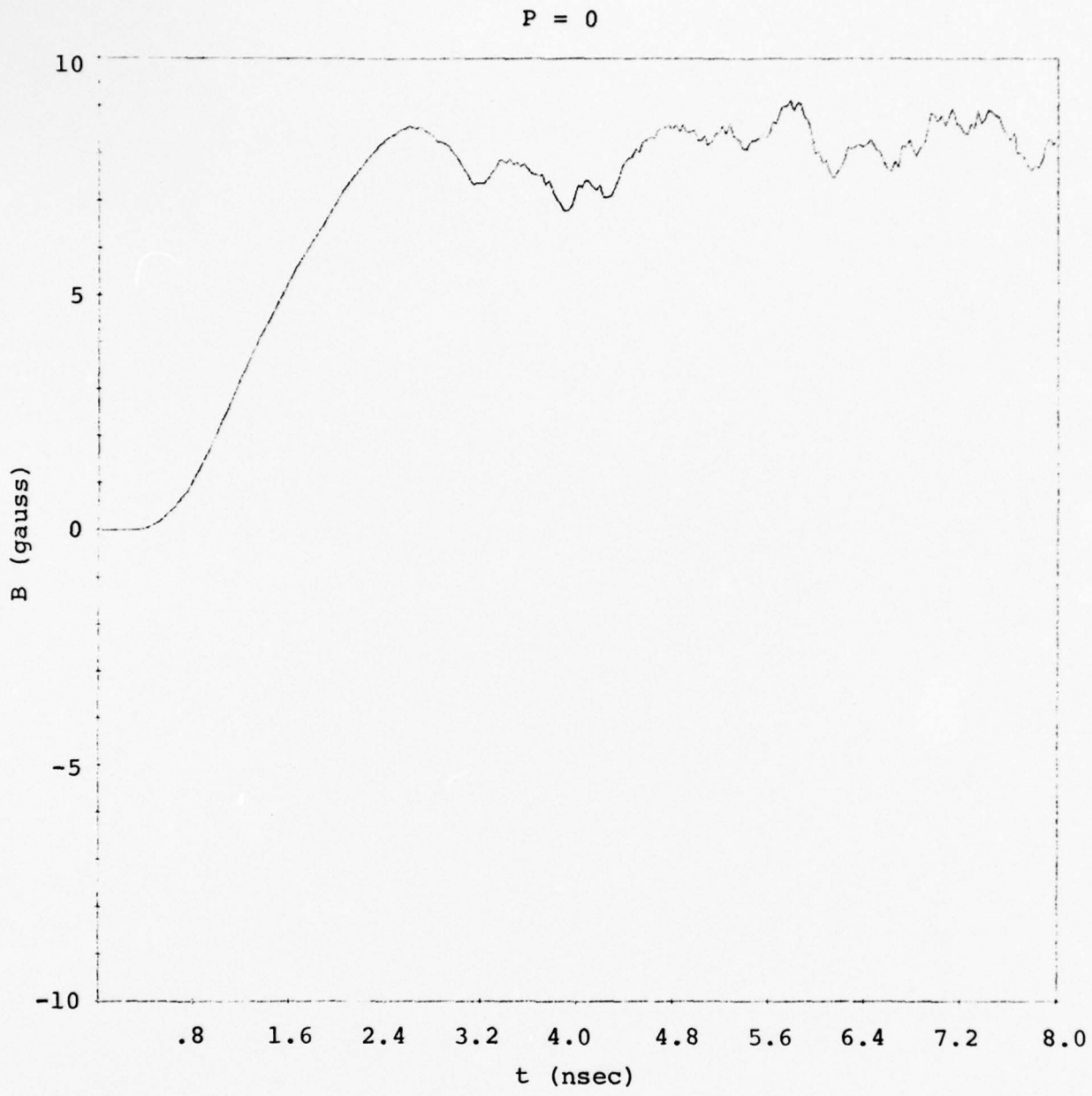


Figure 14. Magnetic field at r = 14 cm, z = 7.0 cm.

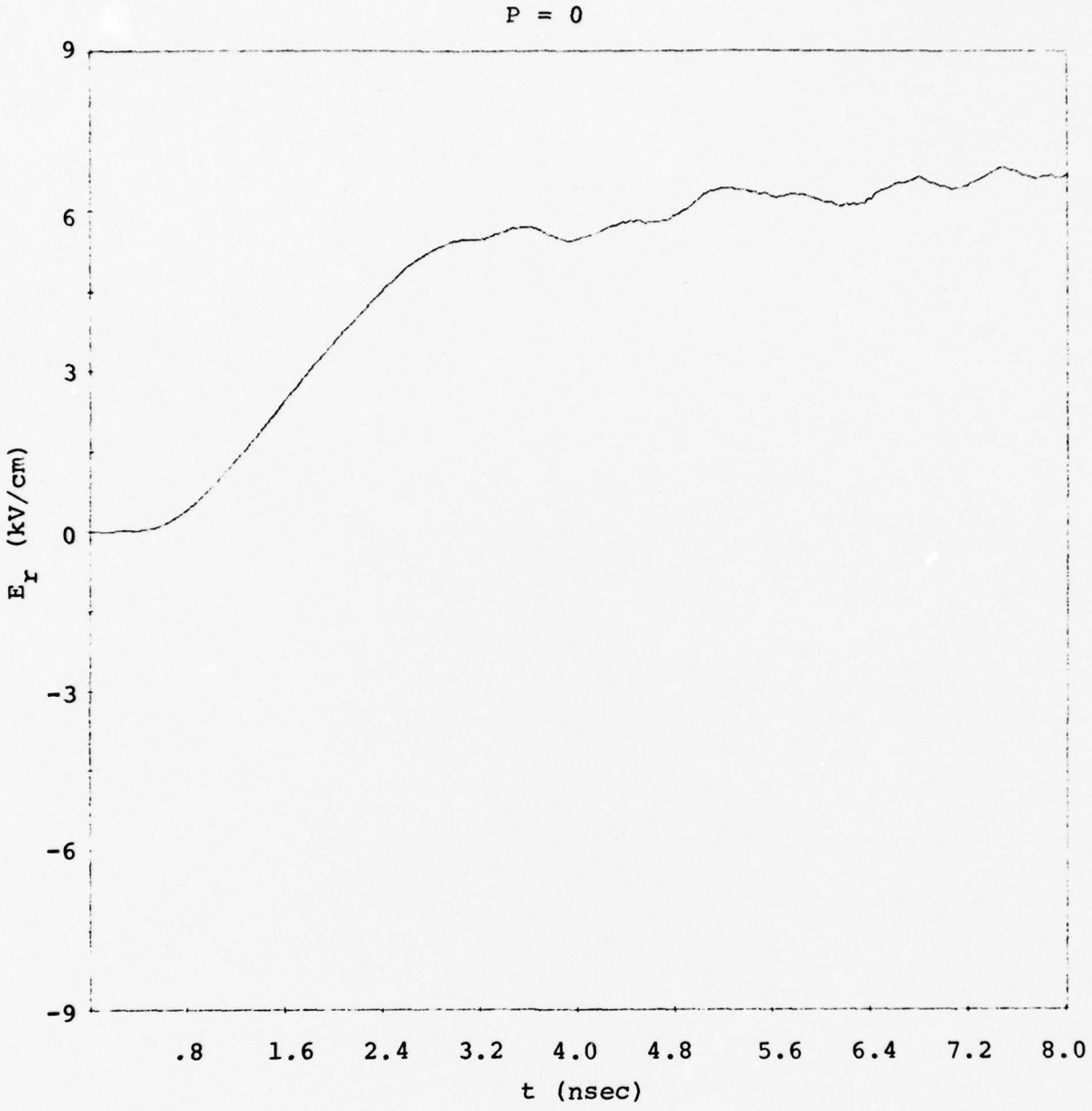


Figure 15. Radial electric field at r = 14 cm, z = 7.25 cm.

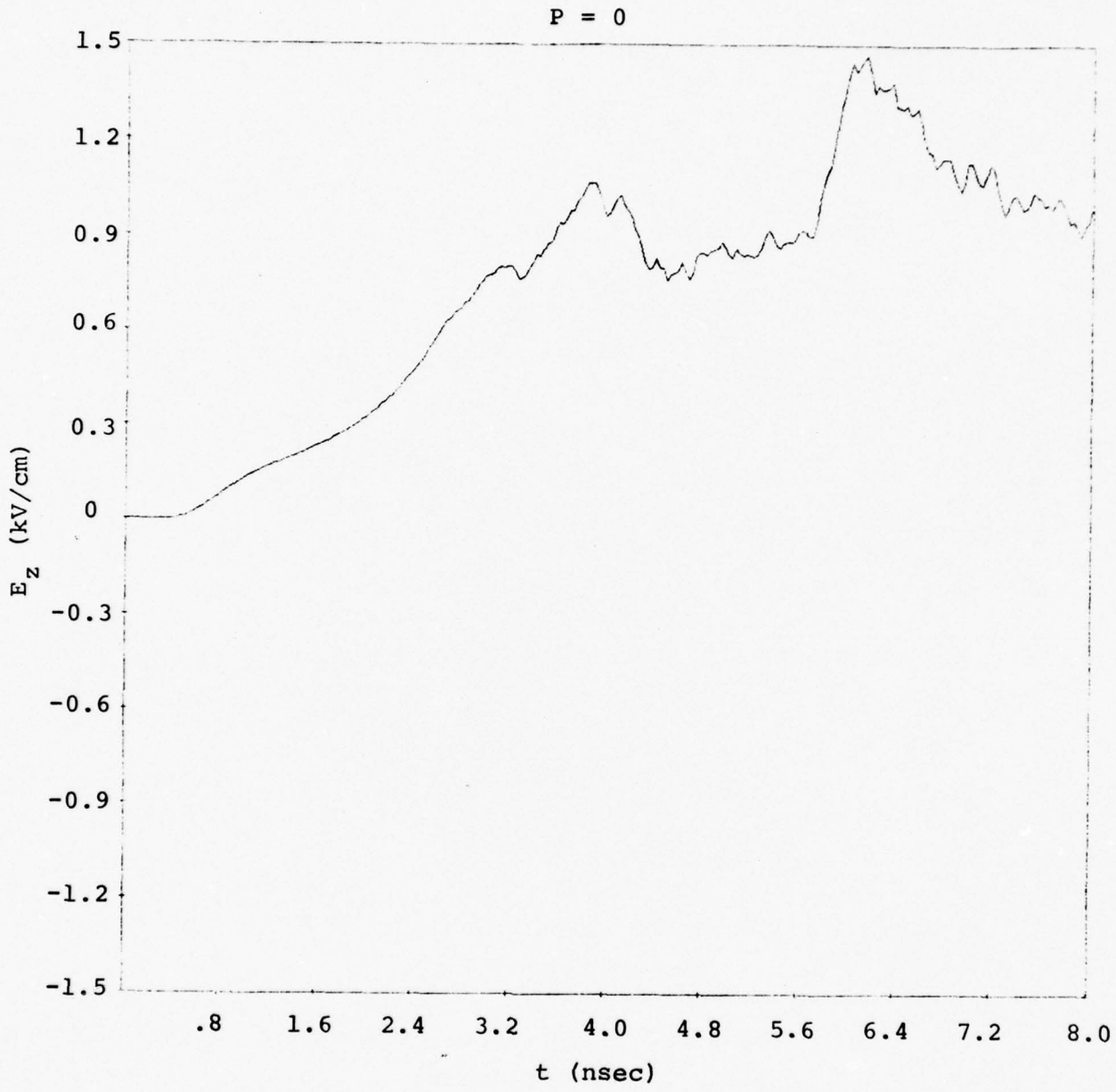


Figure 16. Axial electric field at r = 14.5 cm, z = 7.0 cm.

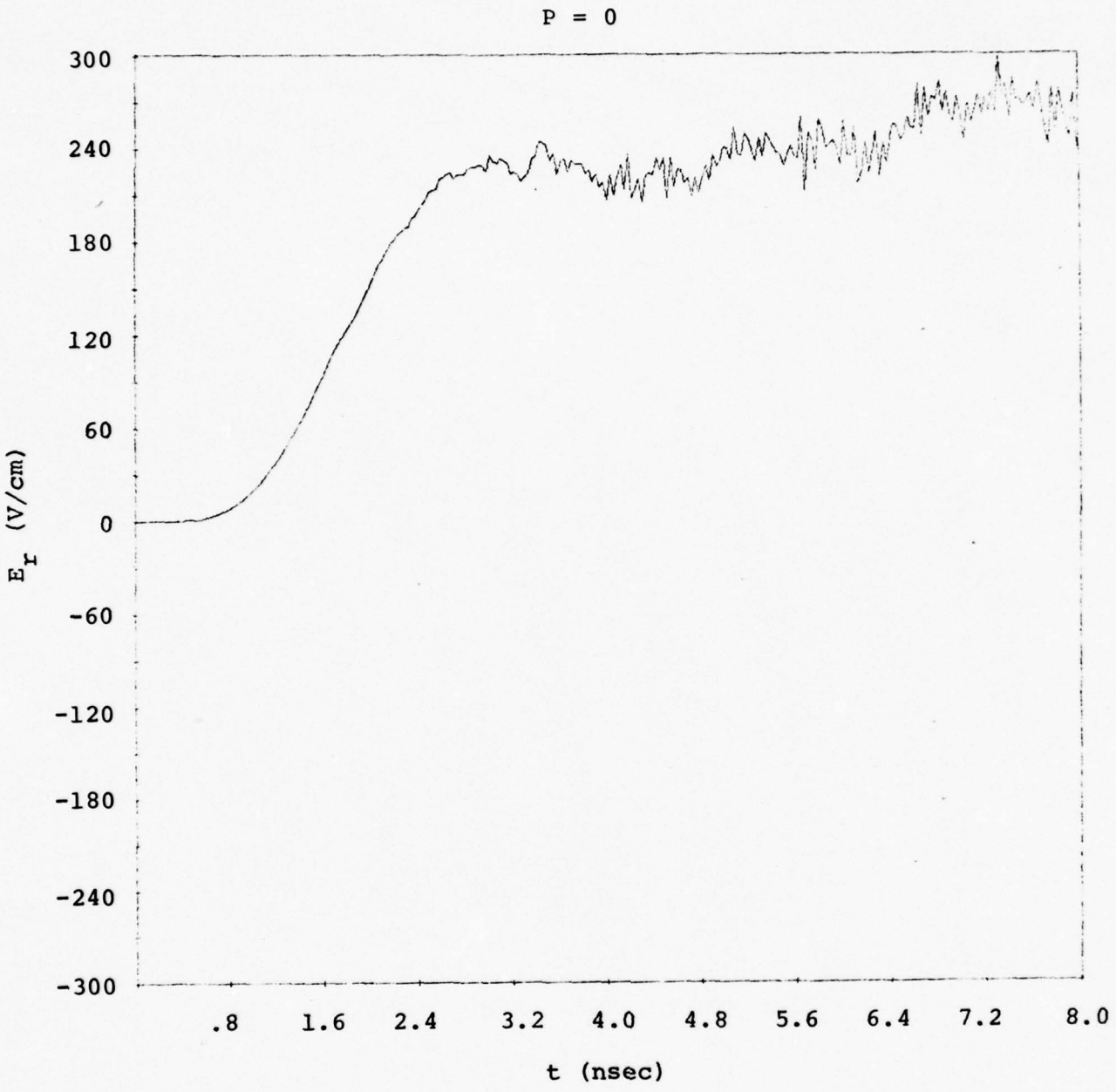


Figure 17. Radial electric field at r = 14 cm, z = 14.75 cm.

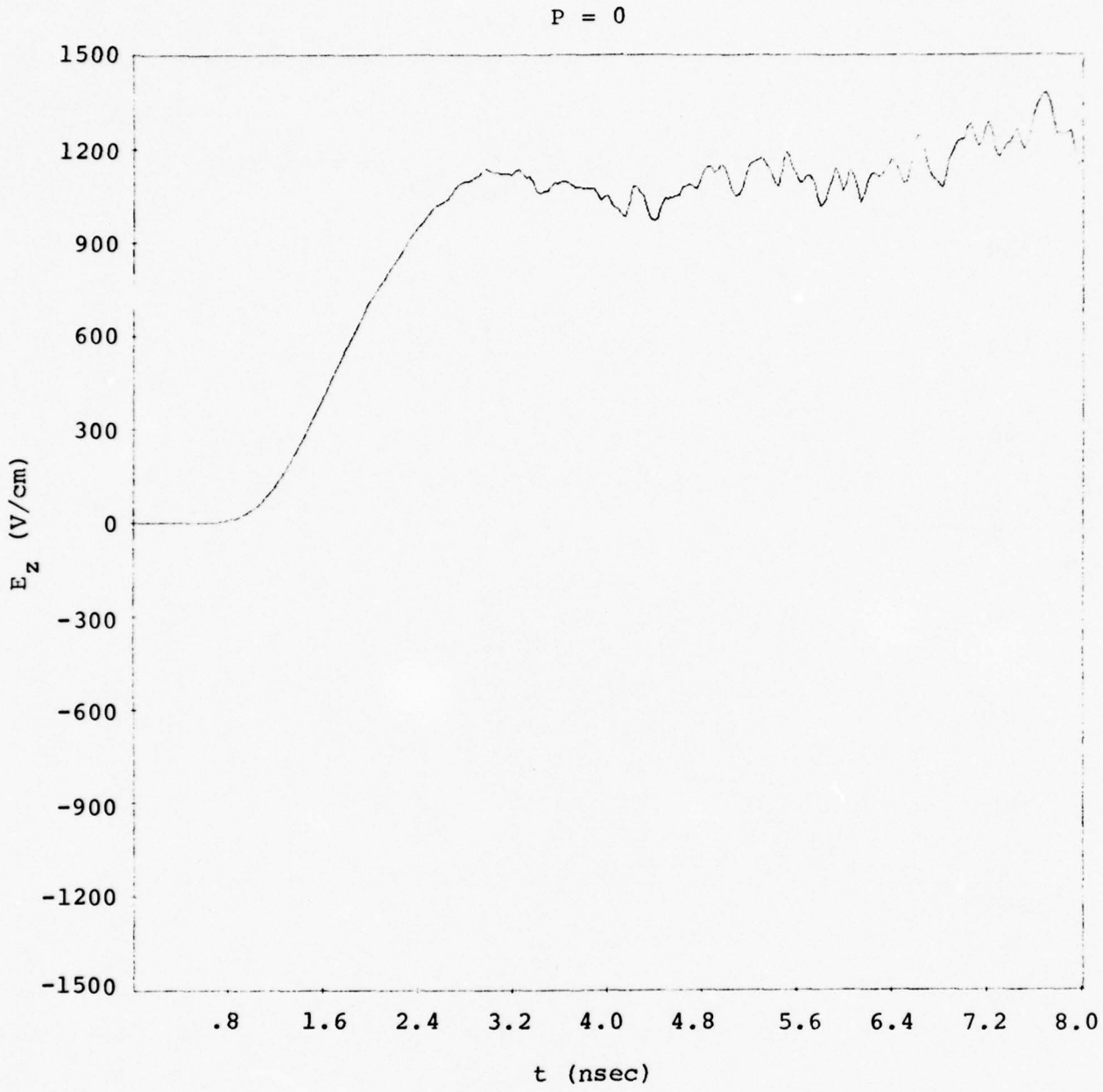


Figure 18. Axial electric field at r = 14.5 cm, z = 14.5 cm.

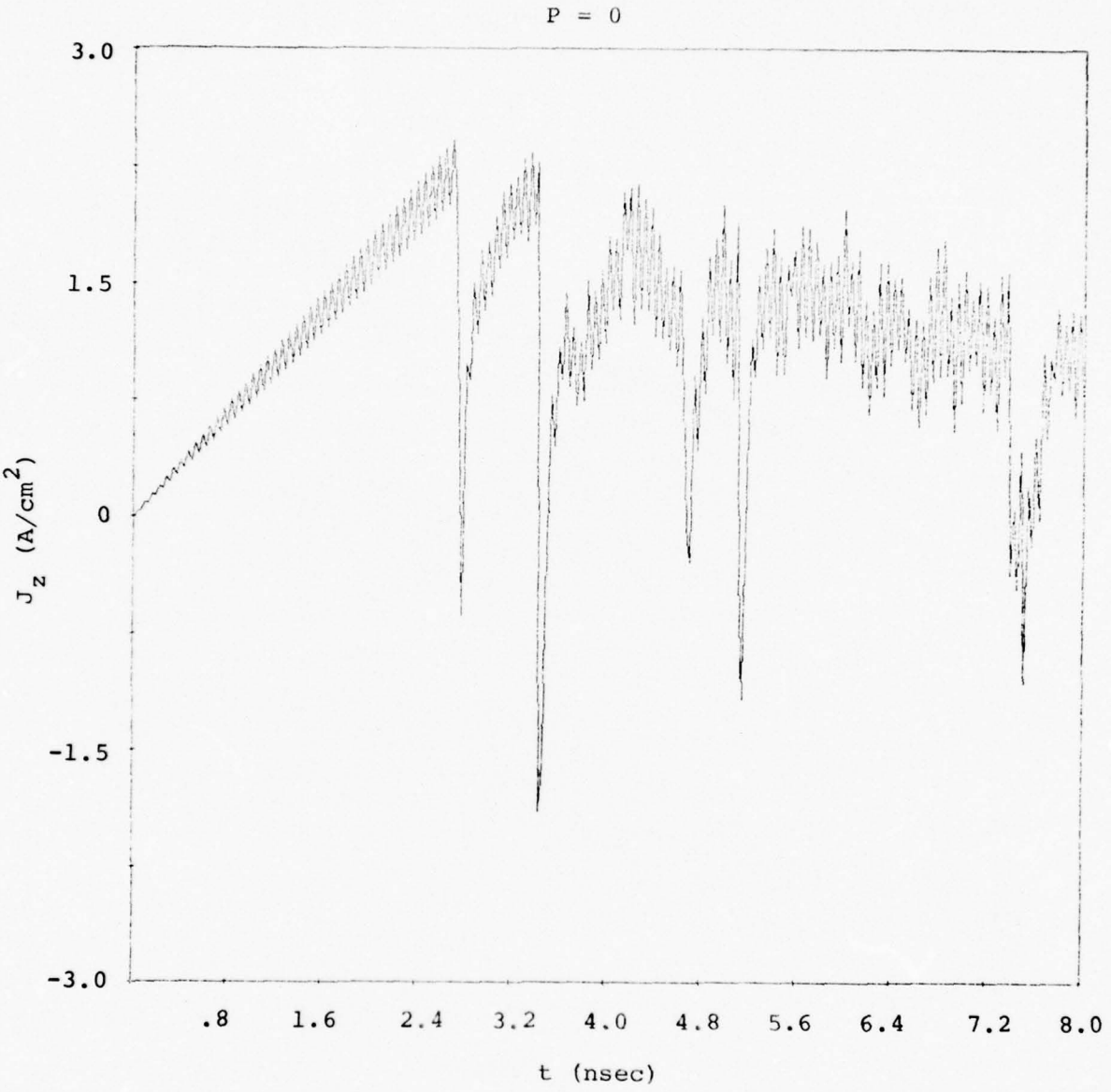


Figure 19. Net electron current density on emitting surface at r = 0.5 cm.

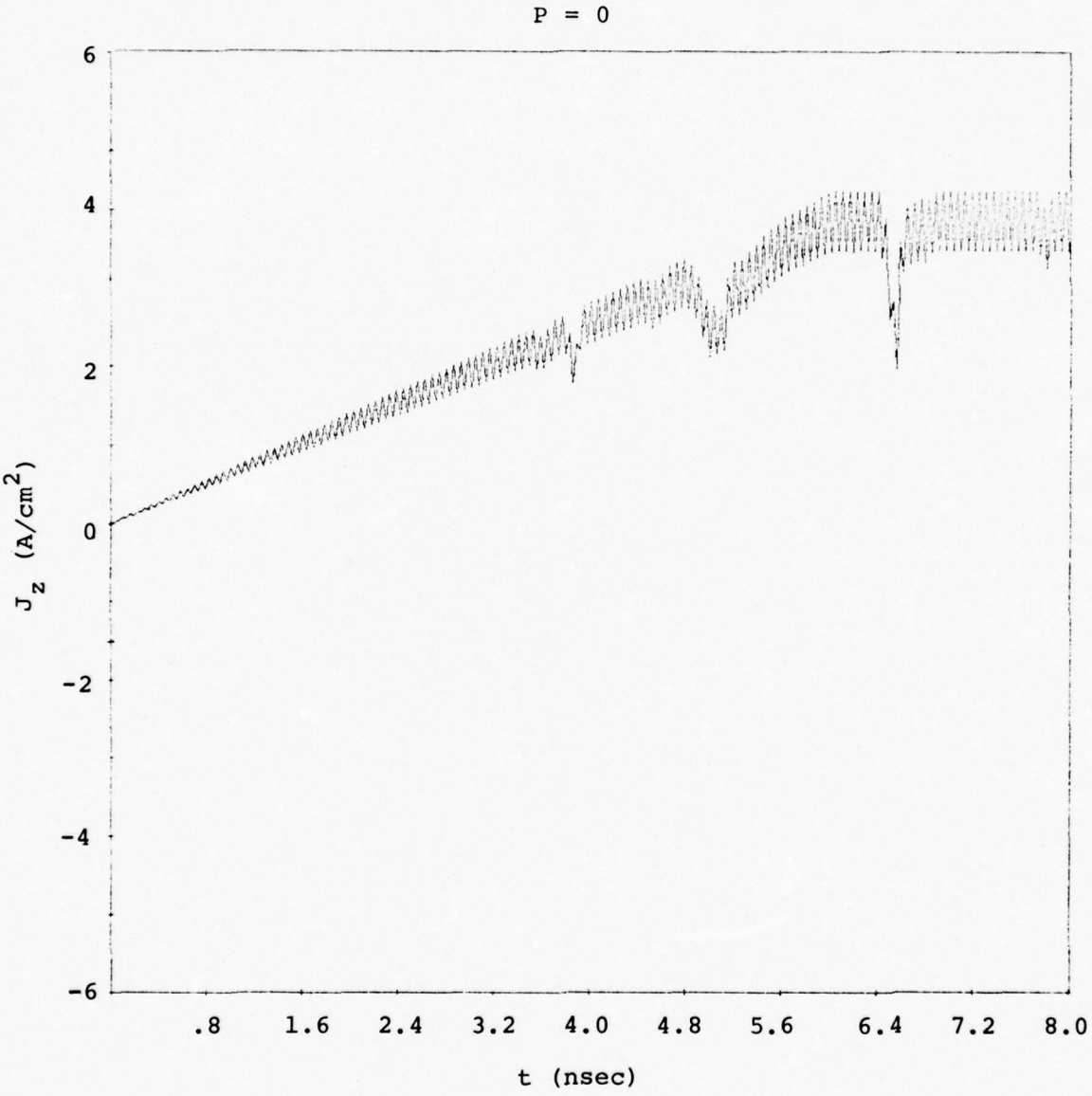


Figure 20. Net electron current on emitting surface at r = 14.5 cm.

this estimate is the neglect of the 2-D effect of radial blowup.

Figures 19 and 20 show the net axial electron current on the emitting surface $z = 0$ at the positions $r = 0.5$ cm, $r = 14.5$ cm, respectively. In the former case, the current grows linearly until current limiting sets in. In the latter case, the current is not limited on account of 2-D effects; namely, smaller axial fields close to the curved edge of the tank at $r = R$. In both cases, the sharp jumps in the current result from the return of a discrete energy group. With the lack of angular spread in the emission, these groups are quite obvious. They would not show up in more realistic emission data. The high frequency oscillations in the current responses result from particle fluctuations. Particles are emitted only every other cycle and this gives rise to the very high frequency noise. It is removed entirely by emitting every cycle. In this calculation, a maximum of 6000 particles was permitted.

The initial rise of the magnetic field (Figures 10, 14) is due to the displacement current, not the electron current. After limiting has set in, the magnetic field shows some oscillatory behavior. This results from cavity mode oscillations. They are relatively weak because the dimensions of the cavity are small compared with $ct_R$ so that the response is basically quasi-static.

P = 0.05 torr.

A series of graphical plots which is similar to the $P = 0$ case is presented here (Figures 21-28). As before, limiting begins at about $t = 3$ nsec. However, it is much less severe as the particle plots show. The space charge barrier is partially neutralized and transmission across the cavity is more complete. Time histories of electric and magnetic fields are shown in Figures 29-39.

According to the estimate given in Section 2, neutralization should not be complete by the end of the problem (8 nsecs) since $t_N \sim 19$ nsecs at this pressure. This result is borne out by the results obtained.

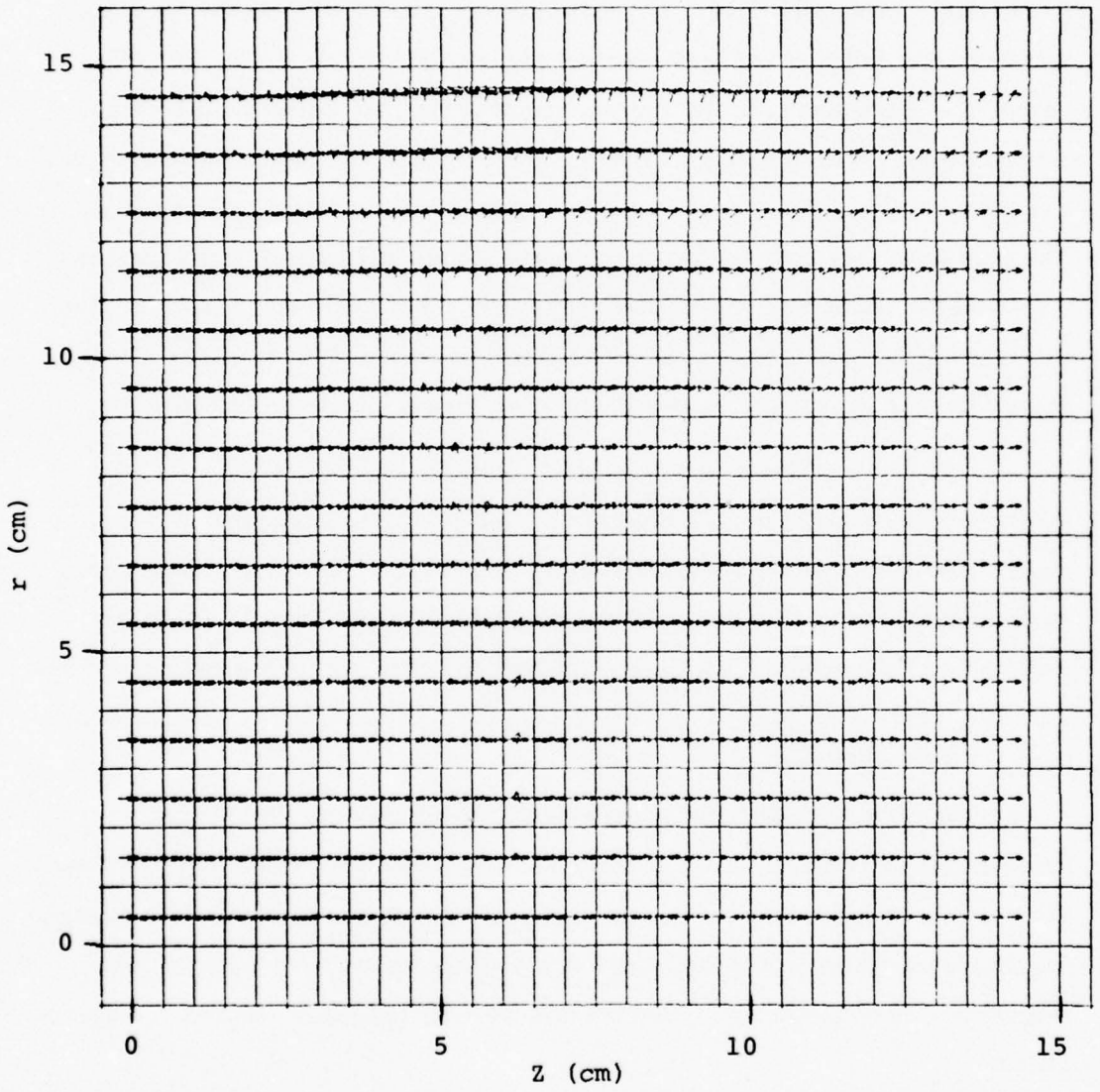


Figure 21. Particle positions at t = 1 nsec, P = 50 mtorr.

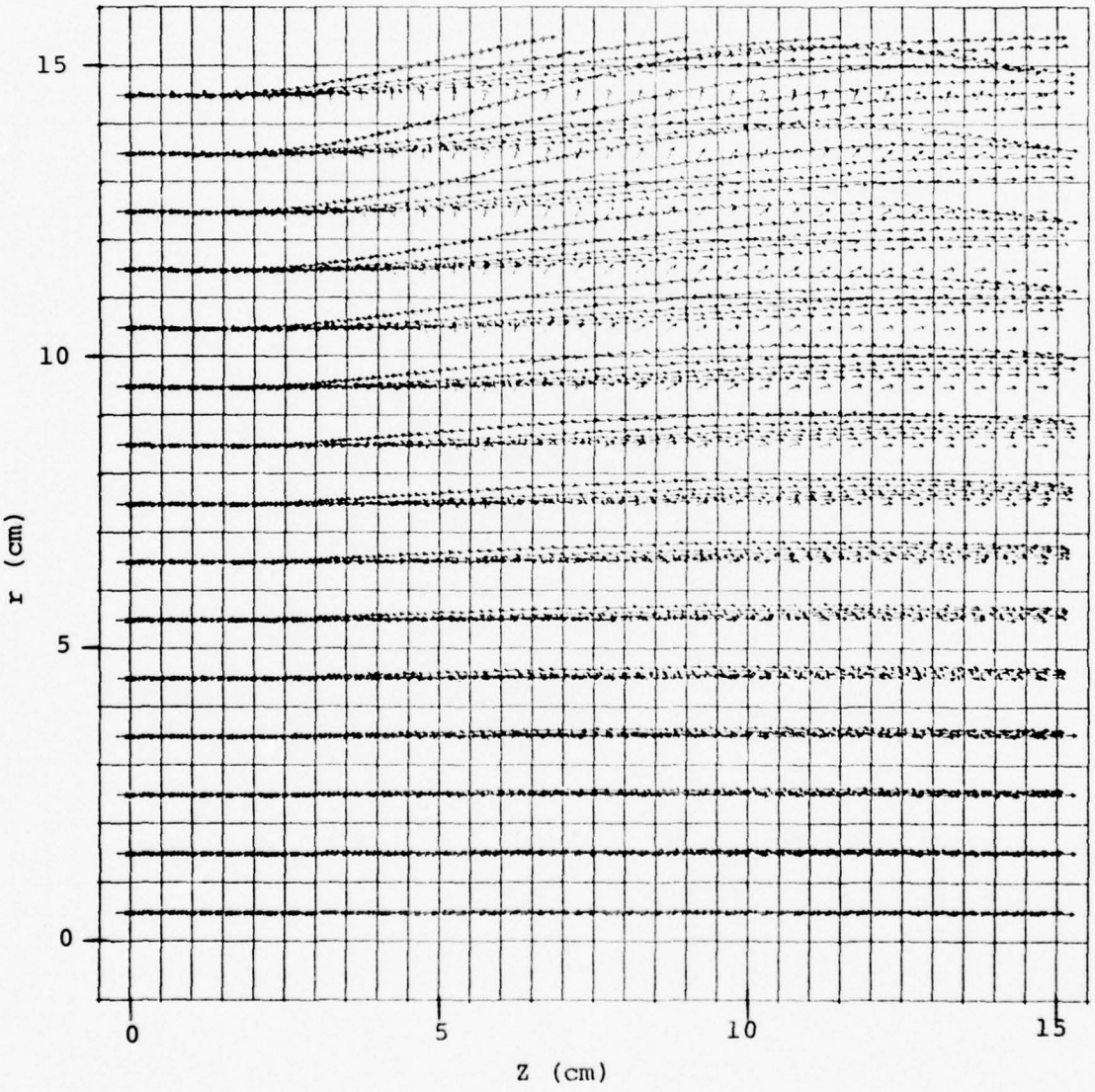


Figure 22. Particle positions at t = 2 nsec, P = 50 mtorr.

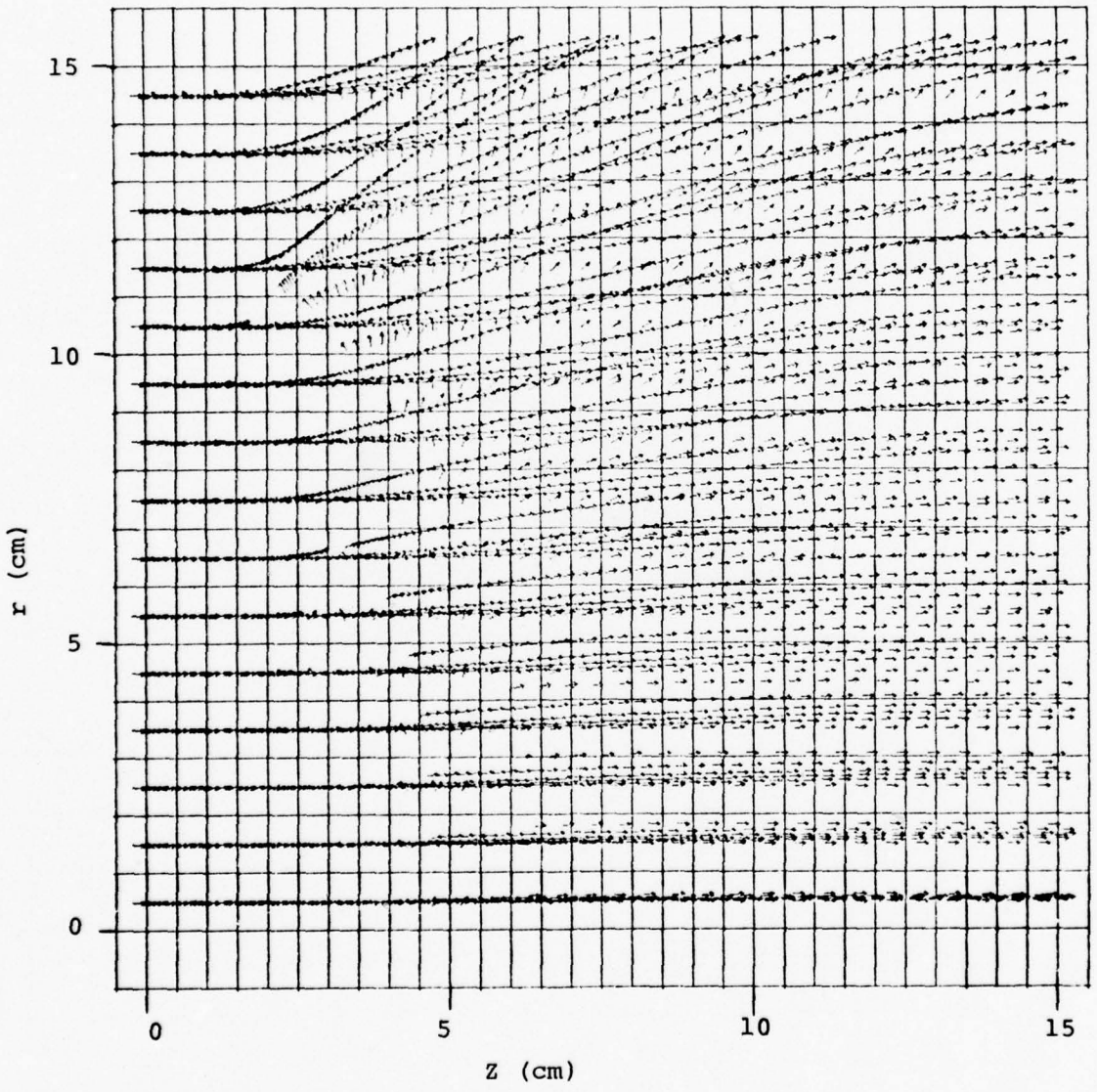


Figure 23. Particle positions at t = 3 nsec, P = 50 mtorr.

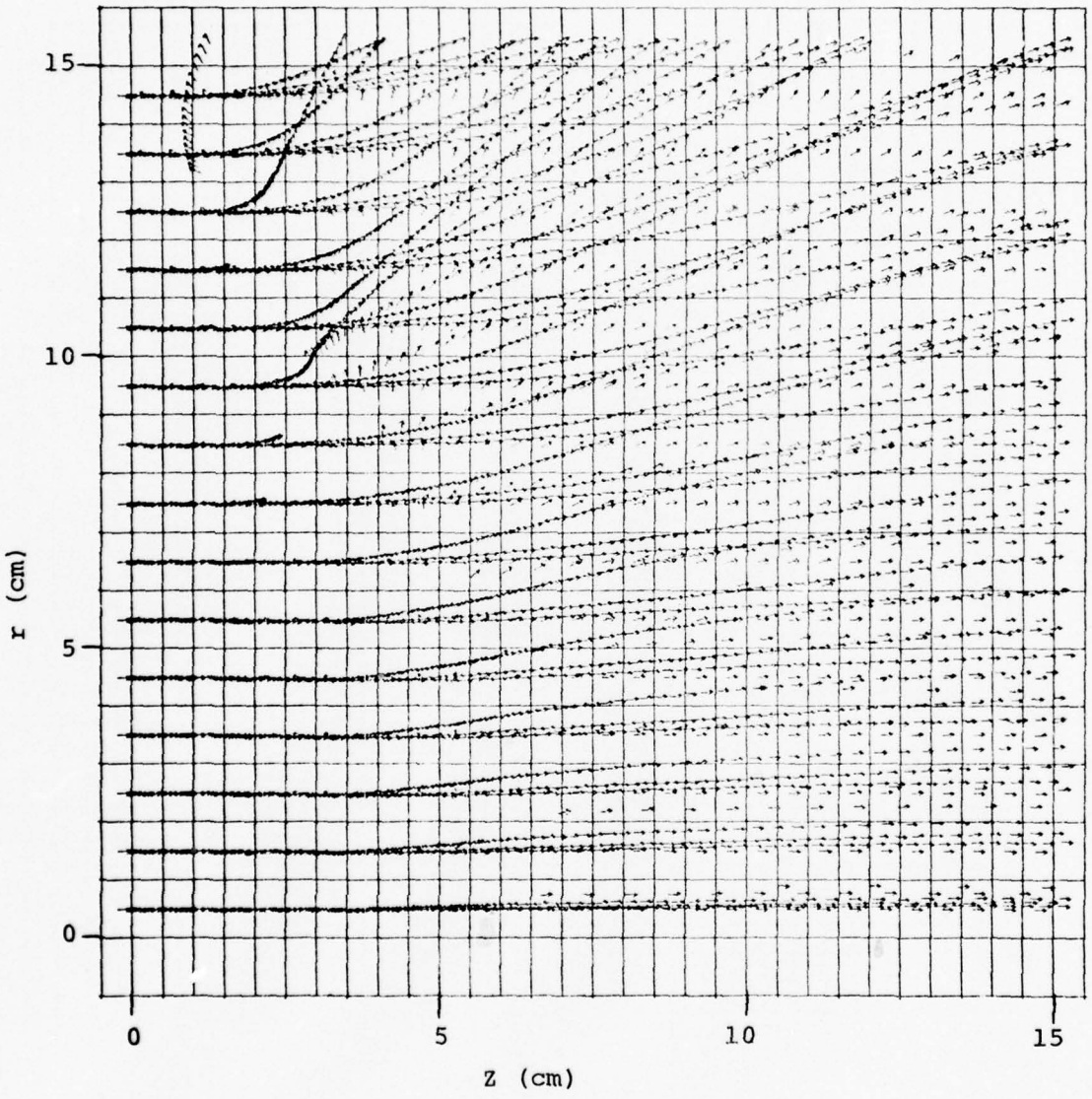


Figure 24. Particle positions at t = 4 nsec, P = 50 mtorr.

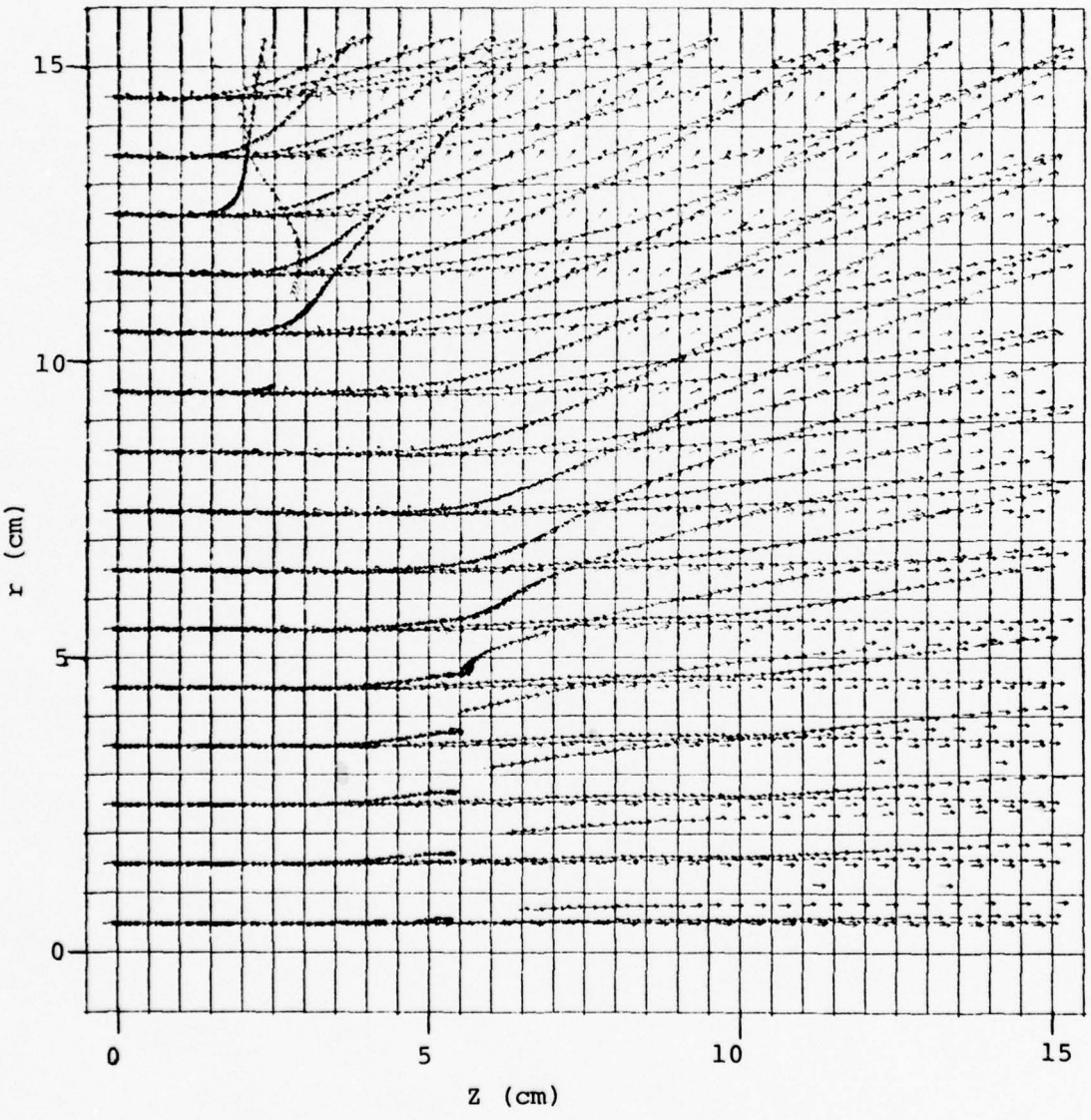


Figure 25. Particle positions at t = 5 nsec, P = 50 mtorr.

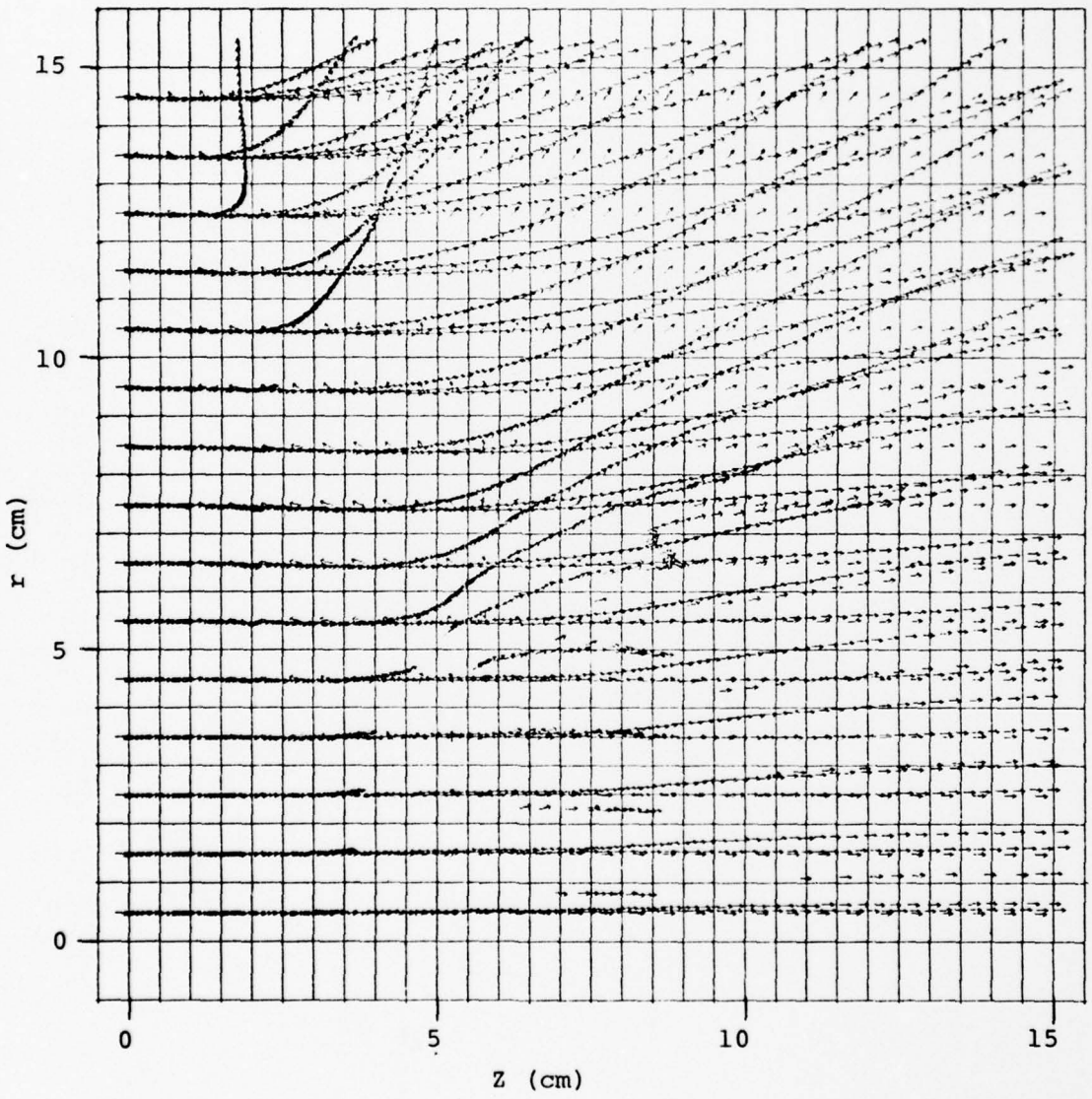


Figure 26. Particle positions at t = 6 nsec, P = 50 mtorr.

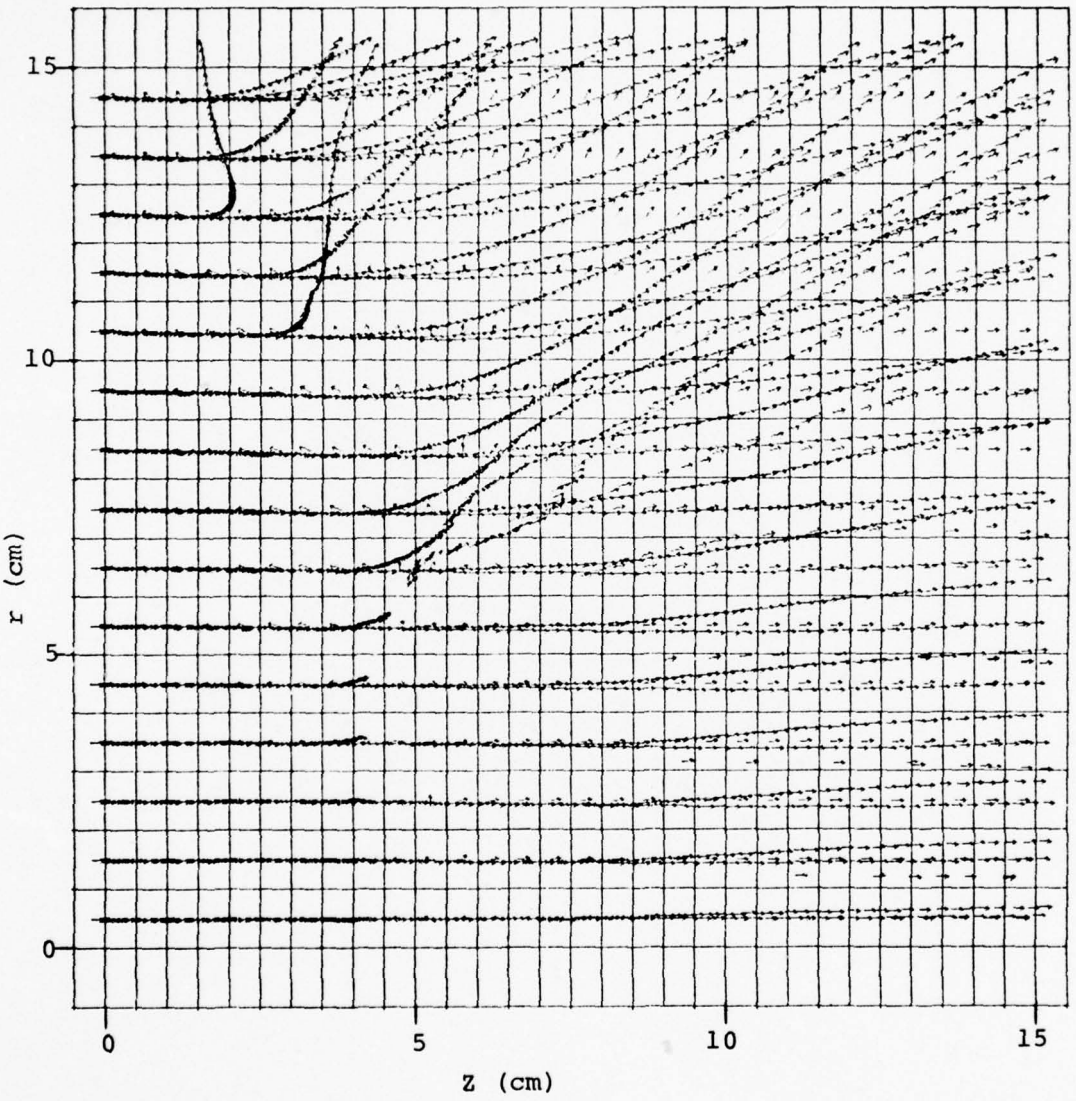


Figure 27. Particle positions at t = 7 nsec, P = 50 mtorr.

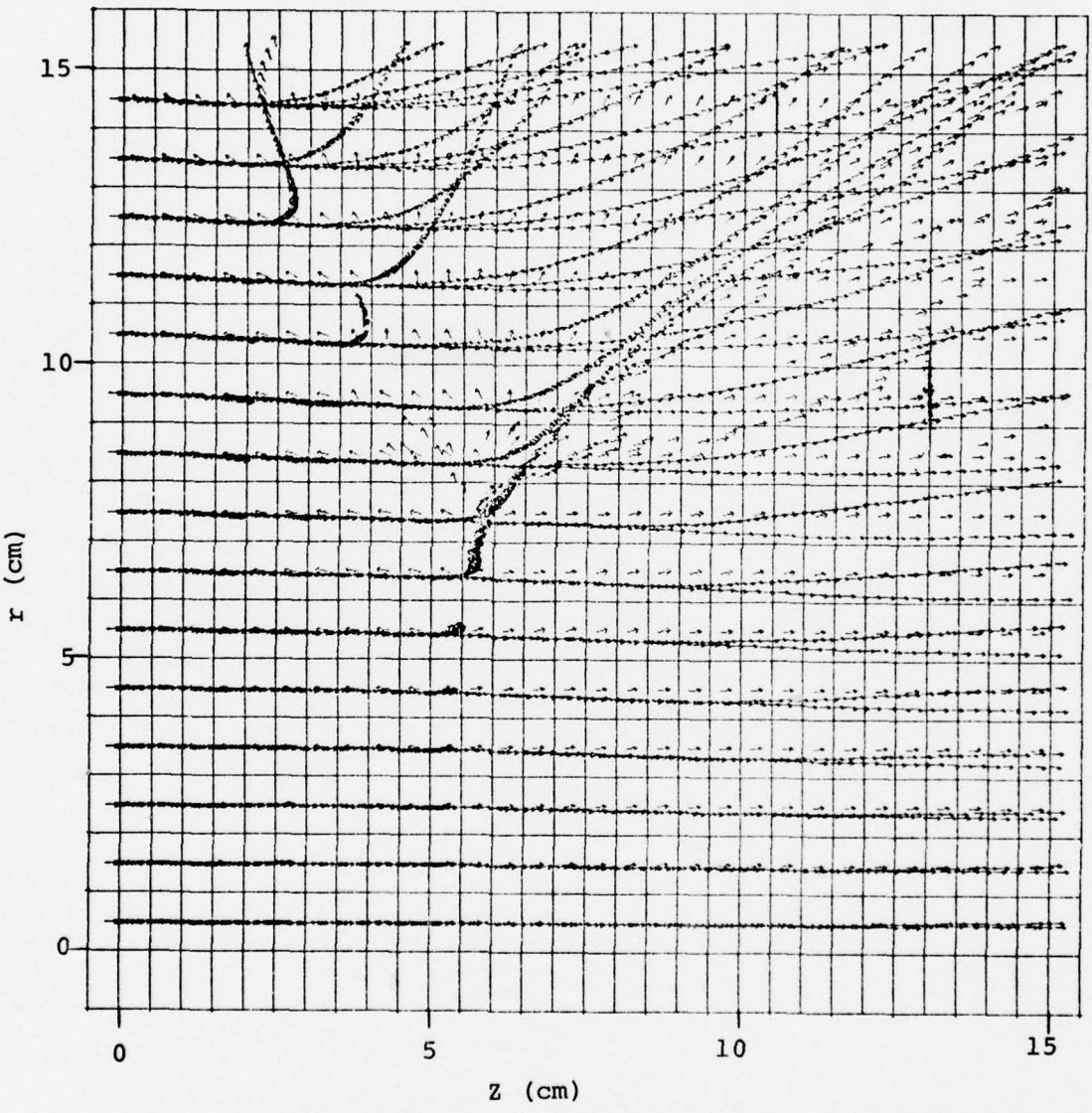


Figure 28. Particle positions at t = 8 nsec, P = 50 mtorr.

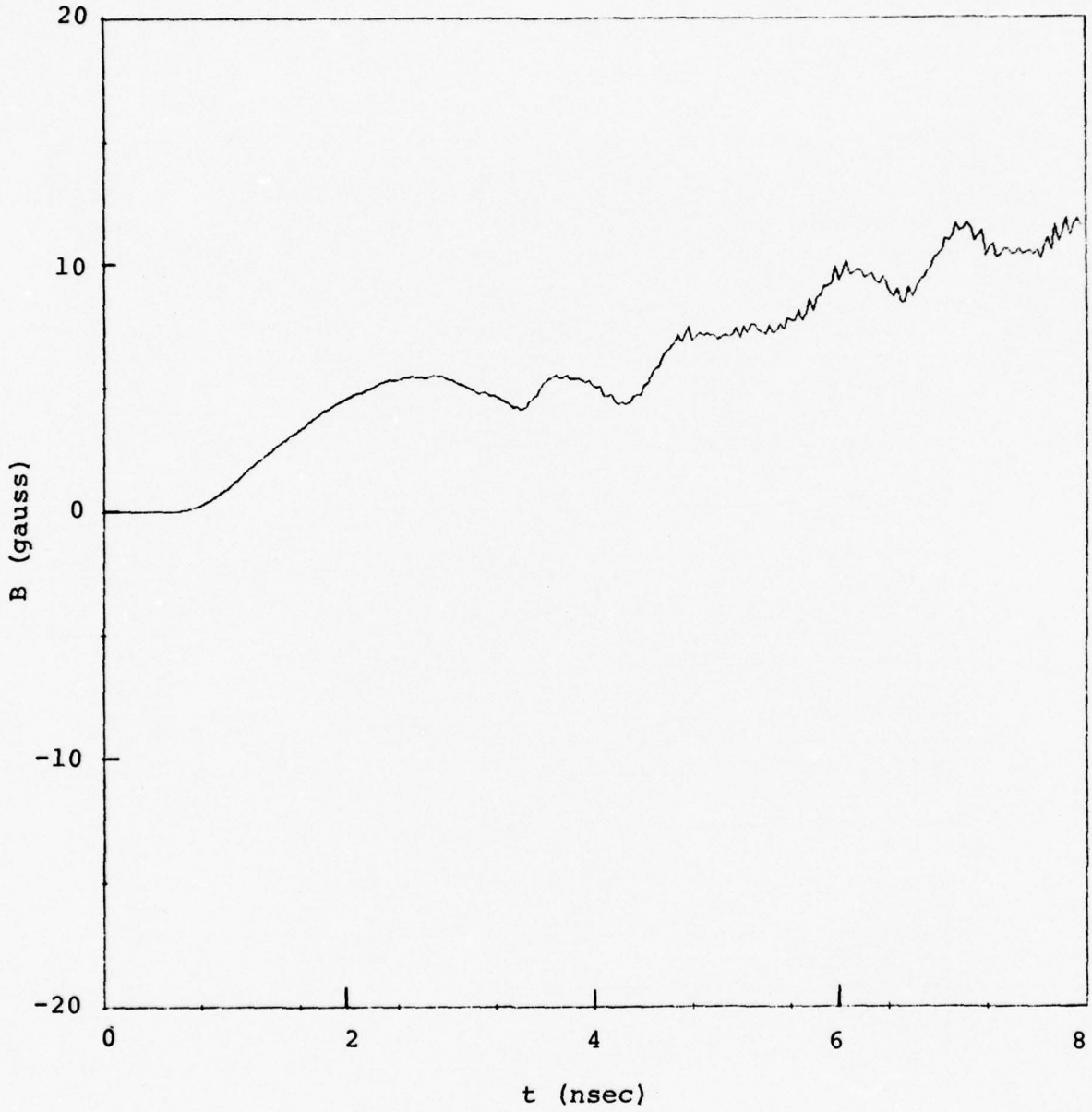


Figure 29. Magnetic field at r = 15 cm, z = 15 cm, P = 50 mtorr.

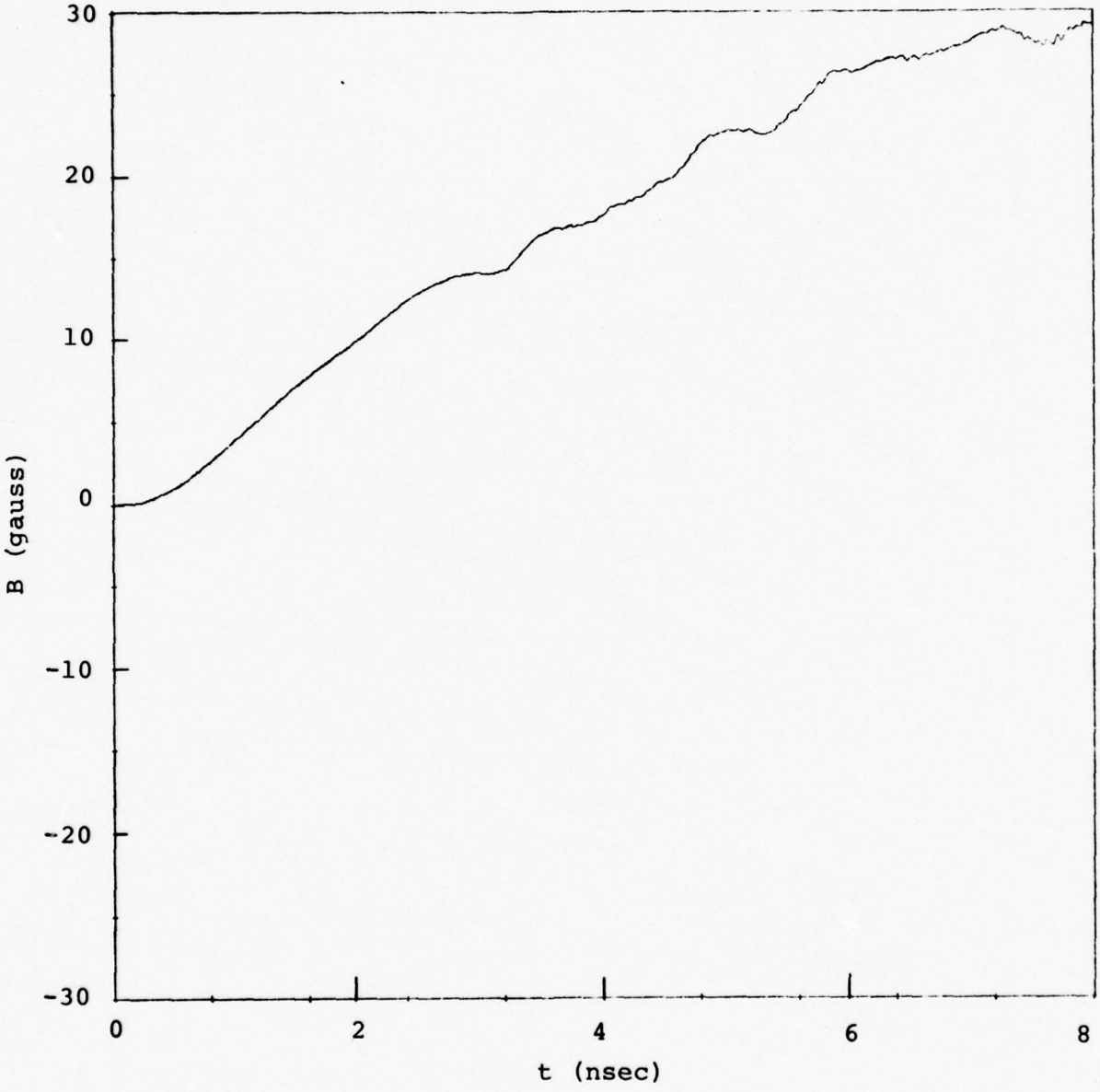


Figure 30. Magnetic field at r = 14 cm, z = 0 cm, P = 50 mtorr.

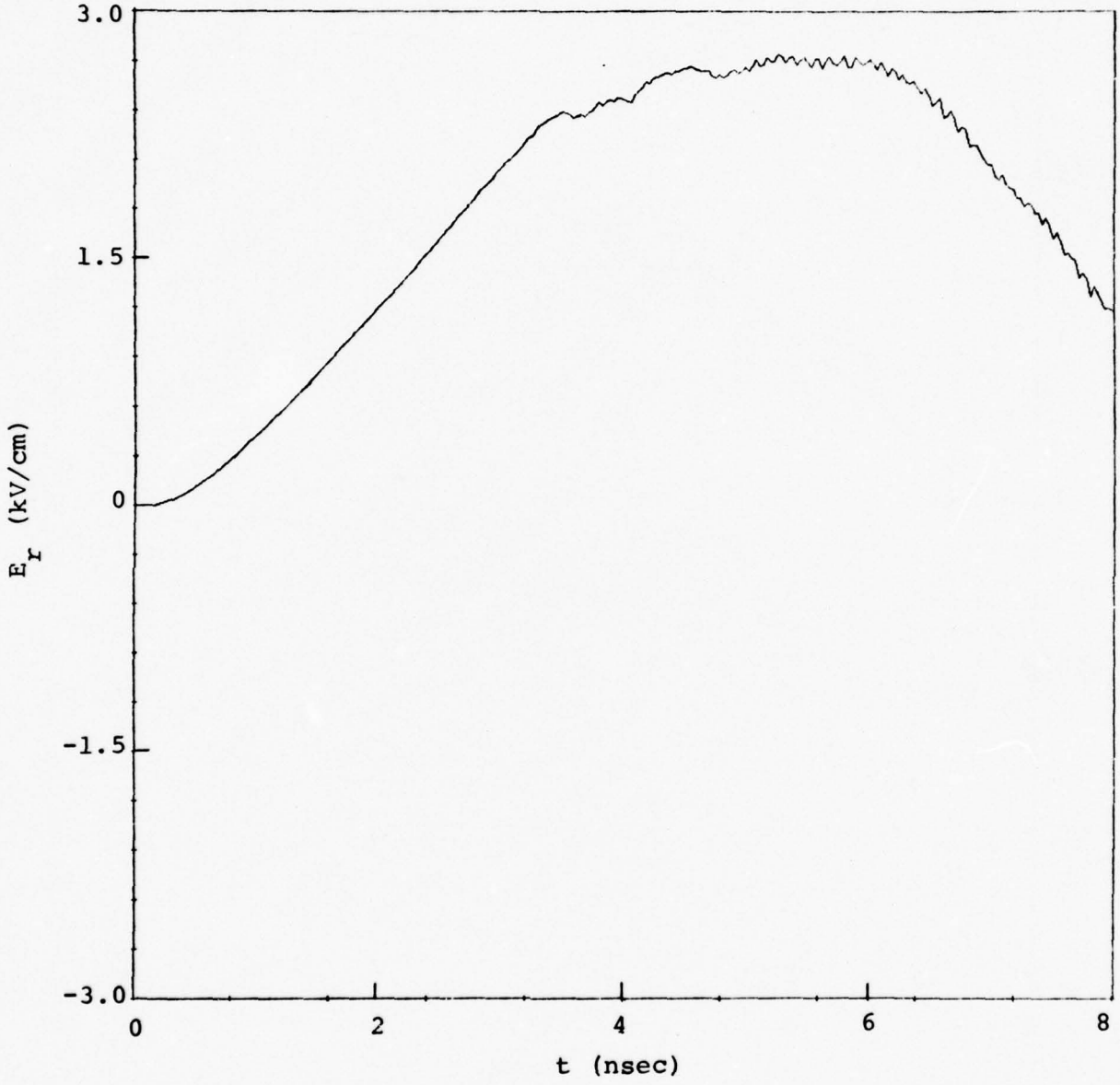


Figure 31. Radial electric field at r = 14.0 cm, z = 0.25 cm, P = 50 mtorr.

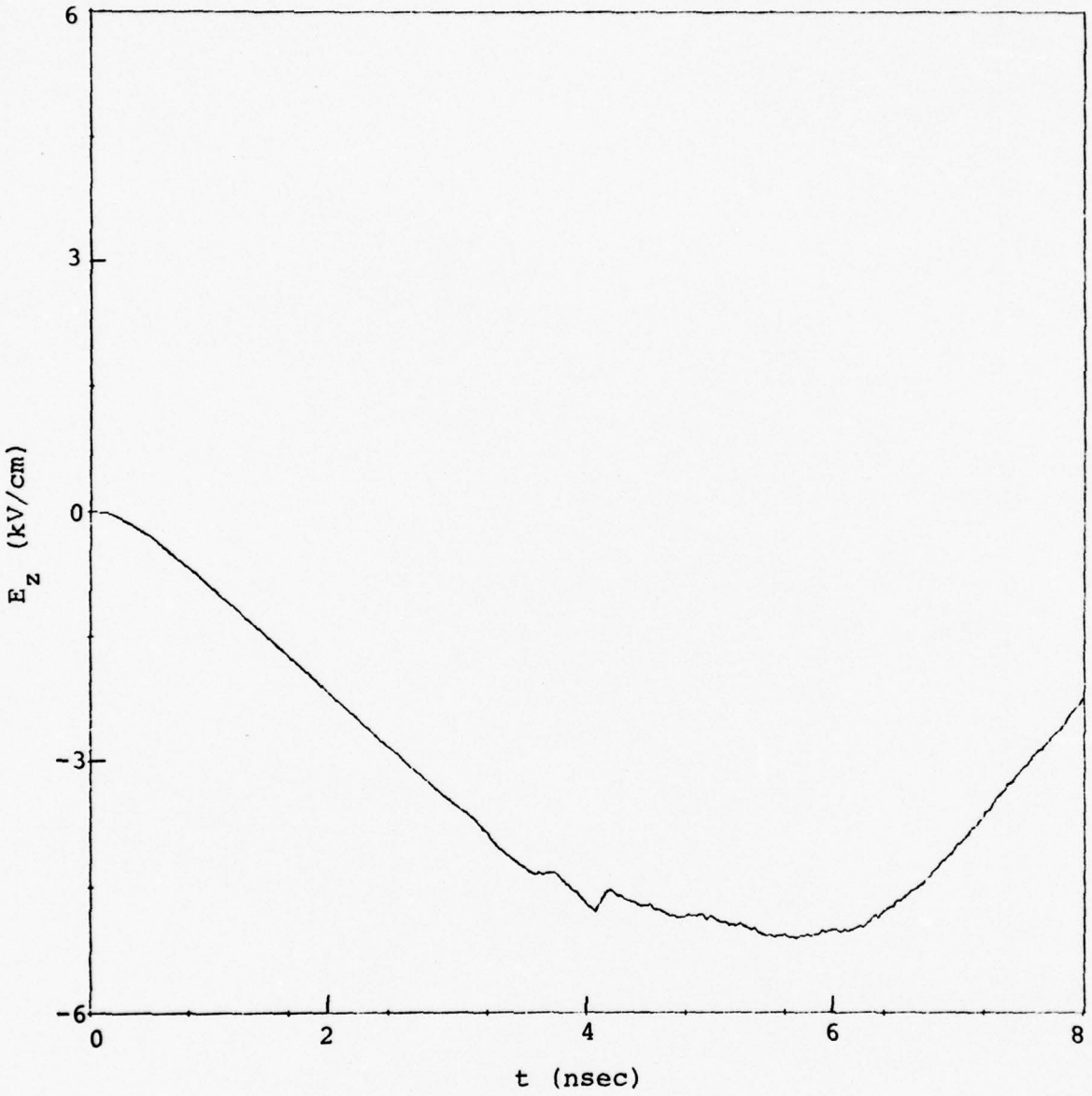


Figure 32. Axial electric field at r = 14.5 cm, z = 0 cm, P = 50 mtorr.

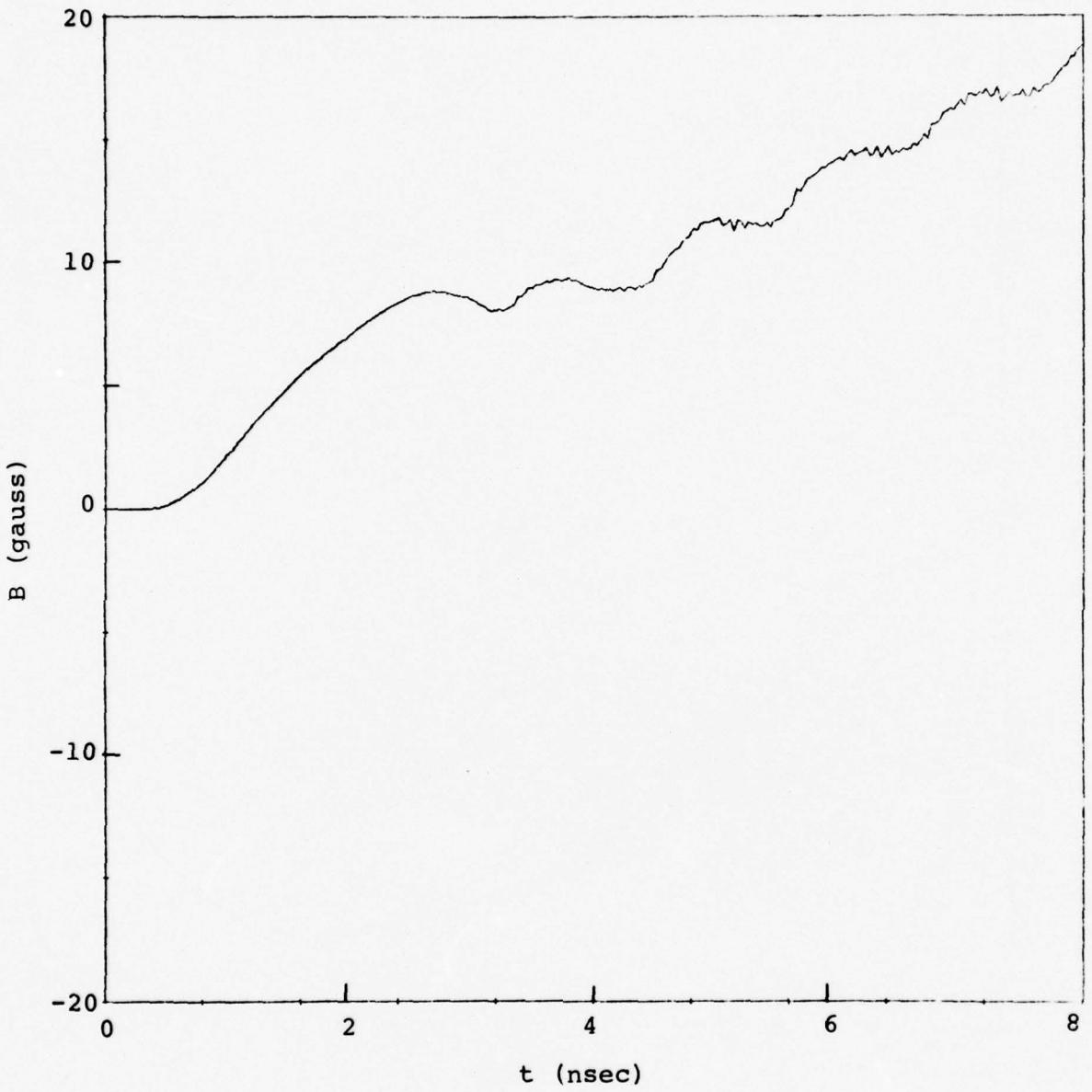


Figure 33. Magnetic field at r = 14 cm, z = 7 cm, P = 50 mtorr.

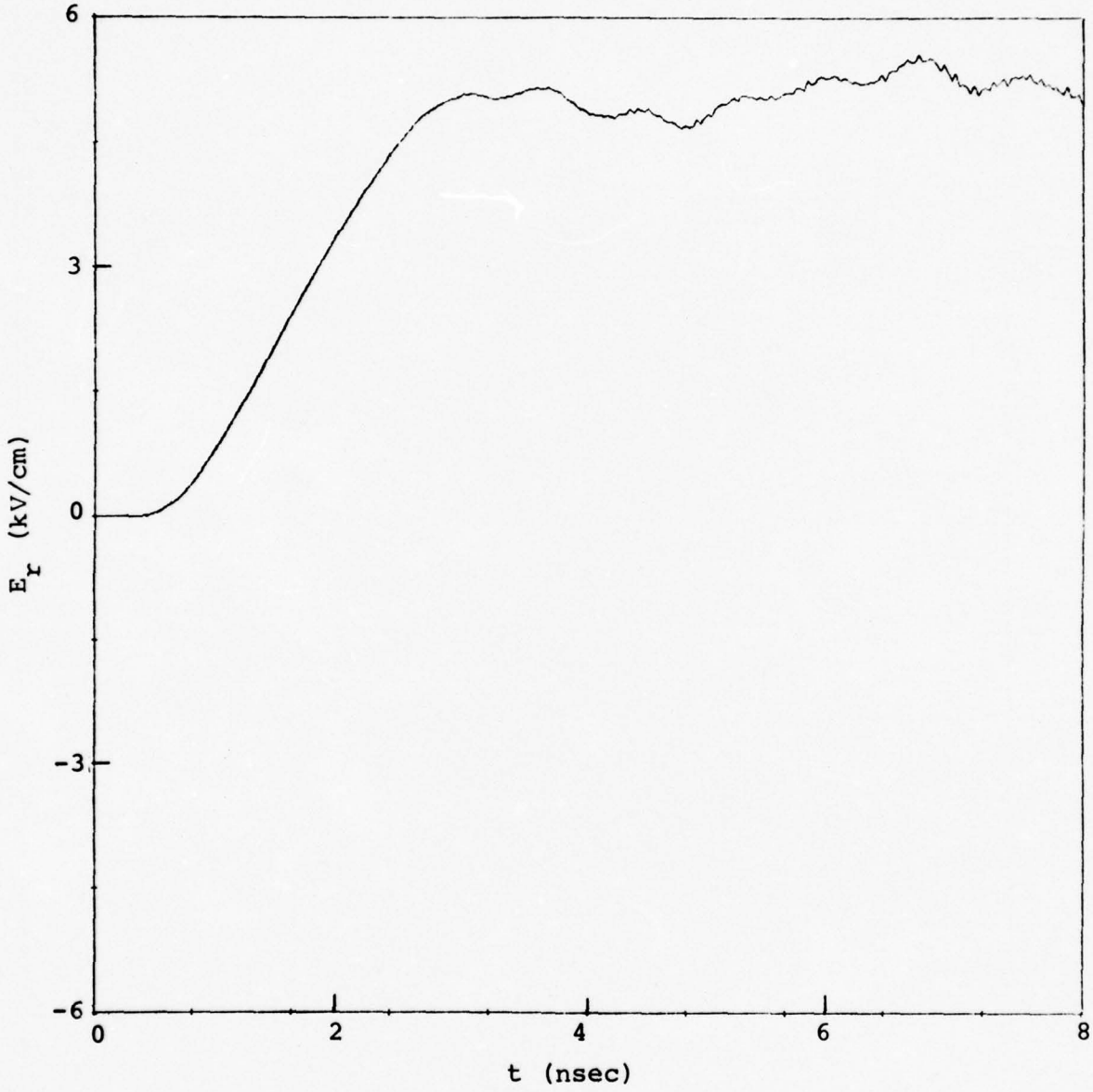


Figure 34. Radial electric field at r = 14 cm, z = 7.25 cm, P = 50 mtorr.

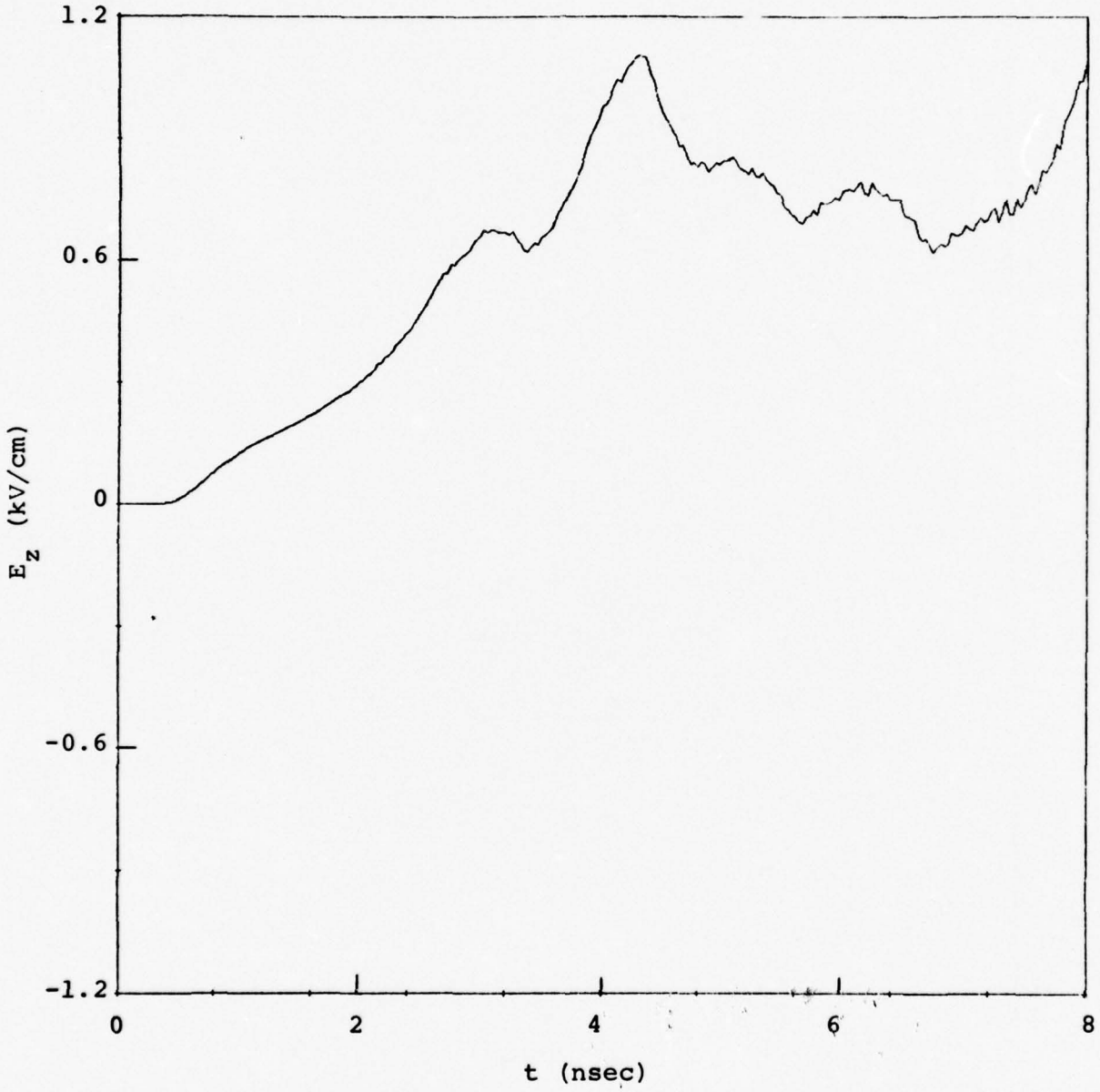


Figure 35. Axial electric field at r = 14.5 cm, z = 7.0 cm, P = 50 mtorr.

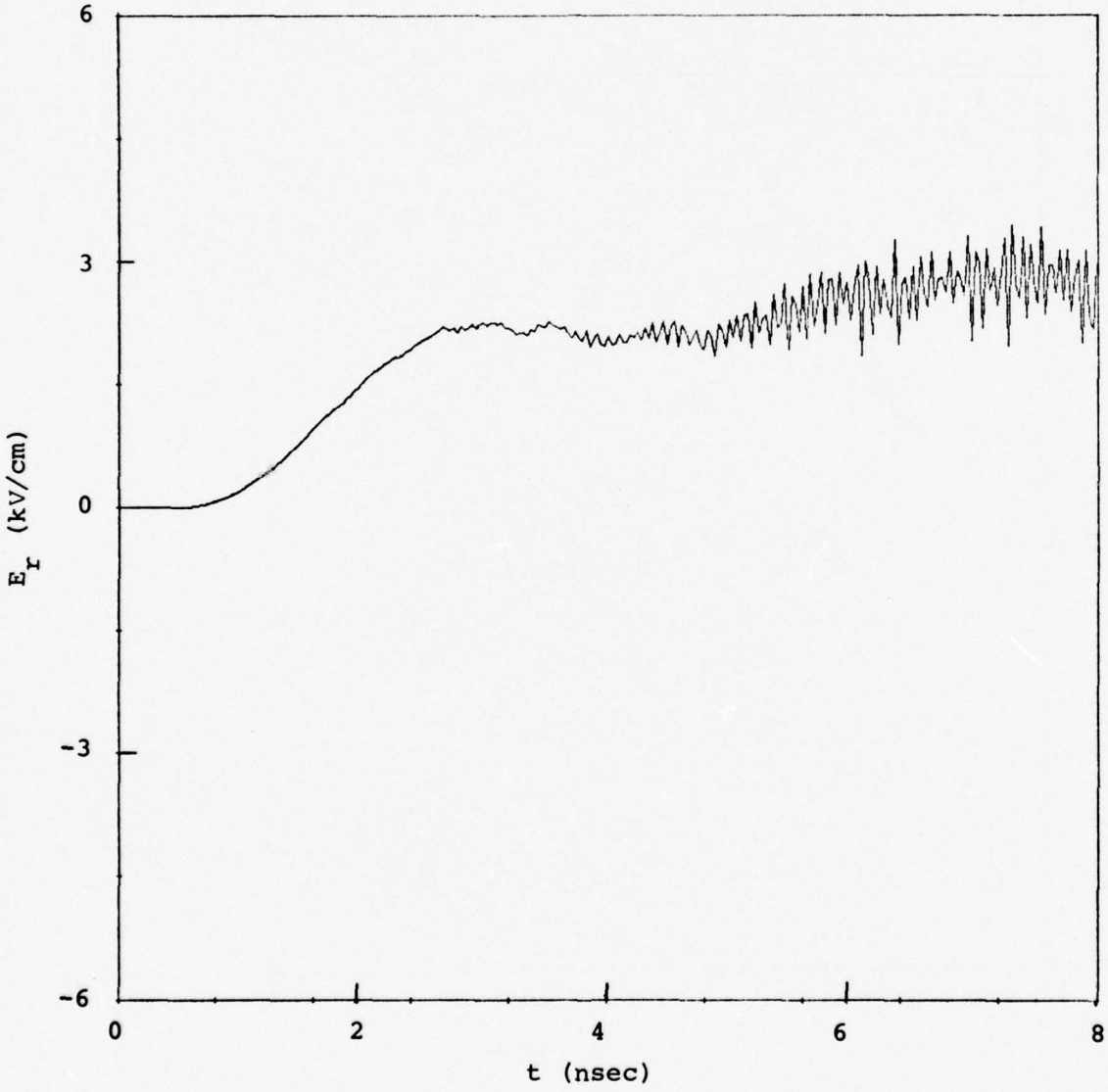


Figure 36. Radial electric field at r = 14 cm, z = 14.75 cm, P = 50 mtorr.

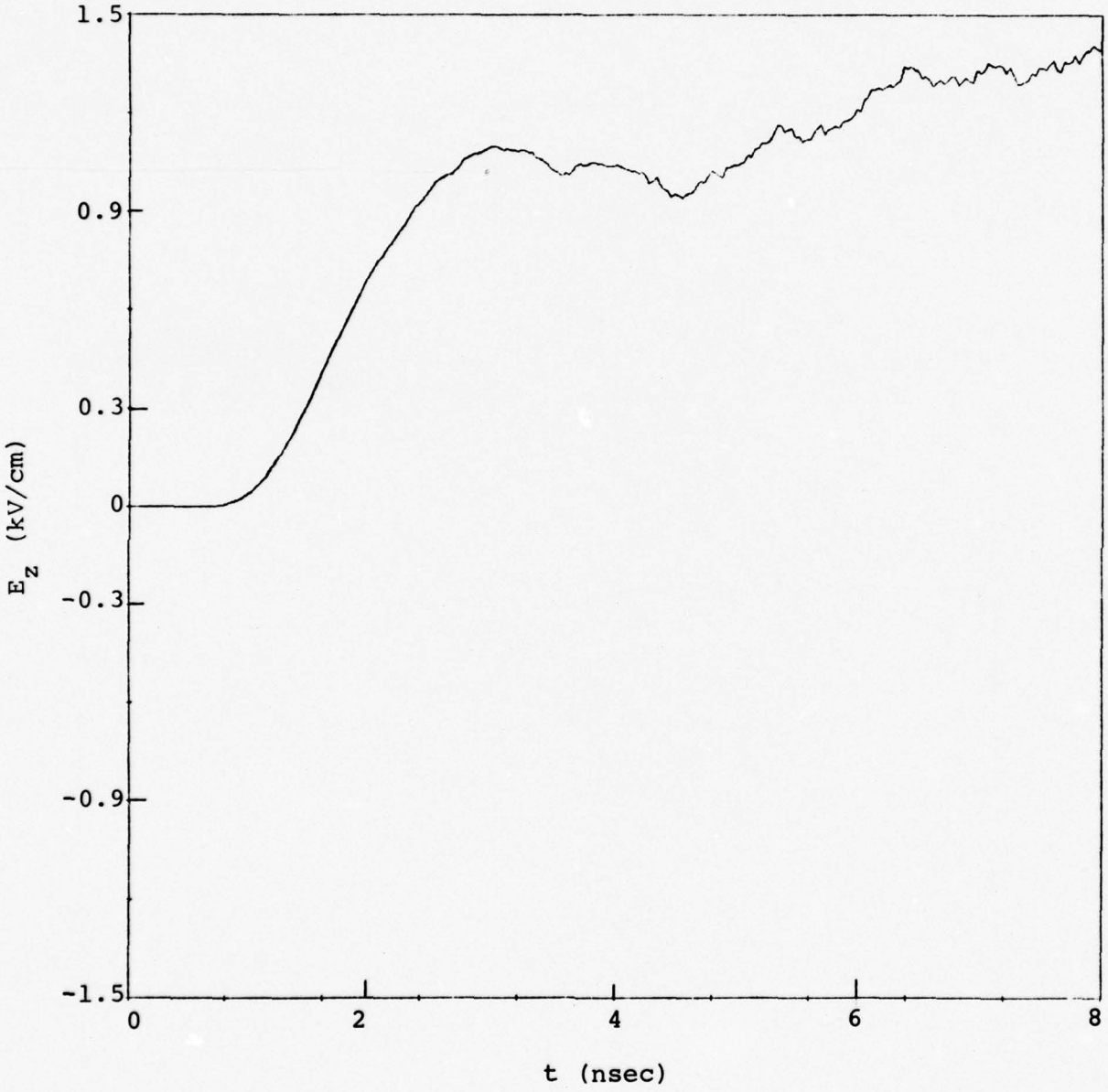


Figure 37. Axial electric field at r = 14.5 cm, z = 14.5 cm, P = 50 mtorr.

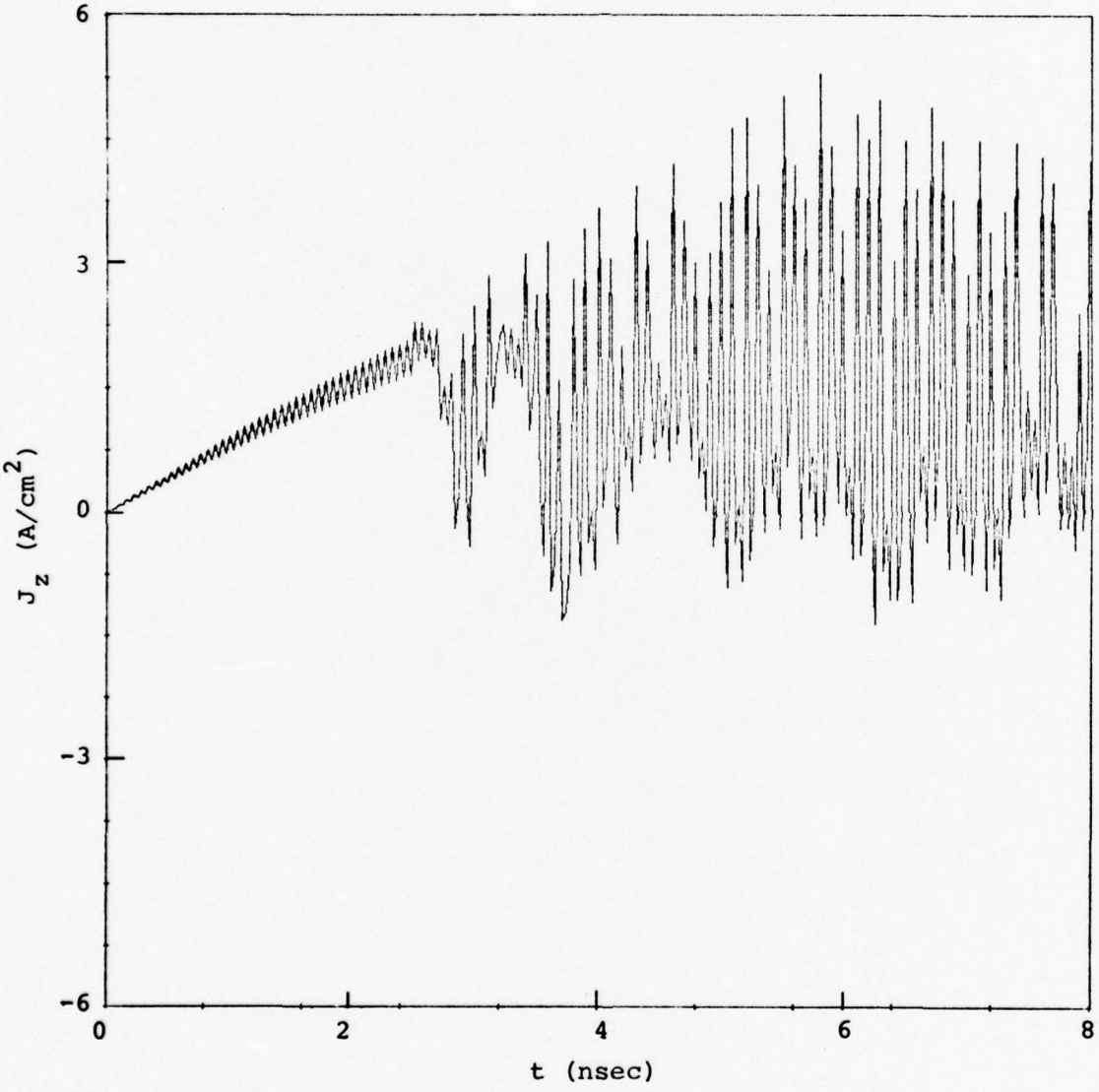


Figure 38. Axial electron current density on emitting surface at r = 0.5 cm, P = 50 mtorr.

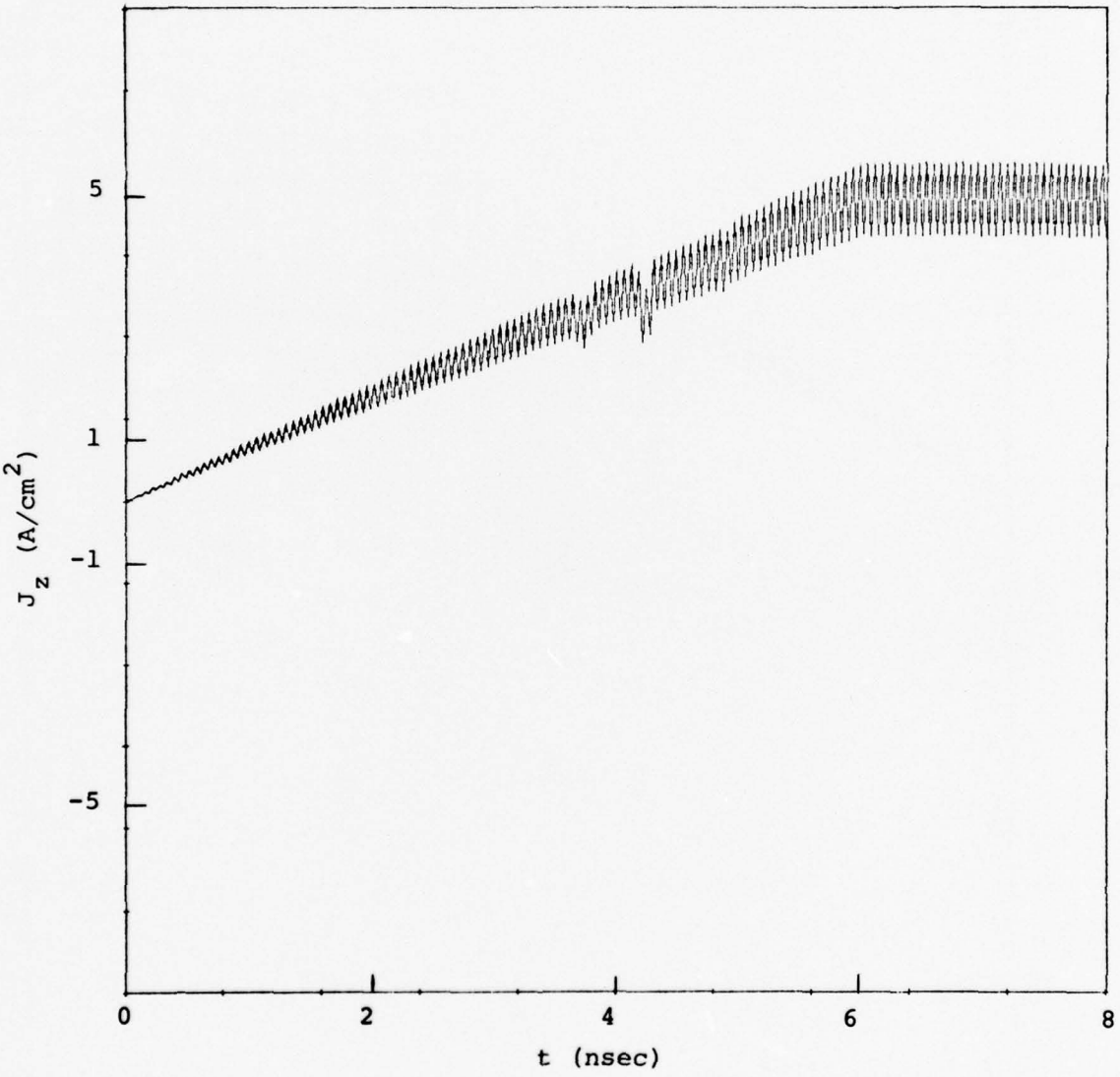


Figure 39. Axial electron current density on emitting surface at r = 14.5 cm, P = 50 mtorr.

The peak transmitted current is (see Figure 29)

$I = 5\ r\ B\ (\text{gauss})$ Amps

$\simeq 900$ Amps

or an average current density of approximately 1.3 $A/cm^2$. It is interesting to note that the current transmitted continues to increase after the time $t = 6$ nsec.

P = 0.2 torr.

This series of graphical plots (Figures 40-47) are similar in form to those of the preceding cases. As before, limiting is in evidence by 3 nsec. However, it is even less severe in this case. The position where turnaround occurs reaches forward toward the opposite face as the gas becomes increasingly ionized and large numbers of secondaries are driven away from regions of high potential to reduce the space-charge. Late in the problem a large number of secondaries, which now dominate, are subject to drift motion in the magnetic field as quasi-neutrality has been attained.

The total current transmitted (from Figure 48) reaches a large value by 6 nsec

$I = 75\ B$

$\simeq 2200$ Amperes

or an average current density of over 3 $A/cm^2$. This amounts to over half the injected current. The result appears to be consistent with those of the previous cases.

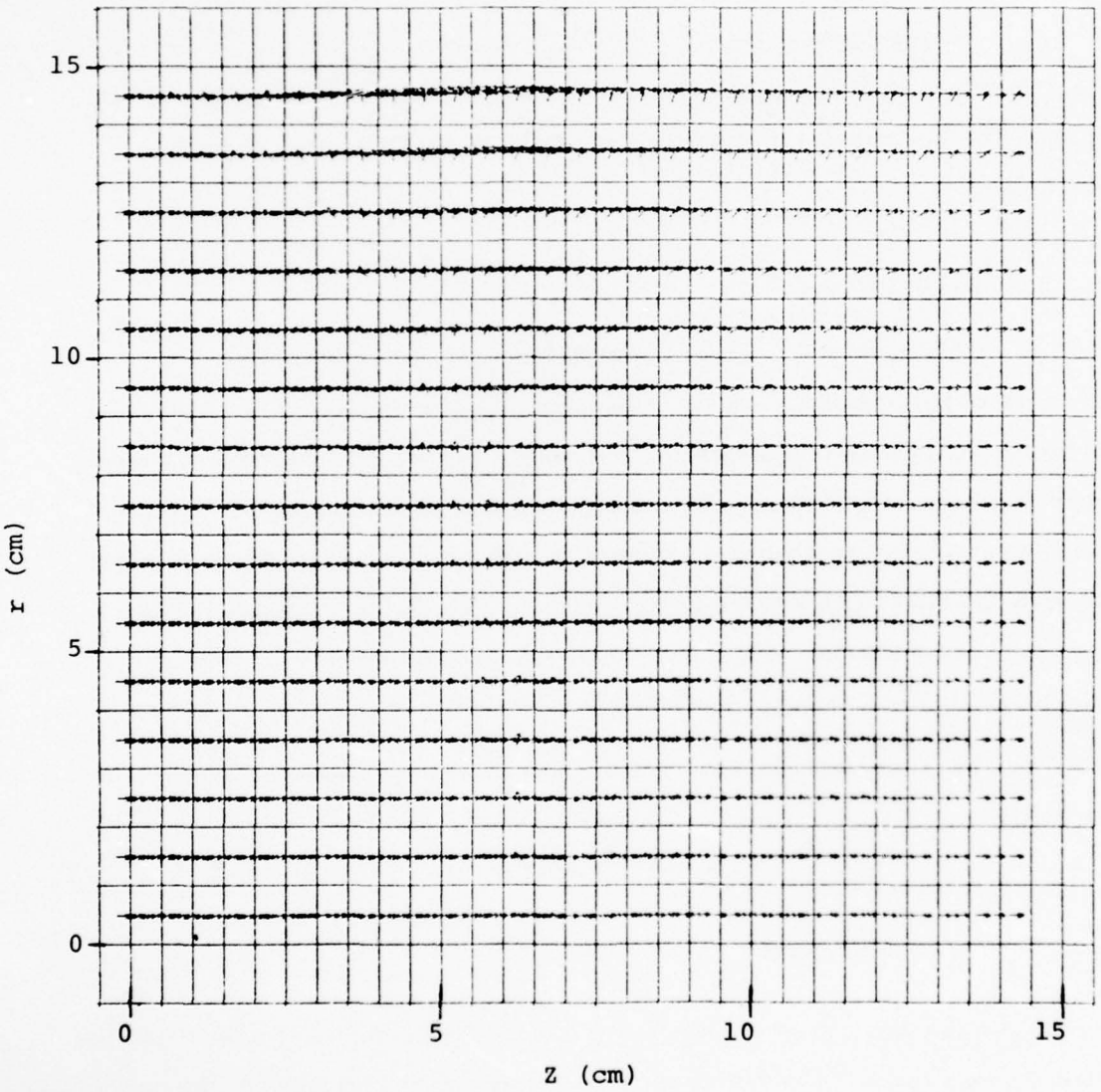


Figure 40. Particle positions at t = 1 nsec, P = 0.2 torr.

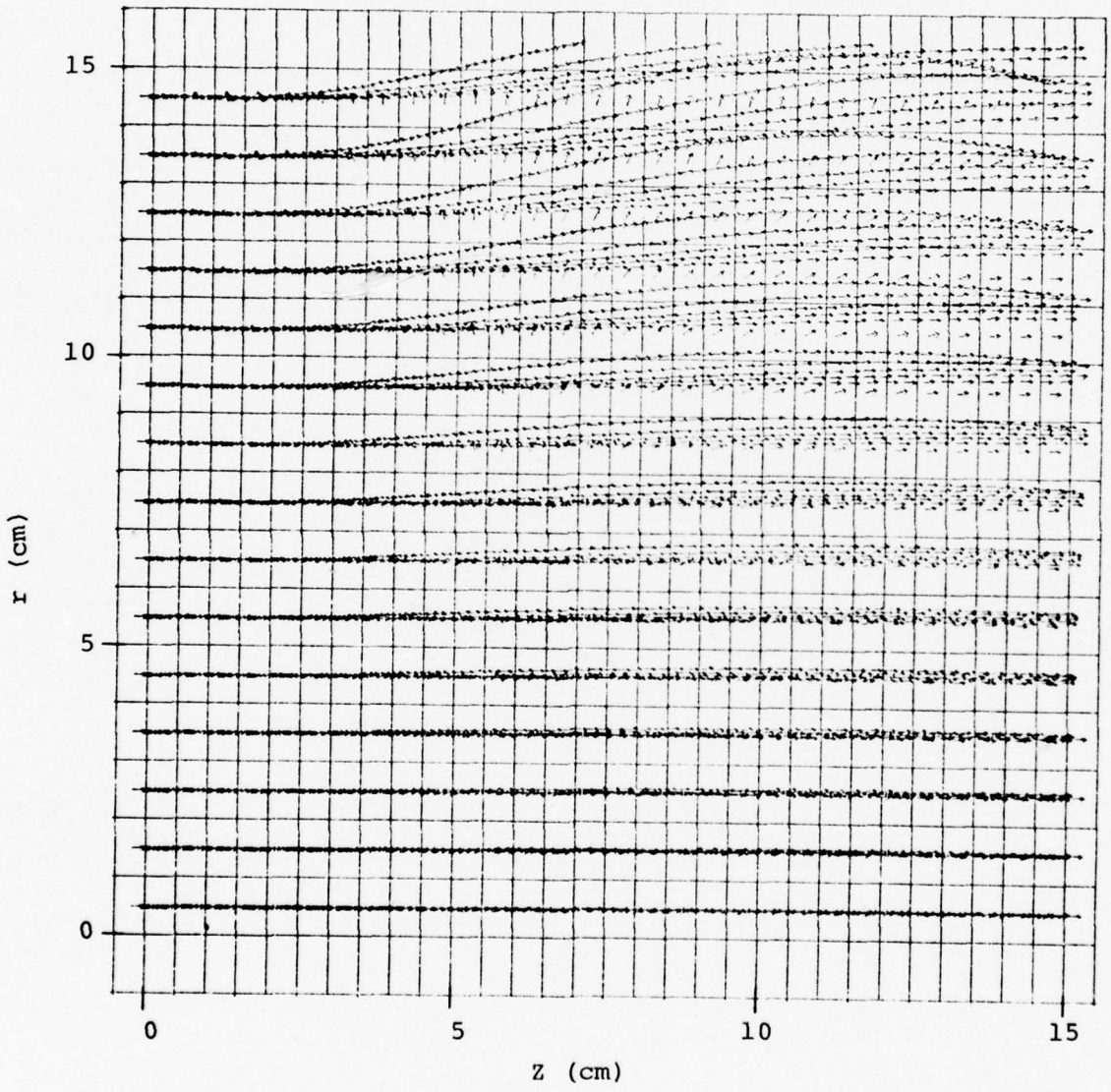


Figure 41. Particle positions at t = 2 nsec, P = 0.2 torr.

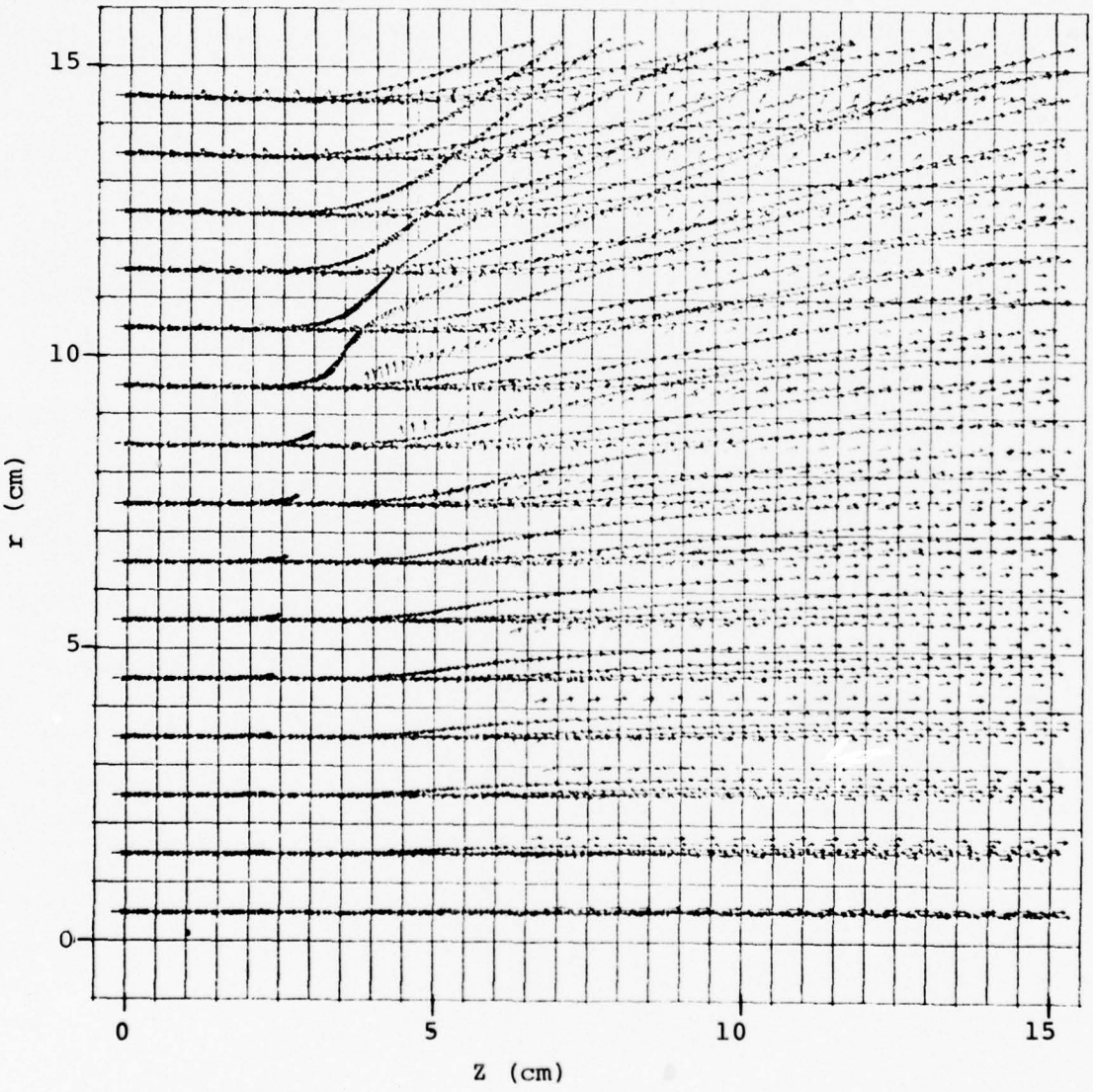


Figure 42. Particle positions at t = 3 nsec, P = 0.2 torr.

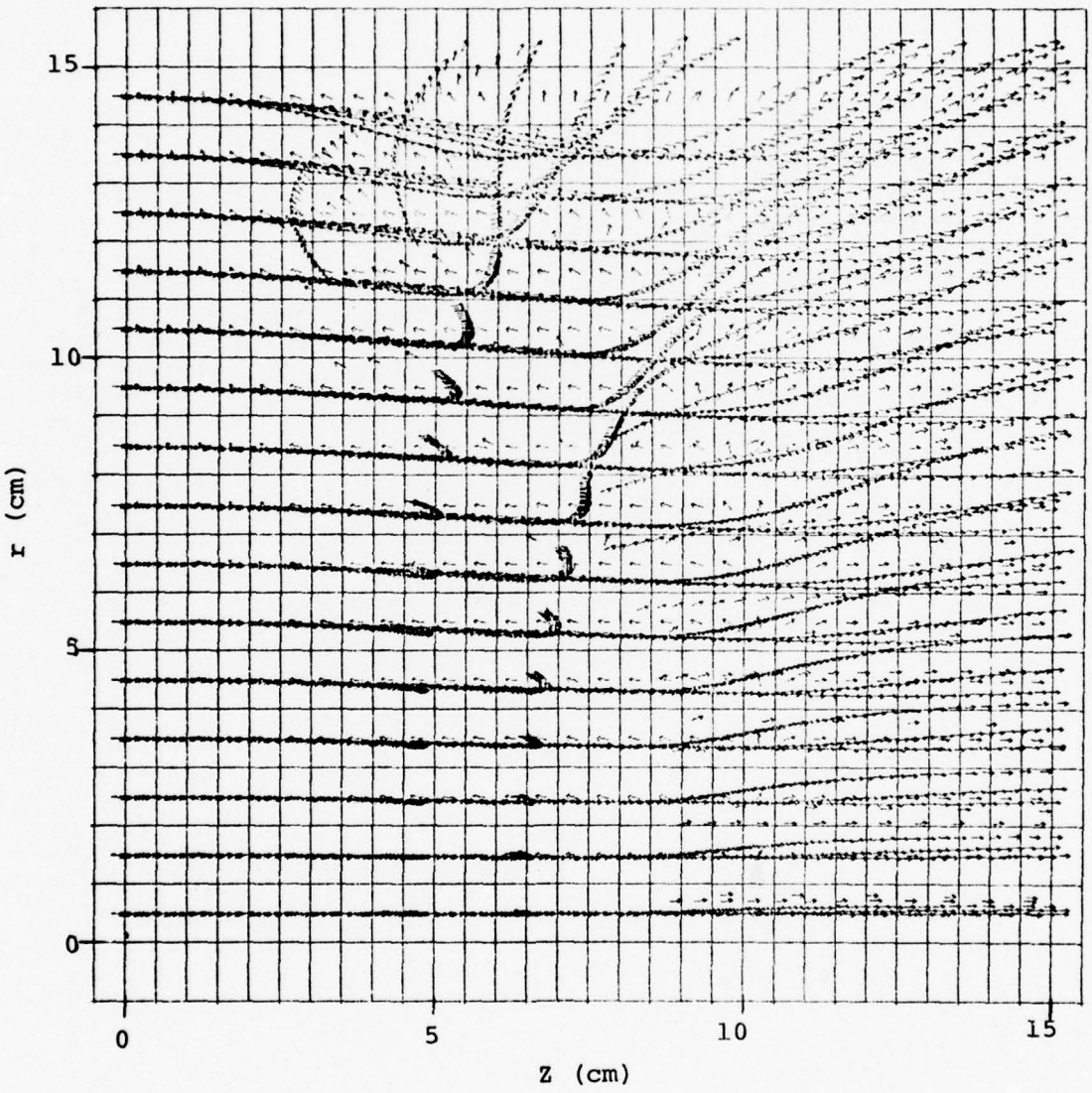


Figure 43. Particle positions at t = 4 nsec, P = 0.2 torr.

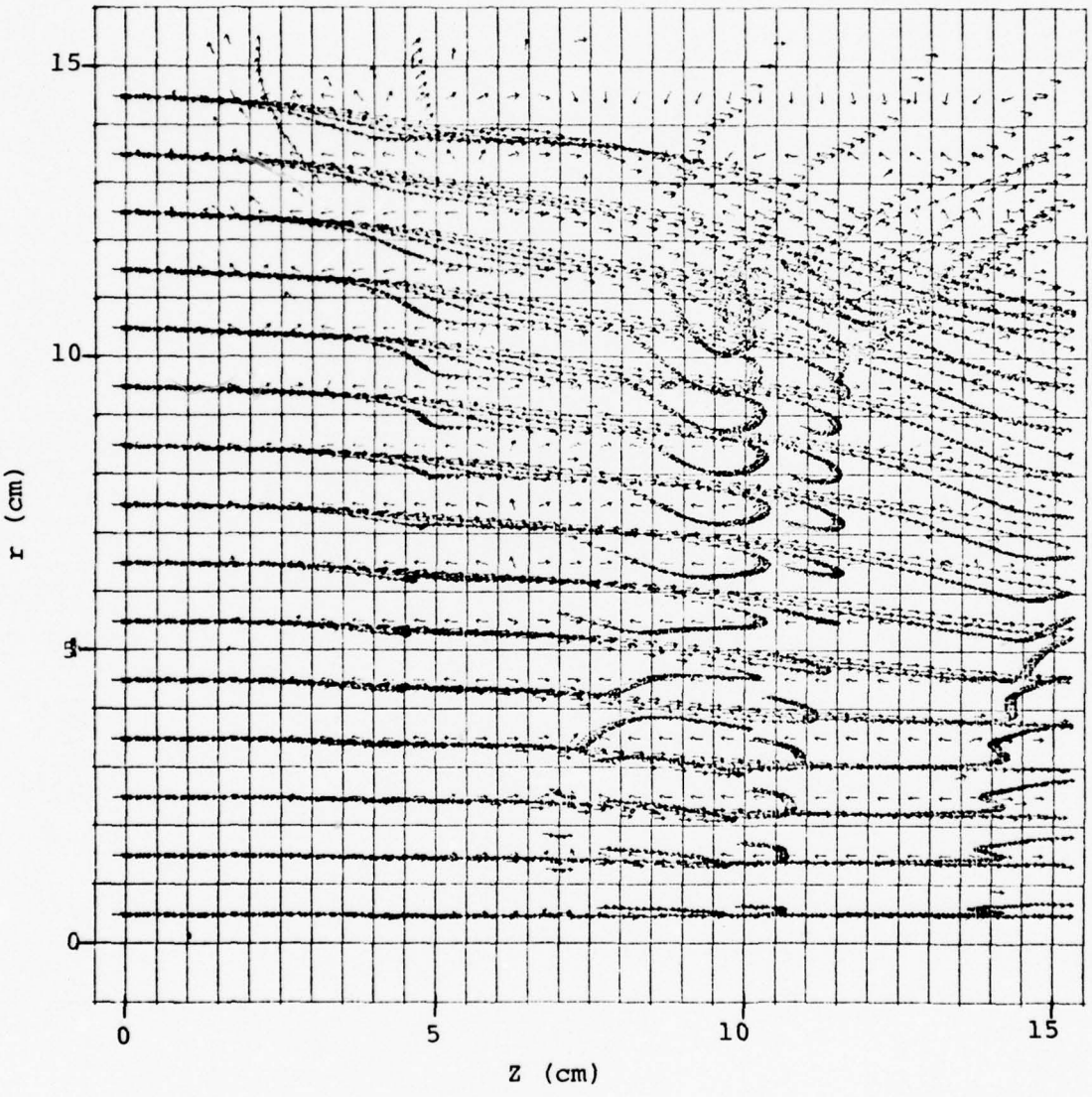


Figure 44. Particle positions at t = 5 nsec, P = 0.2 torr.

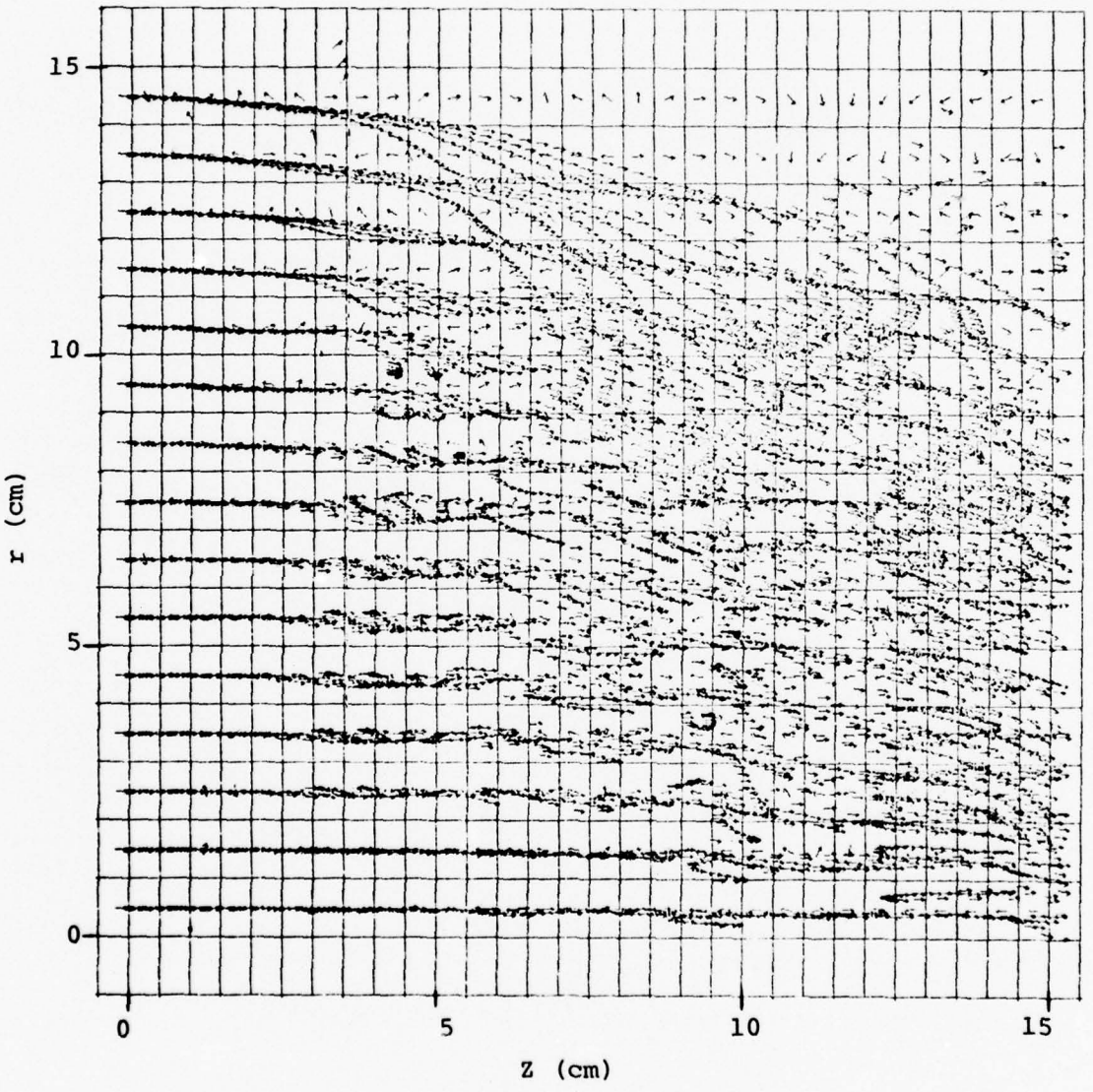


Figure 45. Particle positions at t = 6 nsec, P = 0.2 torr.

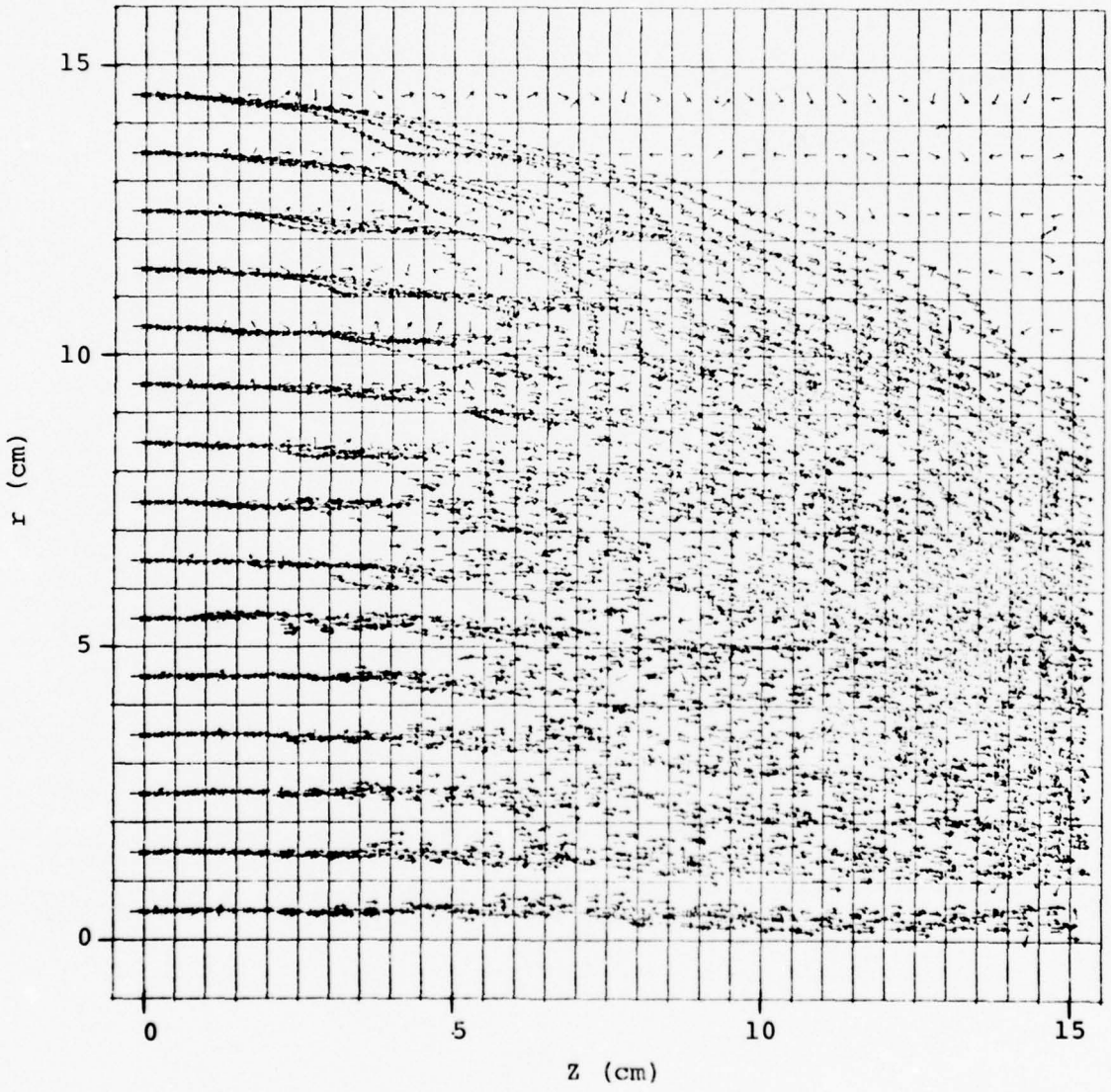


**Figure 46.** Particle positions at t = 7 nsec, P = 0.2 torr.

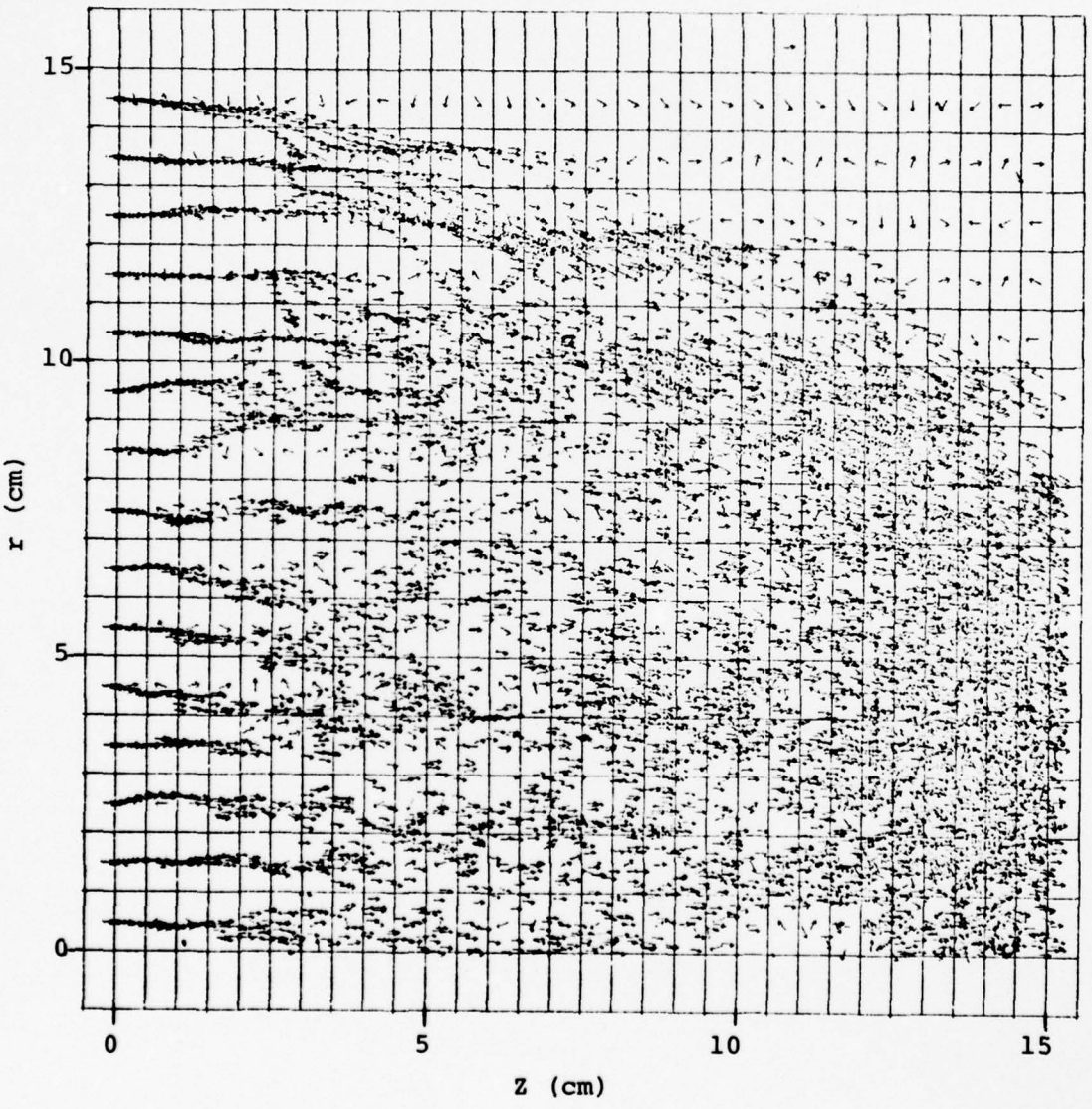


Figure 47. Particle positions at t = 8 nsec, P = 0.2 torr.

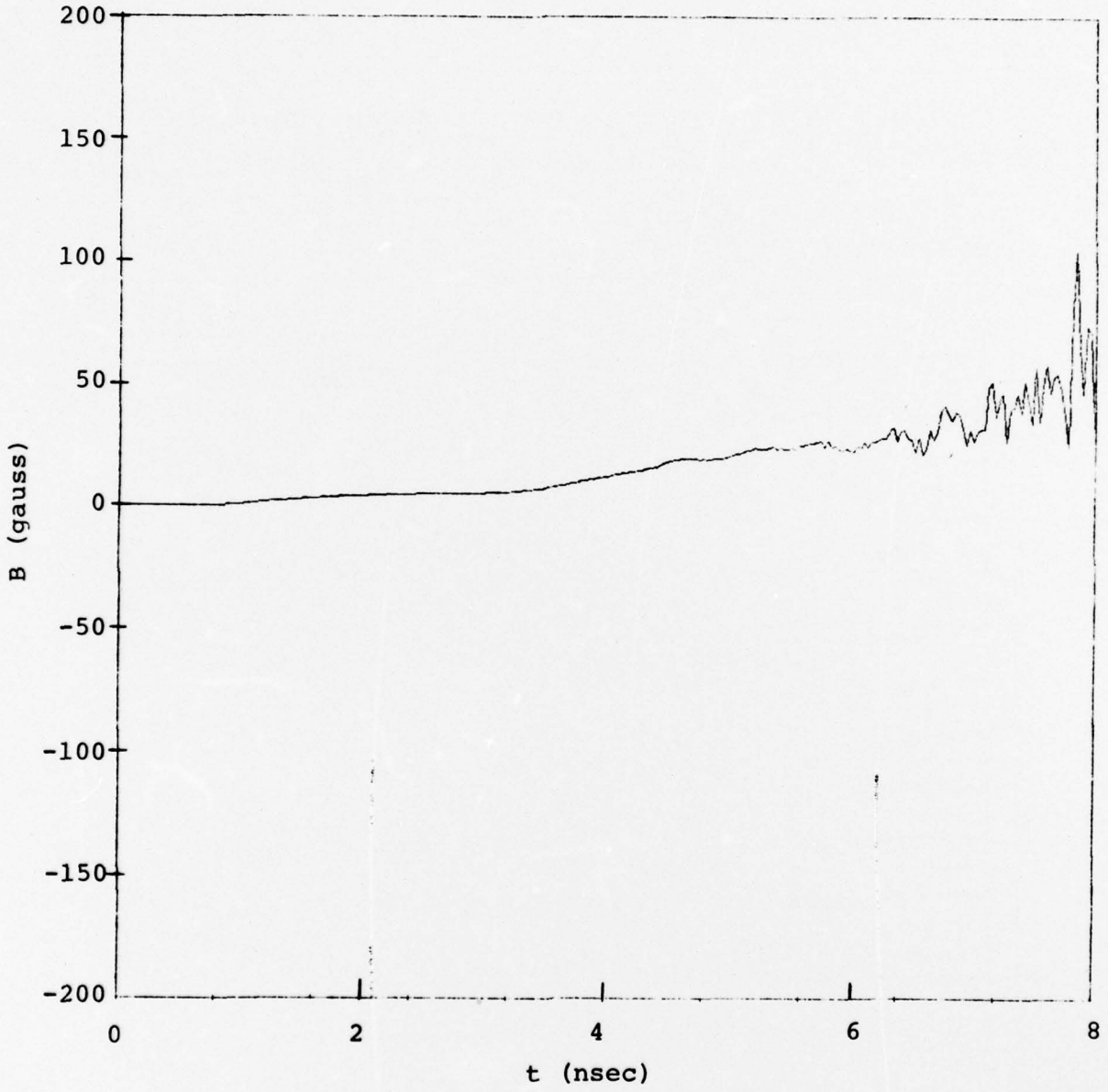


Figure 48. Magnetic field at r = 15 cm, z = 15 cm, P = 0.2 torr. The oscillations after 6 nsec result from a numerical instability.

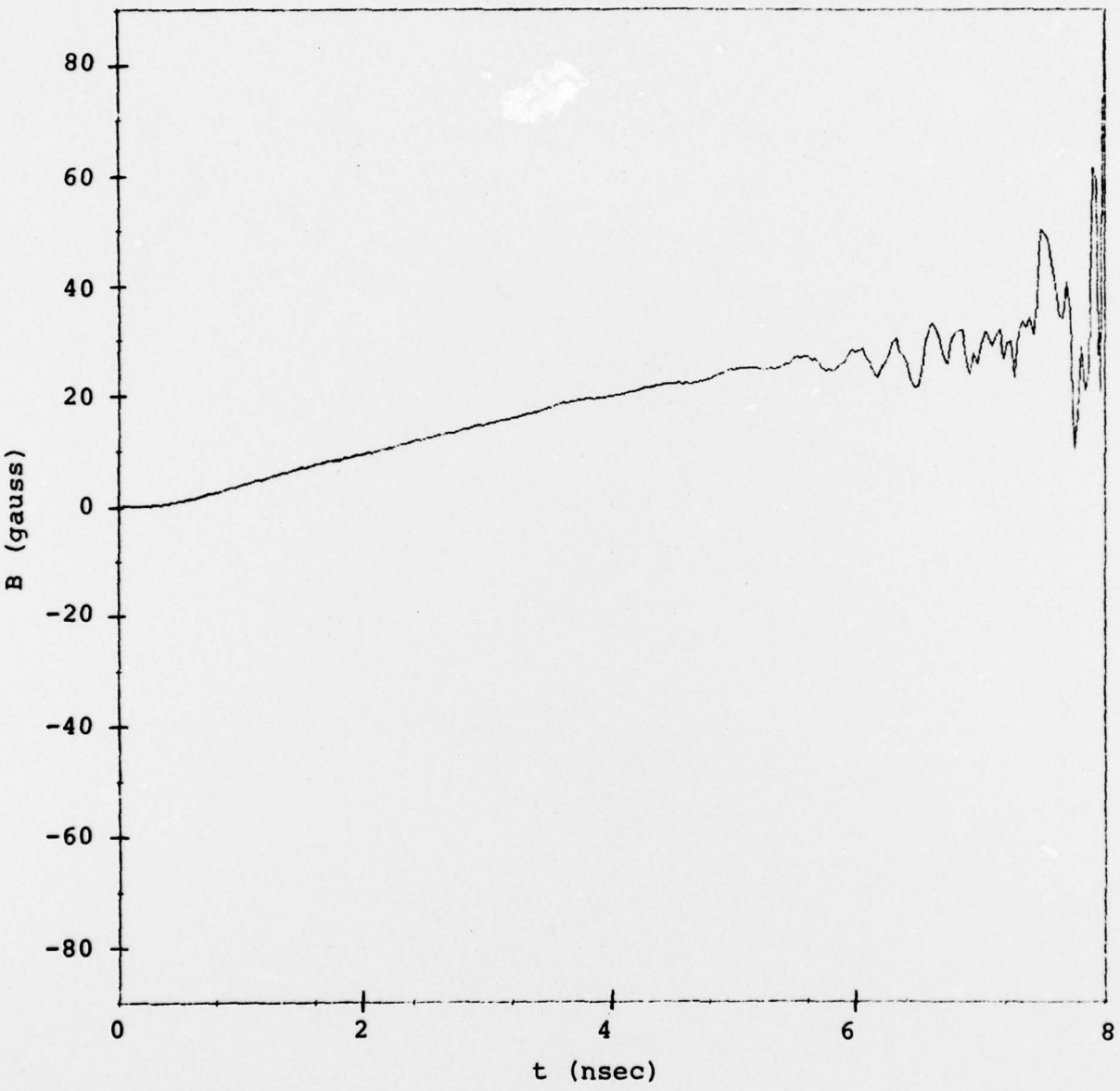


Figure 49. Magnetic field at r = 14 cm, z = 0 cm, P = 0.2 torr.

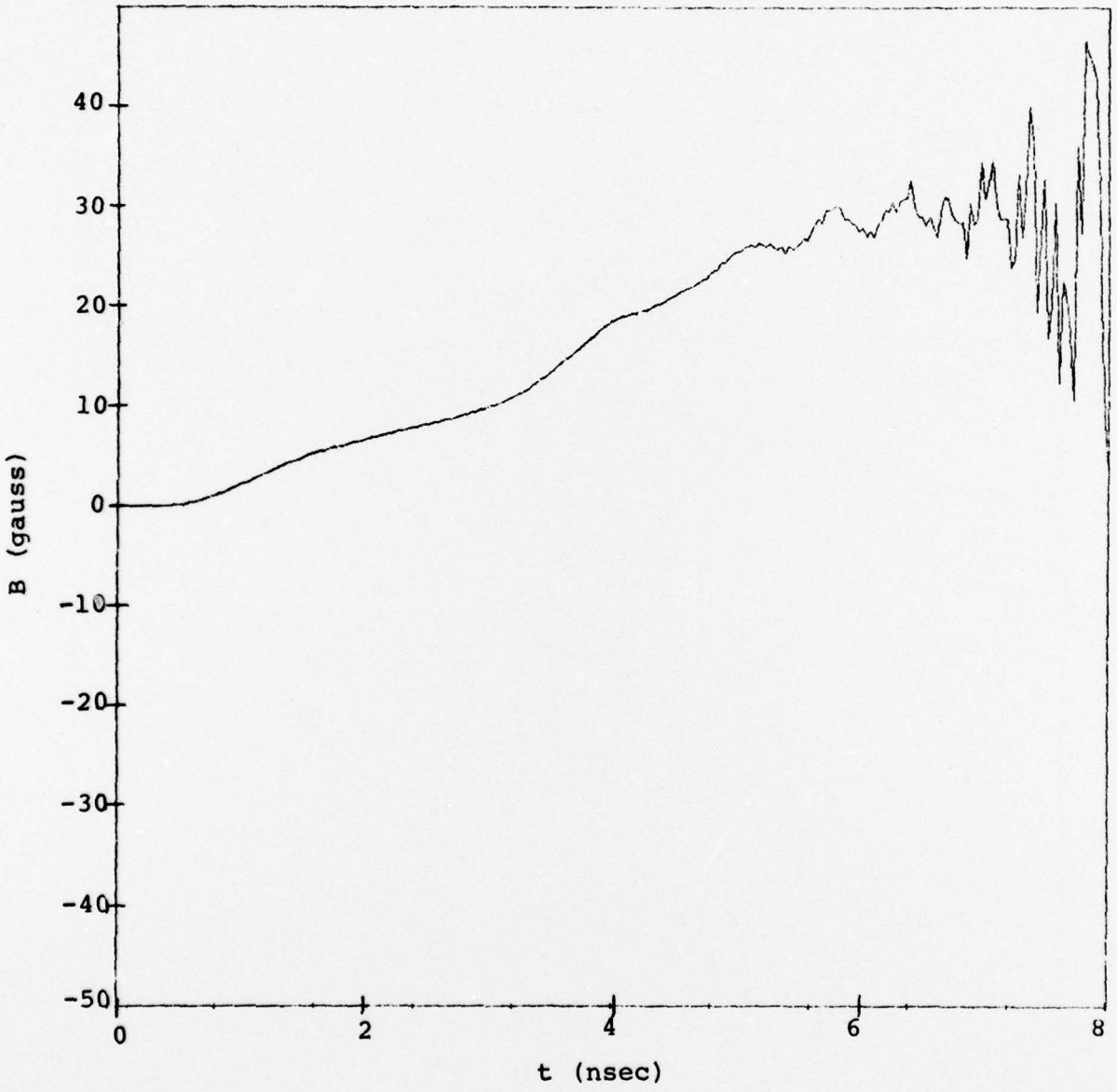


Figure 50. Magnetic field at r = 14 cm, z = 7 cm, P = 0.2 torr.

There are, however, some features of the P = 0.2 torr which are quite different from the two other cases. On account of the higher gas density, quasi-neutrality is reached before the end of the calculation. With energetic beam electrons moving through a cold plasma of secondaries having a comparable number density, conditions are suitable for collective beaming instabilities. In fact, at t = 5 nsec, the spatial profiles of the electric fields exhibit large amplitude variations (not shown here).

Later in the calculation, after 6 nsec, the magnetic field shows large fluctuations of high frequency (Figures 48 to 50) which continue to grow in amplitude. While the fluctuations may result initially from real collective effects, they are certainly not correctly treated at the end of the calculation. By that stage, the stability criterion

$$\omega_p \Delta t < 1/2$$

is violated, resulting in unstable electrostatic oscillations. Here, $\omega_p$ is the electron plasma frequency given by

$$\omega_p \sim 5.6 \times 10^4 n^{1/2} .$$

The electron number density n is given by

$$ne\beta = 0.1 j$$

where $e = 4.8 \times 10^{-10}$ esu and j is in $A/cm^2$. In the vacuum case, we have

$$j \sim 0.5 A/cm^2$$

and, with $\beta \sim 1/2$, we find that $n \sim 2 \times 10^8 cm^{-3}$, or

$$\omega_p \simeq 8 \times 10^8 sec^{-1} ,$$

which clearly satisfies the stability condition.

In the finite gas density case, however, many low energy ($\beta \sim 10^{-2}$) electrons are produced and the current flowing is larger, $j \sim 5$ A/cm$^2$, so that

$$n \sim 10^{12} \text{ cm}^{-3}$$

or

$$\omega_p \sim 5 \times 10^{10} \text{ sec}^{-1} \quad .$$

In this latter case, the time-step, at least late in the problem, is required to be as small as, or even smaller than, the electromagnetic time-step. This effect is discussed further in the Appendix.

# 4. SUMMARY OF RESULTS

The vacuum case results were quite satisfactory and should provide a useful basis for comparison with other code calculations. Even with the relativistic particle pusher included the computation time of 2.5 sec/cycle on the Univac 1108 for approximately 4000-5000 particles is not unreasonable, namely 500 $\mu$sec per particle per cycle. This is over twice as long as the non-relativistic pusher. The results obtained were smooth and free of any large statistical fluctuations.

The P = 0.05 torr case also provided some interesting and useful results. This was the first use of the finite pressure code GFRED. It appeared to behave in a satisfactory manner throughout with computation times similar to those of the pressure treatment in FRED/EM. There were no unusual statistical fluctuations and the results appeared to be consistent.

The P = 0.2 torr case provided a more severe test of the GFRED treatment. It behaved in a satisfactory manner for most of the calculation. However, after rapid multiplication of the secondaries had begun it was evident that abnormal fluctuations were present. This problem could have been solved by reducing the time-step, but for the present work, this was not done. It appears that an extended version of GFRED is required if space-charge neutral cases are to be examined. The existing GFRED treatment works well when the electron density does not impose severe time constraints; but for high pressure cases, a quasi-neutral fluid treatment is needed.

# REFERENCES


1. Katz, I., J. Harvey and A. Wilson, "Particle Simulation Techniques for SGEMP," DNA 3923T (to be published).

2. Boris, J. P., Proc. 4th Conference on Numerical Simulation of Plasmas, pp 3-67, NRL, Washington, D.C., November 1970.

3. Wilson, A., et al., "Theoretical Studies of SGEMP Field Generation," DNA 3654F (to be published).

4. Green, A. E. S., C. A. Barth, J. Geoph. Res., 70, 1083, March 1970.

5. Stolarski, R. S., V. A. Dulock, Jr., C. E. Watson, A. E. S. Green, J. Geoph. Res. 72, 3953, August 1970.

6. Watson, C. E., V. A. Dulock, Jr., R. S. Stolarski, A. E. S. Green, ibid., 3961.

7. Brown, S. C., Basic Data of Plasma Physics, MIT and Wiley, New York, 1959.

8. de Plomb, E., IEEE Trans. Nuc. Sci., NS-20, 20, December 1973.

# APPENDIX

## GFRED - A FINITE GAS PRESSURE PARTICLE CODE

In a number of IEMP/SGEMP environments, the presence of a gas can be important. These environments include air bubbles in cables, residual gas in systems at high altitudes, e-beam cavity experiments, to name a few. In any event, the number density of molecules $n_o$ may range from $n_o \sim 10^{19}$ cm$^{-3}$ to essentially zero. Finite gas pressure effects can cause the space charge neutralization of an electron beam-cloud, thus resulting in reduced electric fields and increased current flow. Or, at higher pressures, gas breakdown is possible.

In order to cover the complete range of gas densities likely to be encountered, it is necessary to have a theory which describes phenomena in a collisionless plasma equally well as in a collision-dominated plasma fluid. It is also necessary to find a theory which goes smoothly between the two regimes.

Before describing the theories developed, it is worth considering briefly the various phenomena which the theory should treat adequately. At 'low' pressures, the beam electrons create, in passing through the gas, secondary electrons. In this regime, they accelerate in the space charge field of the beam electrons and escape to the walls as runaways. The ions move much more slowly and are left to cancel some of the space charge. For sufficiently long pulses, the space charge field becomes neutralized. During such a pulse, the electric field is primarily longitudinal.

At higher pressures, the neutralization takes place at an early stage in the pulse. Thereafter, the electric field is primarily transverse. In this regime, secondary electrons will collide and create further ionization. The secondaries will also be scattered by elastic collisions. As a result, it is necessary to allow for the possibility of secondaries behaving either as runaways or as collision-dominated drifting particles. The effect of the magnetic

field on the electron motion (particularly the fast electrons) may be important. In cases where the secondary electron density is comparable with beam and is characterized by a much lower temperature, it may be necessary to follow effects such as the two-stream instability.

At yet higher gas densities, the ionization by secondaries may result in avalanche and breakdown. Here, the drifting behavior will dominate and the plasma behavior is fluid-like.

Proceeding to the highest gas densities, the collision rate for secondaries is now so small that they cannot gain enough energy between collisions to cause ionization. In this regime, we expect the formation of secondaries to surround the primary trajectories. Recombination may now be important and the primary beam may, itself, be degraded and attenuated.

To cover this complete gas density range is a formidable task. It is fair to say that the vacuum case is now well understood and that the 2-D codes FRED/E, FRED/EM and SQU1D are all tested and fully operational. They are applicable to 2-D geometries of arbitrary shape. FRED/E uses a quasi-static model, whereas the other two are electromagnetic codes. SQU1D is the most complete code, incorporating a capability for handling heavily space charge limited dynamics in an efficient manner.

The first steps toward a complete finite gas density capability have been set up with the codes MANFRED and, more recently, GFRED. The former is a finite density extension of FRED/E, and since it is quasi-static, can be applied to very low density cases where neutralization of the space charge is incomplete. The more recent GFRED removes the quasi-static limitations - it is an extension of FRED/EM. While applicable to a wide range of conditions, it can not, in its present form, be applied to the entire gas density range described above.

GFRED is a 2-D axisymmetric, electromagnetic particle code which incorporates, in an approximate fashion, a description of the ionization of a

finite density gas. The electromagnetic description is carried out as in FRED/EM. The new features are in the treatment of secondaries.

The method adopted to treat plasmas which may be collisionless or collision-dominated is to use a particle description in which the equation of motion is

$$\frac{d\vec{v}}{dt} = -\frac{e}{m}\left(\vec{E} + \frac{\vec{v}}{c} \times \vec{B}\right) - \nu\vec{v} \qquad \text{(A.1)}$$

where $\nu$ is the (energy dependent) collision rate. The latter results from both elastic scattering (at a rate $\nu_s$) and inelastic ionization processes at a rate $\nu_I$

$$\nu = \nu_s + \nu_I \quad .$$

In GFRED, as in most particle simulation codes, particles represent large numbers of electrons. In the particle dynamics, the electron value for e/m is used as in Equation (A.1) above. In calculating currents and charge densities, however, an effective charge $e^*$ is used where $e^*/e$ is the number of electrons represented by that particle. The rate at which a particle of charge $e^*$ creates secondary charge is given by

$$\frac{d\rho}{dt} = n_o \sigma_I v e^* = \nu_I e^* \qquad \text{(A.2)}$$

where $\sigma_I$ is the ionization cross section. It is assumed here that the fractional ionization of the plasma is low so that the electrons collide only with neutral molecules. The collision cross section $\sigma_I$ is zero below an energy threshold of ~20 eV for air. The energy dependence of $\sigma_I$ is based on an analytic fit of experimental data and is described in Refs. 4, 5 and 6. The scattering rate $\nu_s$ is related to the mobility $\mu$ by the expression

$$\nu_s = \frac{e}{m\mu}$$

and the mobility data is provided in Ref. 7.

For energetic particles, the equation of motion reduces to that of a particle in a collisionless plasma because for particle energies $\epsilon$ greater than that of the atomic ionization levels $\nu \sim 1/\epsilon \ \ell n \epsilon$ . On the other hand, for low energy particles, the inertial term is negligible and they drift with a velocity

$$\vec{v} = -\frac{e}{m\nu} \left(\vec{E} + \frac{\vec{v}}{c} \times \vec{B}\right) \simeq -\frac{e\vec{E}}{m\nu} \tag{A.3}$$

In this limit, we have the usual mobility transport model.

This description can thus be used to go smoothly from collisionless to collision-dominated regimes and to treat both energetic primaries and low-energy secondaries. However, some consideration must be given to the high density case where the plasma is collision-dominated. In this individual particle model, secondary electrons are created on each cycle by each of the primary electrons in accordance with Equation (A.2). These particles are then pushed according to the requirements of Equation (A.1). In order to prevent the total number of code particles from exponentiating in this way, it is necessary, at periods $T_c = n_c \Delta t$ (where $n_c$ is an integer and $\Delta t$ is the time step) to coalesce particles whose energies are such that during the time $T_c$ they do not move appreciably. That is, they are coalesced if their velocity $v$ is such that

$$v \, T_c << \Delta x$$

where $\Delta x$ is a cell dimension.

This treatment appears to work well. Despite its simplicity and the ease with which it is incorporated in a standard EM code such as FRED/EM, it does contain most of the physics necessary to describe the behavior of a plasma before avalanche phenomena are important. The advantages of the present model (over others) in this area are listed below.

1) 'First principles' treatment of the secondary electron dynamics - as distinct from using a set of approximate scaling laws[8] to describe neutralization, particle drifting, etc.

2) The theory of the electron dynamics goes smoothly from the collisionless to the collision-dominated limits.

3) The model is simple to incorporate in a code such as FRED/EM and calculations performed using it are fast.

Nevertheless, the model has defects which are evident at sufficiently high pressures. One of these is the neglect of angular scattering during collisions. The other involves the short wavelength electrostatic oscillations which are created when the secondary plasma density becomes very large.

Regarding the former of these, the deflection by a given electron-neutral collision is not taken into account. For calculations in which the collision rate is such that $\nu \Delta t < 1$ for all particles, it would be quite straightforward to take account of the details of the collision. However, very low energy particles may collide many times during a time step. For them, a fluid-like description is necessary. The coalescing of slow particles and the treatment of their dynamics via Equation (A.3) does, in fact, amount to a fluid description. What is neglected is the temperature of the fluid. That is, we assume that the drift velocity v, which is determined from Equation (A.3) is much greater than the random or thermal velocity. While these are good assumptions under conditions of large fields (electrostatic or inductive) at low pressures, they will be invalid at sufficiently high densities.

The other and more important weakness of the GFRED treatment concerns the behavior of the plasma whenever the plasma period $\omega_p^{-1}$

becomes smaller than the time-step. We saw, in Section 3, how the results became unstable whenever the criterion was violated. Use of a smaller time-step is the simple, but limited, solution to the problem. Under conditions of a high plasma frequency, the plasma is essentially neutral, with space charge irregularities occurring on a length scale, $v/\omega_p$, much less than that of the system and on a time scale much shorter than that of other phenomena of interest. The appropriate model for such instances is the adoption of the charge neutrality condition

$$\nabla \cdot \vec{J} = 0$$

to replace the charge continuity condition

$$\frac{\partial \rho}{\partial t} + \nabla \cdot \vec{J} = 0$$

which is inherent in GFRED. Work is now in progress to investigate such a procedure, which when completed, will permit high pressure cases to be examined.

# DISTRIBUTION LIST

DEPARTMENT OF DEFENSE

Defense Documentation Center
12 cy ATTN: TC

Director
Defense Nuclear Agency
ATTN: STSI, Archives
ATTN: DDST
2 cy ATTN: RAEV
3 cy ATTN: STTL, Tech. Lib.

Commander
Field Command
Defense Nuclear Agency
ATTN: FCPR

Chief
Livermore Division, Fld. Command, DNA
Lawrence Livermore Laboratory
ATTN: FCPRL

DEPARTMENT OF THE ARMY

Commander
BMD System Command
ATTN: BDMSC-TEN, Noah J. Hurst
ATTN: SSC-TEN, L. L. Dickerson

Commander
Harry Diamond Laboratories
ATTN: DRXDO-RCC, Raine Gilbert
ATTN: DRXDO-EM, R. Bostak
ATTN: DRXDO-RCC, John E. Thompkins
ATTN: DRXDO-RCC, John A. Rosado
ATTN: DRXDO-EM, John Bombardt
ATTN: DRXDO-TT, Tech. Lib.

DEPARTMENT OF THE NAVY

Director
Naval Research Laboratory
ATTN: Code 7706, Jay P. Boris

Commander
Naval Surface Weapons Center
ATTN: Code WA-501, Navy Nuc. Prgms. Off.

DEPARTMENT OF THE AIR FORCE

AF Weapons Laboratory, AFSC
ATTN: SUL

DEPARTMENT OF DEFENSE CONTRACTORS

Dr. Eugene P. dePlomb
ATTN: Eugene P. dePlomb

Exp. & Math. Physics Consultants
ATTN: Thomas M. Jordan

DEPARTMENT OF DEFENSE CONTRACTORS (Continued)

General Electric Company
Space Division
ATTN: Daniel Edelman
ATTN: Joseph C. Peden, VFSC, Rm. 4230 M

General Electric Company
TEMPO-Center for Advanced Studies
ATTN: William McNamara
ATTN: DASIAC

IRT Corporation
ATTN: Dennis Swift
ATTN: R. L. Mertz

Jaycor
ATTN: Robert Sullivan

Jaycor, Incorporated
ATTN: Eric P. Wenaas
ATTN: Andrew Woods

Kaman Sciences Corporation
ATTN: W. Foster Rich

Mission Research Corporation
ATTN: Roger Stettner
ATTN: Daniel F. Higgins
ATTN: Conrad L. Longmire

Mission Research Corporation
ATTN: V. A. J. Van Lint

R & D Associates
ATTN: Leonard Schlessinger

Science Applications, Inc.
ATTN: J. Roger Hill

Science Applications, Inc.
ATTN: William L. Chadsey

Simulation Physics, Inc.
ATTN: Roger G. Little

Systems, Science & Software, Inc.
ATTN: Andrew R. Wilson
ATTN: Ira Katz
ATTN: James Harvey